

DESIGN AND ASSESSMENT OF AN UPPER EXTREMITY PROSTHETIC SYSTEM

By

Daniel Alvin Bennett

Dissertation

Submitted to the Faculty of the
Graduate School of Vanderbilt University
in partial fulfillment of the requirements
for the degree of

DOCTOR OF PHILOSOPHY

In

Mechanical Engineering

May, 2016

Nashville, Tennessee

Approved:

Professor Michael Goldfarb, Ph.D.

Professor Robert J. Webster III, Ph.D.

Professor Nilanjan Sarkar, Ph.D.

Professor Eric J. Barth, Ph.D.

Professor Gerasimos Bastas, M.D., Ph.D.

To my parents, Dana and Lisa Bennett, who have supported me financially through college,
emotionally through graduate school, and who believe in me in the way only parents can.

Maybe now I will finally get a real job.

ACKNOWLEDGEMENTS

The work presented in this document is the summation of my individual contribution to the upper extremity prosthesis project, but it is by no means a product solely created by my own efforts. There are many people who have helped me a great deal throughout my time in the Center for Intelligent Mechatronics, and without whom the work presented here would have been impossible. Foremost among these is my advisor, Professor Michael Goldfarb, who has guided me over the last five years and has helped my project be the best that it could be. I am particularly thankful for the trust he places in his graduate students to manage their own time and projects, which encouraged me to be productive without making graduate school into something that is all-consuming in my life. I would also like to thank Profs. Sarkar, Webster, Barth, and Bastas for serving as my committee.

The funding for this project has two major sources: the National Institutes of Health (NICHD R21HD068753) and the King Abdulaziz City for Science and Technology (KACST). I would like to thank these institutes for supporting my work and my stipend, and specifically I'd like to thank Dr. Khalid Aldakkan, a former CIM member who facilitated the partnership with KACST, and has provided much support, financial and otherwise, over the course of the project.

The transhumeral prosthesis project has had many contributors over the years, some of whom began the project before I arrived and performed the work that was foundational to my own research, others who have worked alongside me for my entire tenure here, and still others who have come and gone. Tuomas Wiste performed the initial mechanical design of the hand, creating the skeletal anthropomorphic prototypes that gave me a great starting point for my own designs. Drs. Skyler Dalley and Atakan Varol designed the controllers for the Vanderbilt Multigrasp Hand, and I was able to work alongside Dr. Dalley specifically for several years as we developed and

tested the hand prototype. He probably taught me more about my project and building robotic prosthetics than anyone, and it was a pleasure to work with him before he graduated. Don Truex is a wizard when it comes to designing and troubleshooting electronics, and his infinite patience in answering my incessant electronics and coding questions was instrumental in my project. Without his guidance and expertise, my project would have easily taken twice as long. Dr. Jason Mitchell is a fantastic mechanical design engineer who primarily worked on the transfemoral prosthesis project, but was always willing to answer my design questions, and later provided his expertise to design the powered elbow prosthesis. Nasser Alshammary has worked alongside me on the arm team for several years now, and has been a great help in designing the coordinated control schemes for the elbow and wrist joints. Malik Alshareef, Ibraheem Redhwi and Hisham Alhassnan were all here for a shorter time, but also contributed to the design of the transhumeral prosthesis.

I would also like to thank all members of the CIM, past and present, for providing such an enjoyable work environment over the years. I am extremely grateful that I have been able to think of all of you as friends more than just co-workers, which has made all the difference for my experience in graduate school. Specifically, I'd like to mention Ben Gasser, who has frequently served as a sounding board for my design ideas, giving me great feedback, ideas, and design critiques. I would also like to thank Brian Lawson, who has helped me in a similar fashion for much longer, and from whom I have shamelessly stolen my dissertation format. If any future CIM members are reading this for the same reason, you should feel similarly obligated to cite me.

TABLE OF CONTENTS

	Page
DEDICATION.....	i
ACKNOWLEDGEMENTS.....	iii
LIST OF TABLES.....	viii
LIST OF FIGURES	ix
ABBREVIATIONS	xi
 Chapter	
I. Introduction.....	1
1. Upper Extremity Amputee Demographics and Needs	2
2. Overview of Current State of the Art for Upper Extremity Prosthetics.....	3
3. Multi-joint Prosthesis Control Methodologies	5
4. Prior Work on Vanderbilt Transhumeral Prosthesis	7
4.1 Vanderbilt Multigrasp Hand	7
4.2 Multigrasp Myoelectric Controller (MMC).....	9
II. Design of the Vanderbilt Multigrasp Hand	12
1. Manuscript 1: A Multigrasp Hand Prosthesis for Providing Precision and Conformal Grasps	13
1.1 Abstract	13
1.2 Introduction.....	13
1.3 Performance and Functional Objectives	14
1.3.1 Grasps and Postures	14
1.3.2 Digit Forces and Speeds.....	15
1.3.3 Physical Properties.....	16
1.3.4 Power Consumption.....	16
1.4 Multigrasp Hand Design.....	17
1.4.1 Allocation of Actuation for Precision and Conformal Grasping	17
1.4.2 Tendon Actuation and Series and Parallel Elasticity	21
1.4.3 Motor Unit Design	24
1.4.4 Cosmesis and Construction.....	24

1.4.5	Embedded System Design	25
1.5	Characterization of Hand Performance.....	27
1.5.1	Hand Size and Mass.....	27
1.5.2	Fingertip Forces	28
1.5.3	Motion Bandwidth	30
1.5.4	Hand Postures and Grasps	31
1.5.5	Battery Life	32
1.6	Conclusion	33
2.	Addendums to Manuscript 1	34
2.1	VMG Design Iterations.....	34
2.2	Functional Assessment of the Vanderbilt Multigrasp Hand.....	39
2.3	Winding Temperature Estimation and Regulation for Brushless DC Motors	44
III.	Design of a Transhumeral Prosthesis	49
1.	Manuscript 2: Design of a Myoelectric Transhumeral Prosthesis	50
1.1	Abstract.....	50
1.2	Introduction.....	50
1.3	Design Objectives	56
1.3.1	Wrist Objectives.....	56
1.3.2	Elbow Objectives	60
1.4	Design of Arm Components	63
1.4.1	Wrist Design	63
1.4.2	Elbow Design.....	65
1.4.3	Embedded System Design	67
1.5	Performance Characteristics	70
1.5.1	Range of Motion, Size and Mass	70
1.5.2	Joint Speed Measurement	72
1.5.3	Joint Torque Measurement	76
1.5.4	Power Measurements and Battery Life.....	77
1.5.5	Audible Noise Measurement.....	80
1.6	Conclusion	80
2.	Addendums to Manuscript 2	81
2.1	Powered Wrist Rotator Design Iterations	81
IV.	Coordinated Control of a Prosthetic Wrist	85
1.	Manuscript 2: Inertial-Measurement-Based Synergistic Wrist Rotation Control for a Myoelectric Arm Prosthesis	86
1.1	Abstract.....	86
1.2	Introduction.....	86
1.3	Coordinated Control Approach.....	89
1.4	Assessment Procedure	92
1.4.1	Prosthesis Prototype.....	92
1.4.2	Able-bodied Adapter and Motion Capture	94
1.4.3	Obtaining Arm Angles from IMU Measurements	95
1.4.4	EMG Measurement.....	97

1.4.5	Assessment Tasks	97
1.5	Results.....	100
1.6	Discussion.....	103
1.7	Conclusion	104
2.	Addendums to Manuscript 3	105
2.1	IMU Data Interpretation and Sensor Fusion.....	105
2.1.1	Mathematical Representations of Rotation.....	105
2.1.2	Sensor Fusion.....	107
2.1.3	Calculating Orientation from Reference Vectors	108
V.	Conclusion.....	113
1.	Recommended Future Work	114
	REFERENCES	115

LIST OF TABLES

Table	Page
III-1. Wrist and Elbow Performance Characteristics.	73
III-2. Wrist and Elbow Power Usage.	78
IV-1: Coordinated controller parameters.	93
IV-3: Statistical analysis of coordinated controller compared with sequential controller.	103
IV-2: Performance data for the coordinated and sequential controllers.	103

LIST OF FIGURES

Figure	Page
I-1. Comparison of the 3 generations of the VMG.	8
I-2. Graphical representation of the MMC state machine.....	10
II-1. Allocation of actuation in hand prosthesis.	18
II-2. Cross-sectional view of (a) digit II and (b) digit III.....	22
II-3. Exploded view of motor unit, including clutch and pulley.....	24
II-4. Top and bottom views of hand embedded system.	25
II-5. Hand board embedded system architecture.....	26
II-6. Hand with cover removed, showing embedded system and motor units.	27
II-7. Fingertip Forces corresponding to each motor unit.	29
II-8. Bandwidth corresponding to each motor unit.	30
II-9. Canonical grasps and postures provided by the hand prosthesis.	31
II-10. First iteration of third generation VMG actuation scheme.	35
II-11. Self-locking cam mechanism for bidirectional tendon tightening.	37
II-12. Southampton Hand Assessment Procedure (SHAP).....	40
II-13. Able bodied adapter used in SHAP assessments.	41
II-14. Amputee subject performing a SHAP pouring task.	42
II-15. Progression of SHAP scores over time.	43
II-16. Heat transfer diagram for motor thermal model.	45
II-17. Plots illustrating the test of the duty cycle attenuation algorithm.....	47
III-1. CAD model of wrist unit	64
III-2. Elbow prosthesis prototype.....	66

III-3. Block diagram of arm embedded system.....	68
III-4. Top and bottom view of arm embedded system.	69
III-5. Labeled photograph of fully assembled arm prosthesis.....	70
III-6. Solid models and corresponding photographs of elbow prosthesis illustrating its ROM	71
III-7. Closed loop position tracking bandwidth for each wrist transmission configuration.....	74
III-8. Closed loop position tracking bandwidth for elbow.	75
III-9. First generation of wrist prototype.....	82
III-10. Side-by-side comparison of the first and final versions of the wrist.	84
IV-1: Diagram showing location of IMU on arm and motions used in the coordinated controller.	90
IV-2: Wrist controller configurations used in assessment.	91
IV-3: Able-bodied adapter..	94
IV-4: Subject performing Clothespin Relocation Test (CRT).	95
IV-5: Diagram illustrating the procedure of the Compound Manipulation Task (CMT).	99
IV-6: Mean task completion time and standard deviations.....	101
IV-7: Torso displacement means and standard deviations.....	102

ABBREVIATIONS

General Acronyms:

VMG	Vanderbilt Multigrasp Hand
MMC	Multigrasp Myoelectric Controller
EMG	Electromyogram
DOF	Degree of Freedom
DOA	Degree of Actuation
SHAP	Southampton Hand Assessment Procedure
IOF	Index of Function (for SHAP)
ADL	Activity of Daily Living

Anatomical Motions:

OR	Opposition/Reposition
FE	Flexion/Extension
PS	Pronation/Supination
RUD	Radial/Ulnar Deviation

Hand Joint Abbreviations:

CMC	Carpometacarpal
MCP	Metacarpal Phalangeal
PIP	Proximal Interphalangeal
DIP	Distal Interphalangeal
IP	Interphalangeal

CHAPTER I

INTRODUCTION

This dissertation details the research conducted in the Center for Intelligent Mechatronics (CIM) at Vanderbilt University on the development of a myoelectric transradial prosthesis. This work is intended to enhance the ability of amputees to perform activities of daily living, which is primarily a continuation and expansion on previous work developing a multigrasp prosthetic hand that has been the subject of several conference and journal publications [1]–[12]. Specifically, this dissertation covers the mechanical design and evaluation of a multigrasp prosthetic hand and wrist, and the development and assessment of an IMU-based controller to enable the coordinated control of a wrist, hand, and elbow. To provide context for this work, this chapter will provide a brief introduction to the field of powered upper limb prosthetics, detailing relevant background information and current state of the art research directions, and will conclude with an overview of prior work associated with the Vanderbilt upper extremity prosthesis system.

Chapters II-IV are composed of the three journal publications that represent the primary contributions of this body of work. Addendums to each chapter are included to provide context for each publication in the framework of this dissertation, and to present work which did not fit well into the narrative of the publications. Chapter II describes the design and characterization of the Vanderbilt Multigrasp (VMG) hand, with additional sections added regarding the implementation of an algorithm to mitigate motor overheating risk, and the functional assessment of the device

with amputee subjects performing simulated activities of daily living. This manuscript was published in the *IEEE Transactions on Mechatronics* in 2015. Chapter III details the design and characterization of a powered transhumeral prosthesis, including a hand, wrist, and elbow, with an addendum outlining the design process that led to the final iteration of the wrist rotator. This manuscript has been submitted for publication in the *IEEE Transactions on Mechatronics* and is currently in review. Chapter IV presents a novel controller for the coordinated control of a prosthetic wrist and hand using an inertial measurement unit (IMU). This manuscript has been submitted for publication in the *IEEE Transactions on Neural Systems and Rehabilitation Engineering* and is currently in review. Chapter V summarizes the contributions of this dissertation and outlines recommendations for future work.

1. Upper Extremity Amputee Demographics and Needs

In 2005, studies indicated that there were approximately 1.6 million people affected by limb loss in the United States, and this number has almost certainly grown in subsequent years. Many of these individuals (35%) had amputations of an upper extremity. The vast majority of amputations are caused by either dysvascular disease, which has a higher incidence in persons 65 years or older (56%), or trauma, which has a higher incidence in persons under 65 (75%). Since approximately 92% of upper extremity amputations are caused by trauma and upper extremity amputations account for approximately 69% of all trauma-related amputations, it follows that the majority of upper limb amputees are most likely under the age of 65 [13], [14]. This means that even though there is a relatively small number of upper extremity amputees, and even fewer amputees with major (i.e. above wrist) amputations, the population contains a large number of young people who are likely active and thus might find their lifestyles drastically impaired by their loss of limb.

To counteract the loss of function that comes from losing a limb, many amputees turn to prosthetics. Unfortunately, due to the complexity of the limb they are replacing, prosthetic devices almost always fall short of expectations. Surveys have shown that the majority of amputees rate their prostheses as “fair” or “not acceptable” [15]. Common complaints include poor socket fits, low functionality, and poor appearance [16]. Amputees also desire additional wrist movement, better control mechanisms that require less visual attention, and the ability to coordinate two or more joints simultaneously [17]. It is clear that in order to better facilitate the needs of upper extremity amputees, much progress needs to be made in prosthesis design and control methodologies.

2. Overview of Current State of the Art for Upper Extremity Prosthetics

Devices currently available to amputees generally fall into one of three categories: cosmetic, body powered, or electrically powered. Electrically powered devices weren't available at all prior to 1964, when the first myoelectric prosthesis was developed, while cosmetic and body powered devices have been available for much longer. Cosmetic devices have existed since antiquity, and are static pieces that are molded and painted to look like a hand, while serving little functional purpose. Body powered devices have been widely used for over one hundred years, and are composed of Bowden cables, typically a pair, both attached to a shoulder harness worn by the user, such that appropriate movement of the shoulder (e.g. shoulder flexion and scapular abduction) will generate excursion of the cable. For transradial amputations, typically one cable is used to control the opening of a split hook terminal device, which is then closed by elastic bands. For transhumeral amputations, one cable controls both the hand and elbow, whereas a second cable is used to lock or unlock the elbow. Since opening the terminal device (against elastic bands) typically requires

higher cable forces than flexing the elbow, the actuation cable will typically move only the elbow when the elbow is unlocked, and will move only the terminal device when the elbow is locked. Body powered devices are advantageous in that they are highly robust, low cost, and able to offer some measure of proprioceptive feedback to the user, which is generally absent in cosmetic and electrically powered devices. Myoelectric devices are powered by electric motors commanded by a signal derived from a pair of bipolar surface EMG electrodes attached to antagonist muscle pairs. Typically for multiple joint prosthetic systems, a user uses a co-contraction signal (where both antagonist muscles are actuated simultaneously) to switch between control of a hand, wrist, and elbow, as necessary.

Since electric motors have traditionally been rather large with a low power density, older electrical prostheses tend to be as mechanically simple as possible, incorporating as few degrees of freedom as is practical. Thus, prosthetic arms have typically consisted of a single degree of freedom (DOF) hand or split hook, a single DOF wrist (often not powered), and a single DOF elbow. For the wrist and elbow joints this compromise does not sacrifice much function, but for the hand this represents a significant abstraction of the natural human hand. Though single DOF hands are robust and straightforward to control (2 EMG signals provide one-to-one mapping between input and actuator), their inability to adapt to objects results in low contact area and less stable grasps, and their motion tends to appear unnatural due to lack of articulation [18]. However, in the last 15 years, advances in motor, processing, and battery technology have enabled the development of multigrasp hands as an improvement on single DOF devices [4], [19]–[26]. In addition to research prototypes, several prosthetic companies (such as i-Limb, RSL Steeper, and Otto Bock) have released commercial devices to provide these benefits to the amputee community. These hands have many more DOFs and degrees of actuation (DOAs) than previous terminal

devices, and the extra articulation and control they provide has the potential to greatly improve grasping and manipulation of objects.

3. Multi-joint Prosthesis Control Methodologies

Though increased articulation and complexity of prosthetic arms may help amputees to perform activities of daily living, in a way the increased DOFs have compounded the shortcomings of prostheses. Single DOF devices were intuitive to control because there was a one-to-one correlation between the input (EMG signals) and output. With multigrasp hands, however, there are more DOFs to control with the same number of inputs, meaning that existing sequential control schemes will result in devices that are so unwieldy to control that it eliminates the advantages of the additional DOFs. When wrist and elbow DOFs are included in more major amputations, this problem becomes more severe. The most prominent methods researchers have used to solve this problem of control include pattern recognition [27]–[32] and event driven finite-state (EDFS) control [33]–[40].

Pattern recognition involves a-priori training of a classifier to infer user intent (which joints to move/grasps to make) by interpreting a plurality of EMG signals (typically many more than 2) over a series of moving windows in time (frames). At any given frame, if the pattern of measured EMG signals obtained from the user matches the stored values in the classifier, the device performs the selected posture or motion. While pattern recognition shows promise to expand the number of DOFs a user can control, it also has several notable shortcomings. Since it processes data in time frames of fixed duration, there is usually a perceptible delay between a user sending a signal and the device acting on that signal. Additionally, since the EMG characteristics of the muscles change over time, the patterns that trigger each desired event are not constant, and so the classifier requires

retraining periodically to maintain accuracy. These shortcomings will likely be mitigated with further research and development, but will most likely always be present in some way.

Another difficulty with pattern recognition lies in dealing with the absence of a plurality of clear EMG sites on an amputee's residual limb (e.g. in the case of high level transhumeral amputation or shoulder disarticulation), where the EMG signals required by the algorithms can be difficult or impossible to obtain. This problem is present in any control scheme which uses EMG signals, but is more pronounced with pattern recognition, since so many more signals are required. For these cases, a surgical technique known as targeted muscle reinnervation (TMR) can be used to create additional EMG sites [41]. This is accomplished by subdividing a patient's pectoral muscles and attaching several of the nerves that once connected to the muscles in the hand to these new muscle groups. After surgery, a patient can imagine flexing one of their missing arm muscles, which instead causes a flexion in their chest that can be detected by surface EMG electrodes. The signals obtained through this method have been shown to be effective at increasing the available control inputs to a prosthesis.

In EDFS, the controller consists of a series of interconnected states. The controller behavior is well defined within each state, and will transition to a set number of new states depending on the inputs from the user. Control of devices using EDFS tend to resemble moving through a map, where the user can navigate to different grasps or movements in the state by giving different inputs to the system. This system has the advantage of a reduced risk of false positives, near-instantaneous controller response, and no required controller training. The most notable drawback of this method is that not every state is accessible from all other states, meaning it can take somewhat longer to get to a desired pose or motion if it is distant in the state chart. Also, this methodology requires the

user to be trained on the state chart, though this would typically be a one-time event that would be reinforced by regular use of the device.

4. Prior Work on Vanderbilt Transhumeral Prosthesis

Work on the Vanderbilt Transhumeral Prosthesis began with the goal of creating a functional hand prosthesis primarily for transradial amputees. Over the course of the research described here, this focus expanded to include a wrist and elbow prosthesis for transhumeral amputees, but most of the work done prior to the research detailed in this dissertation concerned the development of a multigrasp hand and myoelectric controller, which are referred to as the Vanderbilt Multigrasp (VMG) hand and Multigrasp Myoelectric Controller (MMC), respectively.

4.1 Vanderbilt Multigrasp Hand

To date, there have been three distinct generations of the Vanderbilt Multigrasp (VMG) hand, which can be seen side-by-side in Fig. I-1. The first two generations were designed and constructed prior to the work presented in this dissertation by Dalley and Wiste [1], [4], while the design of the third generation is the subject of Chapter 2. The primary goal that drove the development of all three models was to design and build a hand prosthesis that could achieve the basic grasps required for most activities of daily living (ADLs) with biomechanically appropriate levels of force and speed. Beginning with the first generation and continuing with the second generation, biomimicry was also a high priority. This priority is shown most clearly in the skeletal design of the hand, the high number of DOFs (the design incorporated sixteen out of the approximately twenty DOFs of the natural hand), and the use of tendons to actuate each digit. Additionally, in the first generation the motors that controlled each tendon were located proximally to the hand, similar

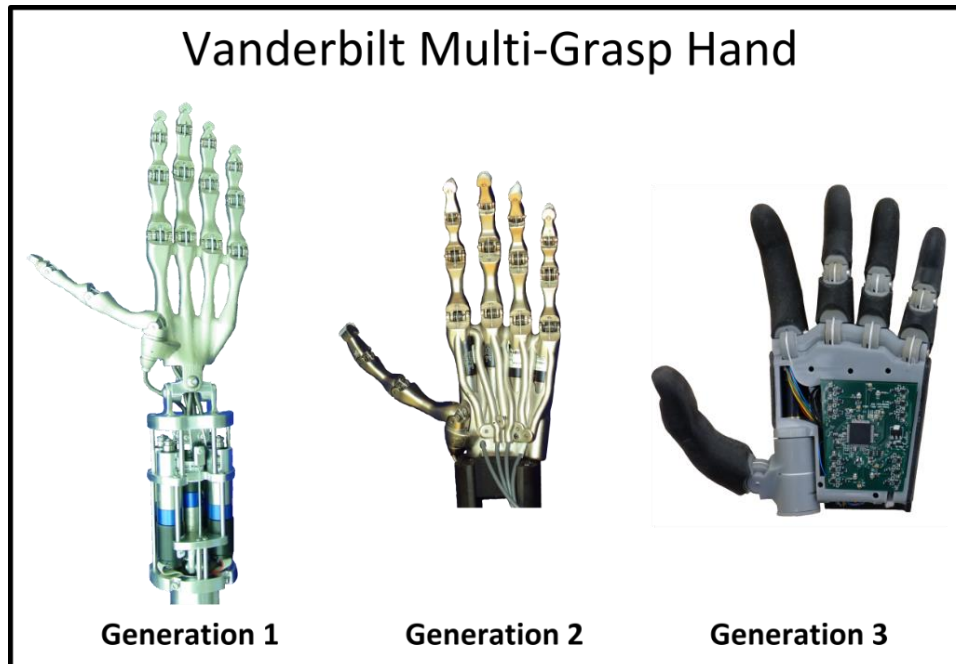


Fig. 1-1. Comparison of the 3 generations of the VMG.

to how many of the muscles that drive the sound hand are located in the forearm. These five motors allowed independent control of thumb flexion, thumb opposition, index finger flexion, middle finger flexion, and coupled control of the ring and pinky fingers.

The second generation hand kept the skeletal design, high DOFs, and tendon actuation of its predecessor, but opted for a less anthropomorphic actuator configuration in order to create a more compact package. Since the size of the residual limb varies between individuals, in order to accommodate the highest number of amputees, the design of the hand needed to be as modular as possible. Thus, it is important that the motors that control the hand be contained within the hand itself. To this end, the motors were reduced in size and number, and the palm structure was altered to create room for the motors. In this configuration only the index finger flexion, the thumb flexion, and the thumb opposition could be controlled independently, while the remaining digits were coupled to a single actuator. This design also incorporated a new 2-way clutch design that prevents

external forces from back-driving the motors, which enables the hand to have a passive load capability that is limited only by the yield strength of the various components.

4.2 Multigrasp Myoelectric Controller (MMC)

The Multigrasp Myoelectric Controller (MMC) [6] was developed alongside the VMG in order to provide intuitive access to the full functionality of a multigrasp prosthetic hand with only the standard 2-site EMG signals used by most commercial myoelectric prostheses. While more sophisticated control methods using multiple EMG sites might have the potential to provide a greater number of control signals, none of those methods have yet matched the reliability and convenience of a 2-site EMG interface. Most commercial myoelectric prostheses attach the two electrodes to antagonistic muscle pairs on either the forearm or the upper arm, depending on the level of amputations. These electrodes provide two control signals (three including co-contraction) that typically correspond to an “open” and “close” command for a single DOF prosthesis. The MMC uses these two signals, along with tendon displacement and force measurements, to navigate an input driven state machine, which can be seen in Fig. I-2.

Each state represents a single grasp form, and the user can move continuously within each state or between adjacent states. When nothing obstructs the digits, the input is treated as a velocity signal, and when the digits come into contact with an object, elastic elements in the hand transform the velocity command into a force command. In other words, higher EMG signals (corresponding to stronger muscle contractions) will cause faster digit movement or stronger grasp force, depending on whether the digits are in contact with an object. Care was taken to make the state chart as intuitive as possible so that amputees would be able to directly apply their experience

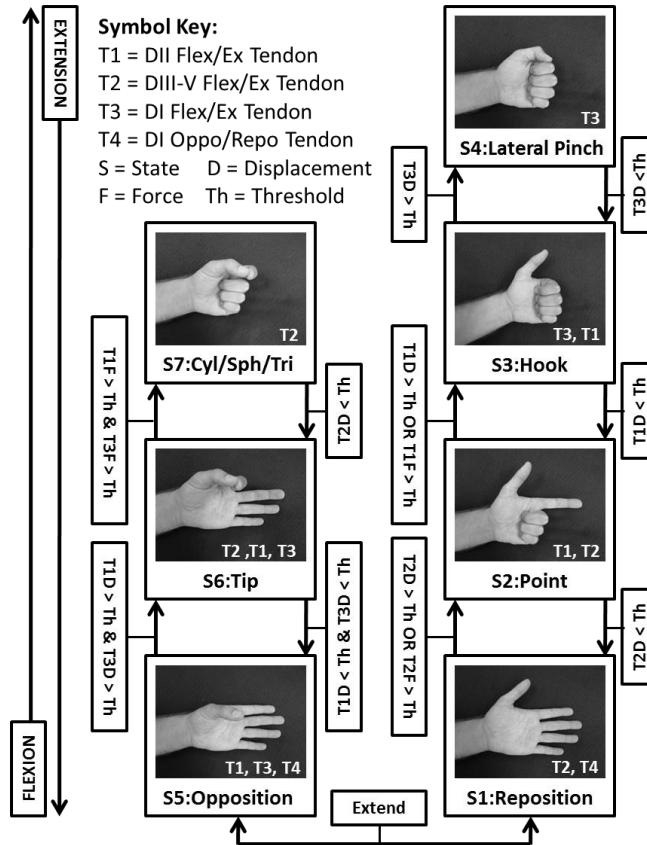


Fig. 1-2. Graphical representation of the MMC state machine.

using their own myoelectric devices. Much like standard myoelectric devices, a signal from the forearm flexors will cause the hand to make closing movements, which correspond to moving upward in the graphical representation of the state chart. Conversely, a signal from the forearm extensors will move downward in the state chart, causing the hand to open. Once in the most open state of the hand, an additional extension signal will cause the thumb to toggle between states of opposition and reposition.

The grasps covered by the MMC were chosen so as to maximize both the applicability of the controller to ADLs and the synergy with the VMG. Studies have shown that the vast majority of ADLs are enabled by only six grasps: tip, tripod, lateral pinch, hook, spherical, and cylindrical [42]. For this reason, these six grasps were chosen as the focus of both the MMC and the VMG designs. The specific layout of the state chart of the MMC was created by sorting the grasps by

thumb position and degree of hand closure. The result is an intuitive controller that users can understand and use within minutes of their initial introduction.

CHAPTER II

DESIGN OF THE VANDERBILT MULTIGRASP HAND

The first and second generations of the VMG proved to be effective test-beds for control methodologies, but the process of experimenting with the hands in standardized hand assessments revealed several shortcomings. Foremost among these was that it was difficult for the hand to grab and manipulate very small objects. This was the result of three factors: the lack of a tactile cosmesis, the small contact area of the digits due to their skeletal shape, and the inability to control digits due to the high degree of underactuation. Additionally, the highly compact configuration required to fit the motors, pulleys and tendons in the hand while keeping the skeletal structure resulted in a prototype that was difficult to assemble and maintain. These shortcomings, and the desire to refine the hand design in the context of the MMC, necessitated a nearly complete redesign of the hand for generation 3. The bulk of this chapter is a reprinting of a manuscript that was published in the *IEEE Transactions on Mechatronics*, which describes the design process and performance of the third generation hand. The paper also presents the design of an embedded system containing brushless DC servo-amplifiers that was designed by Don Truex. The remaining sections provide greater insight into the design process that produced the VMG and present the results of the functional assessments of the hand that were part of the dissertation of Skyler Dalley. The chapter concludes with a brief derivation of a temperature model based current limiter for reducing the incidence of motor burnout in the hand.

1. Manuscript 1: A Multigrasp Hand Prosthesis for Providing Precision and Conformal Grasps

1.1 Abstract

This paper presents the design of an anthropomorphic prosthetic hand that incorporates four motor units in a unique configuration to explicitly provide both precision and conformal grasp capability. The paper describes the design of the hand prosthesis, and additionally describes the design of an embedded control system located in the palm of the hand that enables self-contained control of hand movement. Following the design description, the paper provides experimental characterizations of hand performance, including digit force capability, bandwidth of digit movement, physical properties such as size and mass, and electrical power measurements during activities of daily living.

1.2 Introduction

Upper extremity prosthetic terminal devices have traditionally been limited to a single degree of freedom. In contrast, the human hand has approximately 20 degrees of freedom (DOFs), and can perform a variety of grasps and postures. Recent advances in mechatronics technology enable the development of multigrasp hand prostheses, which contain multiple actuated degrees-of-freedom and can provide to the user a variety of grasps and postures. Presumably, such “multigrasp” prostheses could offer enhanced functionality to upper extremity amputees. Descriptions of several recently-developed multigrasp hands are provided in [4], [19]–[26], [43]–[46]. These hands contain between one and six independent actuators and between eight and sixteen joints, where in each device, the discrepancy between the number of actuators and the number of joints is

accommodated by differential, kinematic, or compliant coupling. The configuration of each of these hands (i.e., the number and allocation of DOFs, number and allocation of actuators, and type and extent of coupling), as described in [1], varies considerably. Specifically, the manner in which to allocate and configure the DOFs, actuators, and coupling in a multigrasp prosthesis is highly variable, and is highly dependent upon the functional objectives of the hand and the nature of the user interface that controls it.

The authors have previously described and characterized the design of a multigrasp hand prosthesis that contained sixteen DOFs actuated by four actuators [4]. Based on experience with that prosthesis, the authors present here a new configuration for a multigrasp hand prosthesis that provides several advantages with respect to the former, as discussed subsequently. To the authors' knowledge, the configuration presented here has not been previously presented in the engineering literature. This paper describes the new hand configuration, the design embodiment of this configuration and the embedded system that controls it, and presents an experimental characterization of hand performance and functionality. A video is also included in the supplemental material that demonstrates operation of the self-contained prosthesis.

1.3 Performance and Functional Objectives

1.3.1 Grasps and Postures

The design objectives for the hand described in this paper are similar to those previously presented by the authors [4], which are briefly restated here for completeness. Grasps can be grossly classified as either precision or conformal types. The most common precision grasps are the tip, tripod, and lateral pinch grasps, while the most common conformal grasps are the hook, spherical, and cylindrical grasps. Note that the purpose of a precision grasp is generally to provide dexterity,

while the purpose of a conformal grasp is generally to provide stability. The former generally involve digits I and II, and possibly III, while the latter generally involve all five digits. The former can be generally characterized by single point contact between an object and each digit (typically at the tip of a digit), while the latter are typically characterized by multiple points of contact, or a continuum of contact, between an object and each digit. These six grasps constitute the vast majority of the grasps used by healthy individuals during the activities of daily living (ADLs) [42], [47]. In addition to these six grasps, the ability to point is an important component of interacting with modern technology interfaces, such as keyboards, cell phones, and touchscreens. Finally, a platform posture is also considered an important component of a complete grasp taxonomy [48], and is useful for holding flat objects, in addition to reaching into confined spaces (e.g., a clothing pocket) or donning clothing over the hand and arm.

1.3.2 Digit Forces and Speeds

In addition to forming these grasp shapes and hand postures, in order to offer functionality representative of the healthy hand, the digits of the prosthetic hand should be capable of forces and speeds representative of those characteristic of healthy individuals when performing ADLs. As discussed in [4], based on studies presented in [49]–[51], the digits associated with precision grasp (digits I and II: the thumb and forefinger) should be capable of at least 11 N, and ideally up to 25 N; the composite force exerted by digits III through V (the middle, ring, and little fingers) should be at least 14 N; and the digits should be capable of joint angular velocities of at least 4 rad/s, which on average corresponds to a bandwidth of 1.5 Hz over half of the range of motion of each joint.

1.3.3 Physical Properties

Surveys of upper extremity amputees indicate the importance of size, weight, and appearance of a prosthetic hand [16], [17], [52], [53]. A precise specification with regard to weight is difficult to obtain; despite this, the mass of the native limb along with the mass of existing commercially available prosthetic hands can be used together to provide a nominal mass target for a prosthetic hand. According to the study by Clauser et al. [54], the mass of the typical human hand is approximately 400 g. Measurements of commercially available prosthetic hands indicate the following: the Otto Bock MyoHand VariPlus Speed (single-grasp myoelectric hand) has a mass of 460 g; the Touch Bionics i-LIMB Revolution has a mass of 515 g; and the mass of the Bebionic hand is 500 g (where all measurements exclude cosmesis and battery). As such, a nominal mass target of 500 g was adopted as an appropriate target specification for the multigrasp prosthetic hand described here. With regard to size, based on the anthropometry study [55], a 50% male hand is characterized by a breadth and length of 9.0 cm and 19.3 cm, respectively, which were adopted as the size specification for the hand described here.

1.3.4 Power Consumption

A hand prosthesis should be capable of operating for a full day between battery charges. Surveys have shown that a majority of amputees use their prostheses more than 8 hours per day; a substantial proportion use them more than 12 hours per day [56], [57]; and some amputees use prostheses up to 16 hours per day [16]. As such, a battery charge should provide for at least 12 hours of use, and ideally 16.

1.4 Multigrasp Hand Design

1.4.1 Allocation of Actuation for Precision and Conformal Grasping

An essential design objective for the hand prosthesis is to provide both precision and conformal grasps. Recall that a distinguishing feature of the latter is the ability to conform to an object being grasped, thus maximizing the area of contact between the hand and object. In the performance of such grasps, one would like the shape of the object to principally determine the configuration of the hand. Conversely, precision grasps are generally used to handle or manipulate objects that are much smaller than the size of the hand. Such grasps are nonconformal (indeed, the notion of conforming to an object much smaller than the hand is not well posed), and therefore the hand must determine its grasp configuration independently of the object shape. In such cases, underactuation should be avoided. In order to provide such functionality, the prosthesis described here incorporates 4 independent actuators. Although a multigrasp prosthesis previously presented by the authors also incorporated 4 independent actuators [4], the allocation of actuation within the hand described here is specified in a unique manner, motivated by providing the aforementioned precision and conformal grasp capabilities. Specifically, in order to facilitate such functionality, the function of the digits were separated into precision and conformal, where digits I and II (i.e., the thumb and forefinger) were assumed to be principally responsible for precision manipulation, while digits III through V were assumed to principally conform to and stabilize objects during whole-hand grasping. As such, digits I and II were designed with three fully-actuated degrees of freedom in order to offer full control of precision grasps, while digits III through V were designed in an underactuated configuration, wherein a single actuator actuates six DOFs through a compliantly-coupled differential, in order to offer the stability of a conformal grasps. The specific actuation configuration is illustrated in Fig. II-1. In particular, one motor unit provides digit I

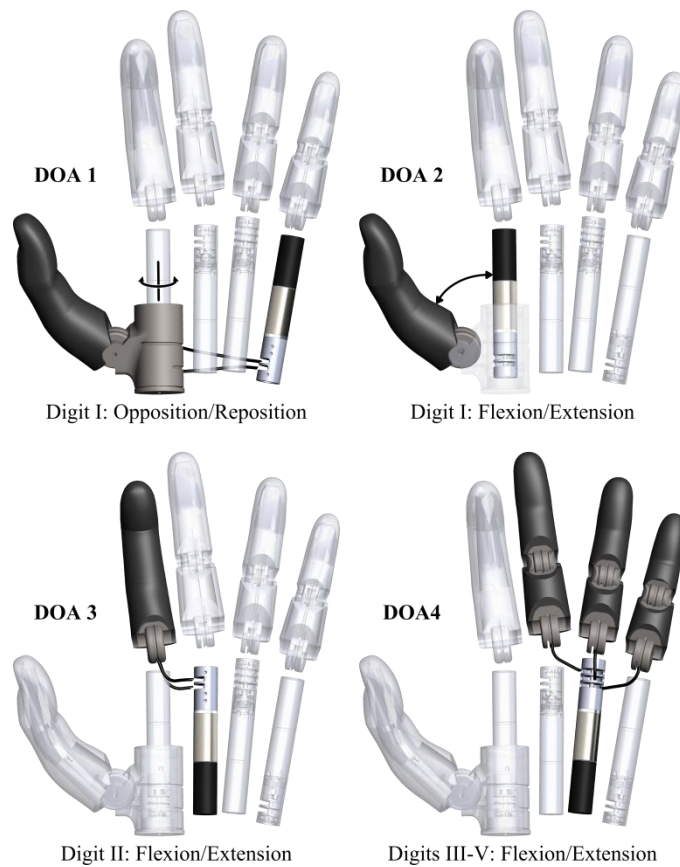


Fig. II-1. Allocation of actuation in hand prosthesis.

(thumb) palmar ab/adduction in a fully-actuated manner at the CMC joint via bidirectional tendon actuation (DOA 1), while another motor unit provides digit I (thumb) flexion/extension in a fully-actuated manner at the carpometacarpal (CMC) joint via bidirectional tendon actuation (DOA 2), while the metacarpal phalangeal (MCP) and the proximal interphalangeal (PIP) joints are fused. A third motor unit provides digit II (forefinger) flexion/extension in a fully-actuated manner at the MCP joint via bidirectional tendon actuation (DOA 3), while the PIP and distal interphalangeal (DIP) joints of the digit are fused. Finally, a fourth motor unit provides flexion of the MCP and PIP joints of digits III through V with unidirectional tendon actuation via compliantly-coupled differential (DOA 4), while the DIP joints of these digits are fused, and wherein extension of the MCP and PIP joints is provided by compliant elements (i.e., torsional springs) in the respective

joints. With this combination of motor units and DOFs, the configuration of digits I and II are determined uniquely as commanded by the motor units, while the configuration of digits III-V are determined by a combination of the motor unit command and the nature (i.e., shape) of the object being grasped. As such, digits I and II are principally responsible for providing precision grasp and manipulation of objects small relative to the size of the hand, while digits III through V provide conformal grasp capability, and in essence stabilize the whole-hand grasping of objects roughly the same size as the hand. In this manner, the hand is able to explicitly provide both precision grasp and manipulation, in addition to whole-hand conformal grasp capability.

In order to present the configuration of the hand in a more technically explicit manner, one can define a kinematic mobility (M) of each degree-of-actuation (DOA) by assessing the number of DOFs that remain after the actuator configuration is prescribed. In the case of a fully-actuated joint, there is no kinematic mobility of the system once the actuator configuration is determined (i.e., $M=0$). Thus, the configuration of a system with zero mobility is determined entirely by the configuration of the actuator, while the configuration of a system with mobility greater than zero is determined by a combination of the actuator configuration and the external and internal forces acting on and within the DOA. For the case of systems actuated in a unidirectional manner (e.g., actuated by a unidirectional tendon working against a compliance), the mobility will be different when loaded against the direction of actuation (M^+) and when loaded along it (M^-). One can define a kinematic controllability as:

$$C = 1 - \frac{M}{DOF} \quad (\text{II-1})$$

Note that a kinematic controllability of 1 indicates that the actuator has full control in determining the kinematic configuration of the DOA (i.e., the configuration is determined by the actuator, irrespective of external loading), while a kinematic controllability of 0 indicates the actuator has

no ability to control or influence the kinematic configuration of the DOA (i.e., the configuration is determined entirely by external loading). Given these definitions, the mobility of the four DOAs of the hand are given by:

$$M_1 = M_2 = M_3 = 0, \quad M_4^+ = 5 \text{ and } M_4^- = 6 \quad (\text{II-2})$$

where M_1, M_2 and M_3 are the mobility of the digit I and II DOAs, and M_4^+ and M_4^- are the mobility of the digit III through V DOA in each respective direction of actuation (+ in flexion and – in extension). In terms of kinematic controllability, when actuated in flexion (or palmar abduction for DOA 1), the respective DOAs are characterized by:

$$C_1^+ = C_2^+ = C_3^+ = 1 \text{ and } C_4^+ = \frac{1}{6} \quad (\text{II-3})$$

while when actuated in extension, the respective DOAs are characterized by:

$$C_1^+ = C_2^+ = C_3^+ = 1 \text{ and } C_4^+ = 0 \quad (\text{II-4})$$

Thus, the configuration of digits I and II are fully and uniquely determined by the actuator commands when loaded in either flexion or extension. The configuration of digits III through V is determined by the combination of the actuator command and external loading (i.e., the shape of the object being grasped) when loaded against flexion, with the object shape having more relative influence than the actuator command; while the actuator has no control over the configuration of digits III through V when those digits are loaded against extension.

As a point of reference, a previous hand design presented by the authors [4] incorporated the same number of DOAs, but the respective DOAs were characterized by substantially different kinematic controllability. Specifically, the hand was characterized by mobility of each DOA when loaded against flexion of:

$$M_1^+ = 0, \quad M_2^+ = M_3^+ = 2, \quad M_4^+ = 8 \quad (\text{II-5})$$

and when loaded against extension of:

$$M_1^- = 1, \quad M_2^- = M_3^- = 3, \quad M_4^- = 9 \quad (\text{II-6})$$

These respective mobilities result in kinematic controllability when loaded against flexion of:

$$C_1^+ = 1, \quad C_2^+ = C_3^+ = \frac{1}{3}, \quad C_4^+ = \frac{1}{9} \quad (\text{II-7})$$

and kinematic controllability when loaded against extension of:

$$C_1^- = C_2^- = C_3^- = C_4^- = 0 \quad (\text{II-8})$$

As such, only the palmar abduction of digit I was fully controllable (C_1^+), and only when loaded against palmar abduction. The configuration of each remaining DOA when loaded against flexion was determined by the combination of the respective actuator command and external loading on the digits (i.e., object properties). The influence of the object on the DOA configuration was greater for digits III through V than for digits I and II, but was the primary influence on DOA configuration in all cases. In the case the digits were loaded against extension (or palmar adduction), the actuators had no influence on the kinematic configuration of each DOA. As such, although the hand described in [4] also included four actuators, the relative mobility and controllability between the two prosthesis prototypes is markedly different.

1.4.2 Tendon Actuation and Series and Parallel Elasticity

The ability of the hand to provide full kinematic controllability when loaded in either direction, as described in equations (II-3) and (II-4), is provided by incorporating bidirectional (as opposed to unidirectional) tendon actuation in the three respective DOF/DOAs of digits I and II. In addition to offering full kinematic controllability, such actuation provides higher output impedance (i.e., more rigid posture) in the associated digits. Additionally, the bidirectional tendon configuration eliminates the need for parallel springs in the fingers, which are otherwise required to provide

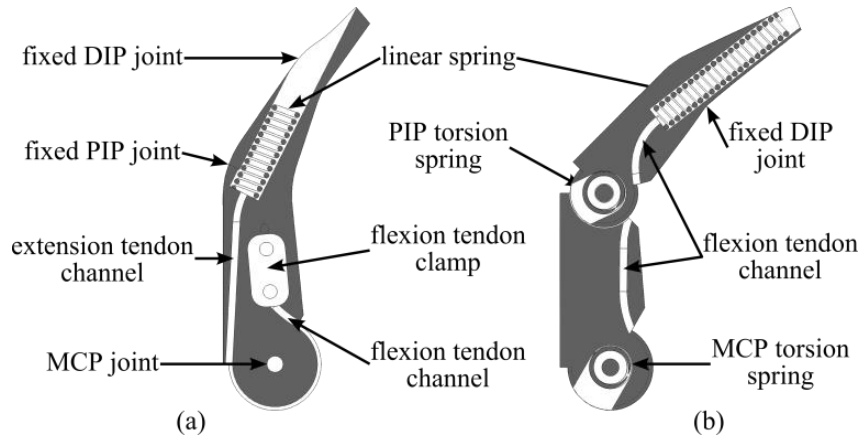


Fig. II-2. Cross-sectional view of (a) digit II and (b) digit III.

extension in the unidirectional tendon configuration. As such, the tendons need not work against the restoring force of the parallel springs, and thus the motor units when used in a bidirectional tendon configuration generate greater maximum fingertip and grasp forces than when used in a unidirectional configuration. Fig. II-2a shows a representative bidirectional tendon configuration. Specifically, the figure shows a cross-section of digit II and its tendon configuration, which is generally representative of the tendon routing in the three bidirectional-tendon fully-actuated axes. Note that the bidirectional tendon path lengths must be matched, such that the overall tendon path is constant (i.e., the tendon on the anterior aspect of the joint is configured to remain in contact with the constant-radius joint). In order to eliminate backlash, a linear spring (10.5 N/mm) is located in the fingertip which imposes series elasticity on the extension side of the tendon and maintains a pretension on the bidirectional tendons. Note that, since this spring is in the extension tendon, it has no significant effect on behavior during grasping.

Although bidirectional actuation provides important advantages for the fully-actuated (precision grasp) DOFs, unidirectional tendon actuation provides important advantages for the (conformal grasp) underactuated DOA. Most evidently, a unidirectional configuration reduces the total amount of spooled tendon by a factor of two, which is particularly important given the fact

that three digits are being actuated, and thus the total space savings (especially in the motor unit pulley) is significant. Perhaps more importantly, however, the unidirectional tendon configuration is well-suited to enabling conformal grasp via a compliantly-coupled mechanical differential. Fig. II-2b shows a representative cross-section of digit III and its tendon configuration, which is generally representative of the tendon routing in the three digits associated with the underactuated DOA. Like the bidirectional tendon configuration, the unidirectional tendon includes a series stiffness in the fingertip; unlike the bidirectional configuration, however, the stiffness is on the flexion side of the digit, and the spring (0.75 N/mm) is configured with a considerably lower stiffness than the preload spring on the bidirectional extension tendon in order to provide a greater degree of displacement. The resultant effect of these springs is to provide a differential coupling between the three conformal digits when loaded against flexion, such that the digits can be differentially displaced in addition to the differential movement between the MCP and PIP joints within each digit. In addition to the tendon series springs, the MCP and PIP joints of the associated digits include torsional springs (40 mNm/rad) within each joint (see Fig. II-2b) which provide return torques to maintain tendon tension and provide for digit extension, and also provide a parallel stiffness that determines the nature of joint movement in the absence of contact with an object. Note that, regarding the latter, although the torsional springs in the MCP and PIP joints are all of the same stiffness, the radius of the tendon path around the MCP is 30% larger than the radius around the PIP, and as such the MCP will undergo 30% greater flexion than the PIP when moving through free space, in order to provide a cascading pattern of joint movement.

1.4.3 Motor Unit Design

Each DOA is actuated by a motor unit consisting of a Faulhaber 1226 brushless DC servomotor, a 64:1 planetary gearhead reduction, a custom two-way clutch unit, and bidirectional or unidirectional tendon pulleys, as per the specific DOA. Each bidirectional tendon pulley consists of a double pulley for the flexion and extension sides of the tendon, respectively, while the unidirectional tendon pulley consists of a triple pulley, one for each of the flexion tendons in digits III through V. The clutch provides high drive efficiency in the forward path, but precludes back-drivability, such that the configuration of the hand can be maintained without electrical power consumption. The motor unit design and configuration is shown in Fig. II-3. With the exception of the bidirectional pulleys, the motor units are similar to motor unit designs presented in previous publications by the authors [4].

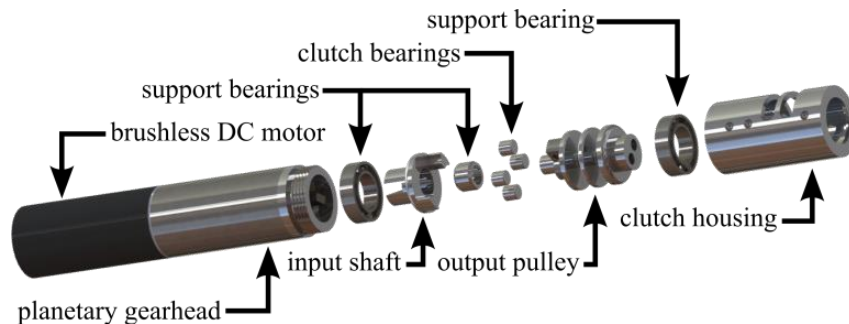


Fig. II-3. Exploded view of motor unit, including clutch and pulley.

1.4.4 Cosmesis and Construction

The primary form of the hand prosthesis consists of two materials: a high-modulus material forms the load-bearing geometric and kinematic structure of the hand, while a low modulus material provides a “soft tissue” covering that provides compliance and shape to facilitate grasping and manipulation of objects. Both materials are produced by additive manufacturing processes. The

high modulus material is a thermoplastic with a flexural modulus of approximately 1750 MPa and a flexural strength of approximately 60 MPa (3D Systems Accura Xtreme), while the low modulus material is an elastomer with a Shore A durometer of 40 (PolyJet Tango Black). The elastomer is slipped on the “skeletal” structure of each digit, and bonded to the anterior and posterior sides of the palm using adhesive.

1.4.5 Embedded System Design

An embedded system was developed for the hand in order to enable fully self-contained control of all DOAs of the hand. The embedded system was designed to be powered by a 14 v battery (located elsewhere in the prosthetic arm); to accept and execute motion and/or force commands from a high-level controller via a controller area network (CAN) serial interface; and to return processed position and force information for each DOA to the high-level controller via the CAN bus. The embedded system consists of a single, four-layer circuit board that is fully contained within the palm of the hand prosthesis. The “hand control board” contains four custom brushless motor PWM

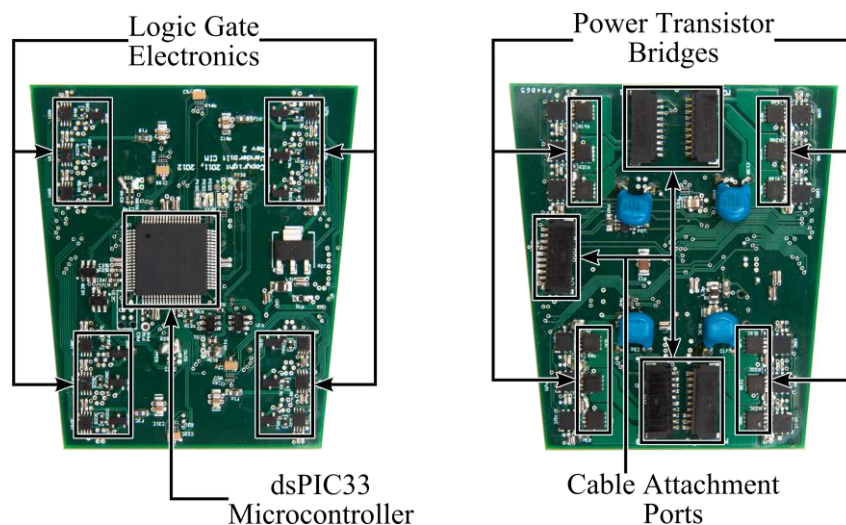


Fig. II-4. Top and bottom views of hand embedded system.

servoamplifiers, each operating at a pulse-width-modulation (PWM) frequency of 20 kHz, and each capable of maximum continuous current of 3.5 A. All four servoamplifiers are controlled by a single microcontroller (Microchip dsPIC33). In addition to the dsPIC, the components on both sides of the board associated with the servoamplifier channels are outlined in Fig. II-4. In addition to providing Hall-based brushless motor commutation and servoamplification, the dsPIC also provides closed-loop PID position control of each DOA, with each closed loop running at a sampling rate of 1 kHz. Finally, the hand board sends real-time sensor information regarding tendon excursion (from Hall sensors) and tendon force (via motor current), at a sample rate of 1 kHz, over the CAN bus to the high-level controller. Note that sensing tendon excursion via the Hall sensors at the motor provides a direct measurement of digit configuration for the fully-actuated digits I and II, but provides only an average configuration for the underactuated digits III-

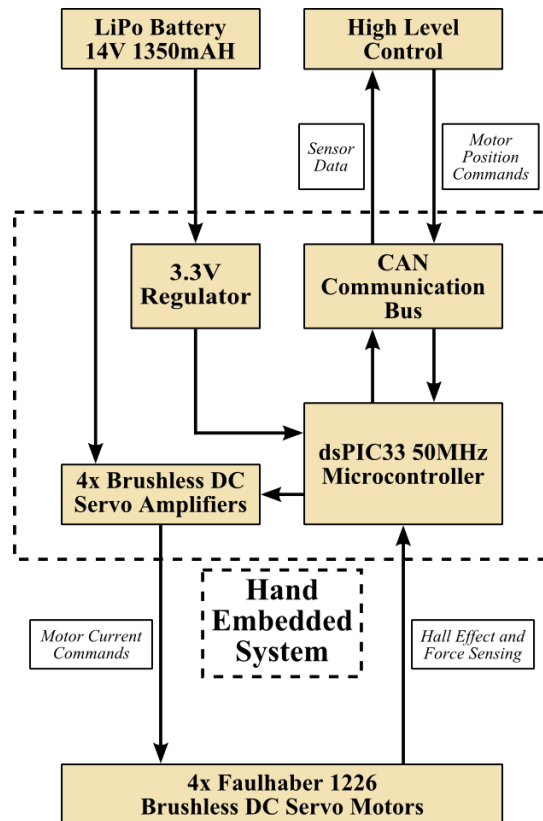


Fig. II-5. Hand board embedded system architecture.

V (i.e., the single measurement provides the average flexion in the six actuated joints, but cannot distinguish between all sets of configurations corresponding to a given tendon displacement). It should be noted that, even if the system were able to independently sense the configuration of all (six) joints in digits III-V, the only the average flexion is controllable by the single actuator. A block diagram of the functionality of the embedded system is shown in Fig. II-5. The location of the embedded system within the palm of the hand is shown in Fig. II-6.



Fig. II-6. Hand with cover removed, showing embedded system and motor units.

1.5 Characterization of Hand Performance

1.5.1 Hand Size and Mass

The mass of the prosthetic hand, including the embedded system encased in the palm, is 546 g. The major dimensions of the hand are 8.9 cm across the widest portion of the palm, and 20 cm from the base of the palm to the tip of digit III. Based on anthropometric norms as given in [55], these dimensions correspond to the breadth and length of a 35th percentile and 85th percentile male hand, respectively. Note that while the breadth is constrained by the layout of the palm, the length

of the hand is not as substantially constrained, and could be shortened without difficulty by decreasing the length of the fingers. Shortening the finger length by 1 cm, which is well within the dimensional constraints of the finger design, would render the overall dimensions equivalent to that of a 35th percentile male (9 cm breadth, 19 cm length). The hand dimensioned as such would further correspond to a hand breadth and length of a 99th and 85th percentile female hand, respectively.

1.5.2 Fingertip Forces

Fingertip forces were measured by applying 2.5 A of current to the motor unit for a duration of one second. Note that each motor unit incorporates a two-way clutch, and as such it is presumed that sustained grasping would be performed passively, first by squeezing the object for a short period (e.g., one second), then turning off the motor current and allowing the combination of the series elasticity and two-way clutches to passively hold the respective grasp force. An Exttech Instruments 475044 force gauge was attached orthogonally to the fingertip to measure the resulting fingertip force. Three trials were taken at four different tendon excursions, spaced evenly at 0, 25, 50, and 75% excursion of the tendon, and the average force for each tendon excursion recorded. For digits III through V, the force gauge was attached to all three fingers at once, and the combined force provided by the three fingers was measured together. Fig. II-7 shows the maximum fingertip force data corresponding to these measurements. Specifically, the two direct-drive DOAs corresponding to flexion of digits I and II are each capable of maximum fingertip forces between 25 and 30 N, depending on tendon excursion. Note that variation in fingertip forces in these DOAs may be due to variation in frictional characteristics of the joints and tendon paths, and may also reflect variation in the actuator pulley diameter due to tendon spooling onto the pulley at increasing

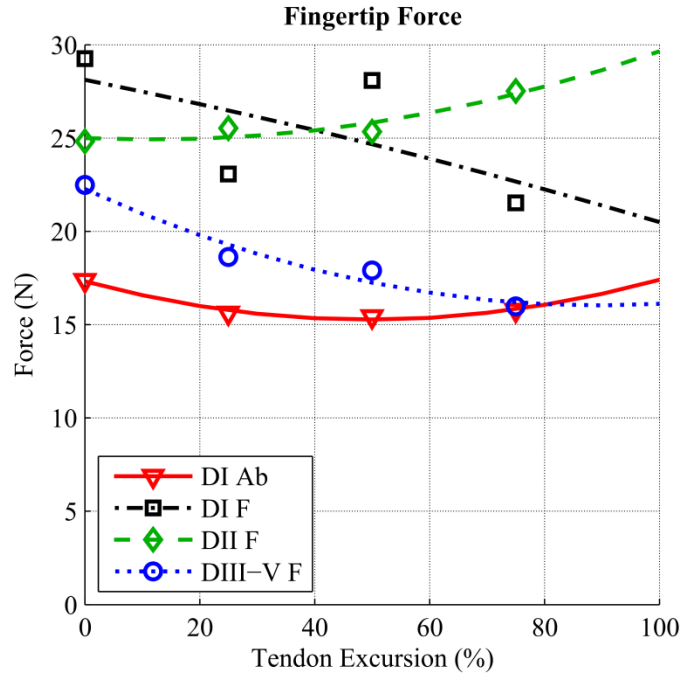


Fig. II-7. Fingertip Forces corresponding to each motor unit.

tendon excursions. For a typical tip grasp, digit I (i.e., the thumb) remains nearly extended (approximately 0% tendon excursion), while digit II (i.e., the index finger) becomes almost fully flexed (~80% tendon excursion), such that the maximum tip grasp force is estimated to be approximately 29 N. The combined efforts of digits III through V provide grasp forces between 16 and 23 N, depending on tendon excursion. Assuming a nominal tendon excursion of 50%, the maximum fingertip grip strength of the hand, obtained by combining the fingertip forces of digits II through V, is approximately 45 N. The grip forces are obviously greater if contact with a given object occurs proximal to the fingertips. Note that the grasp forces provided by the prosthesis are well within the ranges typically required by activities of daily living, as previously discussed.

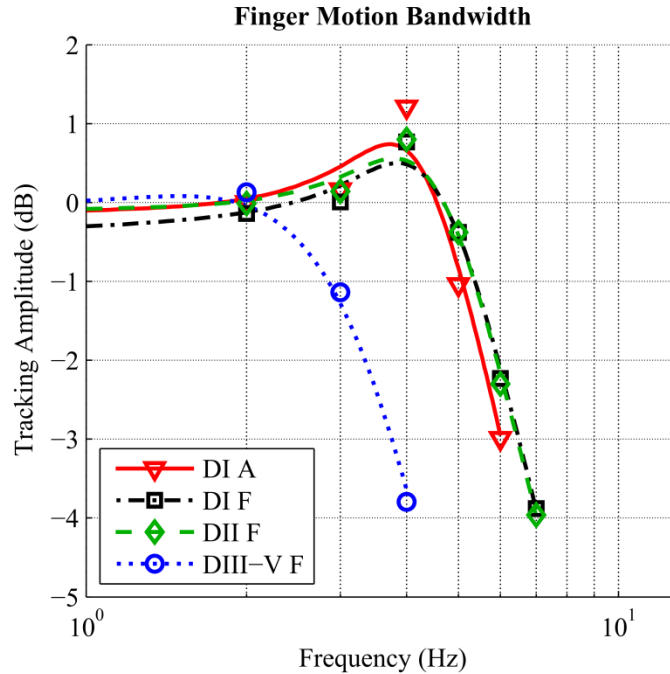


Fig. II-8. Bandwidth corresponding to each motor unit.

1.5.3 Motion Bandwidth

The motion bandwidth of the fingers was measured during unloaded movement, wherein each motor was driven with a sinusoidal position command, at an amplitude of half of the total tendon excursion, with the center point of oscillation corresponding to the center of the range of motion. As discussed previously, the embedded system provides PID servocontrol of each motor unit, and as such the movement bandwidth was assessed by recording the relative magnitudes of the commanded and measured tendon movement. The results for each of the motors units are shown in Fig. II-8. Note that the direct drive DOAs each have a -3 dB bandwidth of approximately 6 Hz, while the underactuated (unidirectional) DOA exhibits a -3 dB bandwidth of approximately 3 Hz. Note that both are well above the 1.5 Hz bandwidth that nominally characterizes activities of daily living, as previously discussed.

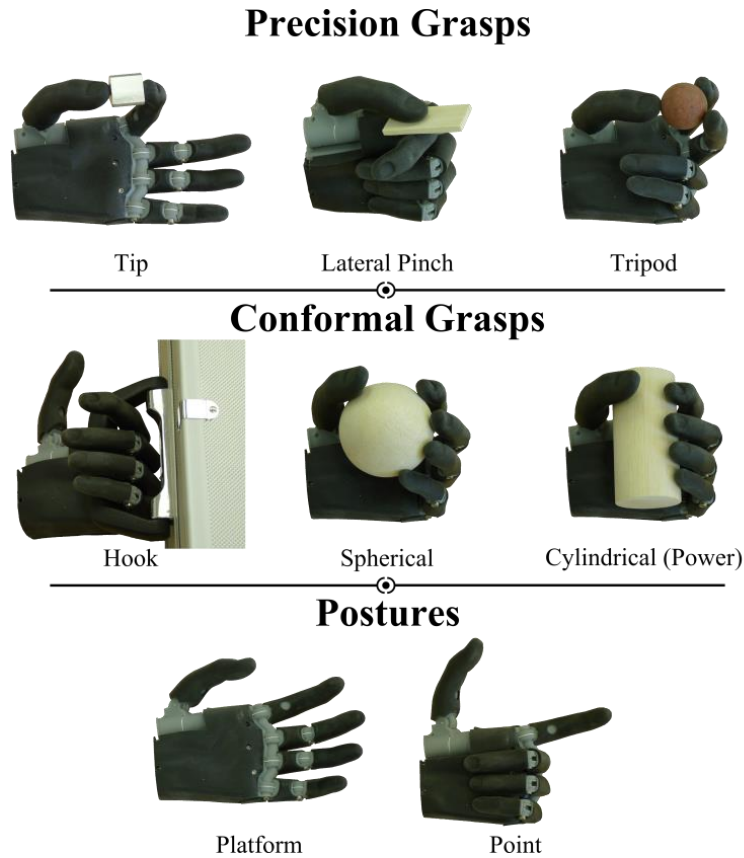


Fig. II-9. Canonical grasps and postures provided by the hand prosthesis.

1.5.4 Hand Postures and Grasps

Fig. II-9 shows the ability of the assembled hand prototype to achieve the aforementioned eight grasps and postures under motor control. A video is included in the supplemental material that dynamically demonstrates these grasps and postures. A method by which the hand can be controlled by the user to provide these postures and grasps via a standard two-site myoelectric interface is described in [6].

1.5.5 Battery Life

The electrical power required by the hand was characterized by assessing the electrical power consumed by the two basic activities performed by the hand, which are movement and grasping. With regard to movement, electrical power is required to move from one hand posture or grasp configuration to another. With regard to grasping, electrical power is required to form and to release a grasp, although the presence of the two-way clutches renders the power consumption independent of grasp duration. Specifically, power is required to achieve a given grasp force, but once achieved, the clutches “lock in” the grasp, such that electrical power is no longer required. As such, the electrical power requirements of the hand were characterized by two assessments. First, in order to characterize the power required to perform movements, the amount of electrical power required to move between a canonical set of postures was measured. Specifically, the electrical power was measured starting in the cylindrical (or power) grasp and moving to the tip, platform, point, hook, and lateral pinch grasps, then reversing the sequence back to the cylindrical grasp. Note that the remaining grasps are subsets of these grasps, but depend on the presence of objects. While this sequence was performed, the current drawn from a 14 v battery by the embedded system in the hand was measured using a current probe (Agilent model 1146A), and the power integrated over the duration of the movement in order to obtain the electrical energy required from the battery to perform this sequence of movements. The measurement was repeated ten times using the previously described sequence, with an average current requirement of 2.18 A-s, which at the battery voltage of 14 v results in an average energy requirement of 30.5 J (to move through the sequence and back).

The electrical power requirements to grasp and release an object were characterized by grasping a 500 mL water bottle filled to a mass of 500 g (approximately full), grasping with a force

sufficient to securely lift the bottle, then releasing the bottle. Like the posture sequence, this activity was performed ten times, with an average current requirement of 2.25 A-s, and therefore an average energy requirement of 31.5 J, which incidentally was nearly identical to the energy required to perform the posture sequence.

The battery being used in these tests was a 14 v, 1.35 A-h lithium polymer battery, which has a mass of 133 g. As such the battery provides a gravimetric energy density of 511 J/g. Given this battery (or one of similar gravimetric energy density), the hand could grasp and release a water bottle approximately 16 times per gram of battery weight, or could move through the full suite of hand postures approximately 17 times per gram of battery weight. For the 133 g battery used in the hand prosthesis prototype, the hand could perform approximately 2100 power grasps, approximately 2300 movement sequences, or perform some combination of these activities, on a single battery charge.

1.6 Conclusion

The authors describe here a hand prosthesis that incorporates a unique configuration of four actuators to explicitly provide both precision and conformal grasp capability. The authors describe the actuation configuration of the hand in terms of kinematic controllability. A performance characterization indicates the hand prosthesis provides levels of force and speed appropriate for performing the activities of daily living. The physical properties of the hand are additionally representative of the size and mass of a typical male hand. Electrical power measurements indicate that the prosthesis is able to provide over 1600 grasps or movement sequences on one charge of a 100 g battery. The authors believe the composite grasp capability and biomechanically

representative performance characteristics of such technology have considerable potential to enhance the functionality and thus improve quality of life of upper extremity amputees.

2. Addendums to Manuscript 1

2.1 VMG Design Iterations

Though the number of actuators and DOFs were fixed at an early point in the design of the third generation VMG, the final configuration of the actuators and the transmission between input and output required significant design iteration to finalize. The number of DOFs was based primarily on the desired function of the hand (separation of conformal and precision grasps), and the number of actuators was primarily dictated by the anthropomorphic envelope and size of motor units, but connecting the two remained a challenge. The first design challenge revolved around the configuration and actuation of the two DOFs in the thumb. Earlier designs of the VMG used tendon actuation exclusively for each DOF, including the thumb flexion and opposition, whereas the first prototypes of the third generation hand opted to directly drive the thumb opposition with a larger motor. In the previous designs, the thumb joint (carpometacarpal, or CMC joint) was attached to the palm via a very narrow piece of plastic, since anthropomorphism required it be placed at a specific angle and location to the side and above the palm, and the motor units occupied the majority of the palm volume. This specific configuration led to this piece causing the majority of hand breakages. In order to add enough material to increase robustness while remaining inside the anthropomorphic window, the CMC joint needed to be placed one of the four actuation motors in the palm. With the motor concentric to the CMC joint in this case, the simplest configuration was to directly drive the joint with the motor. Since this joint is used only for positioning, not active



Fig. II-10. First iteration of third generation VMG actuation scheme.

loading, size of the palm was reduced by replacing the larger motor with the same motor as the other three actuators, resulting in the actuator configuration shown in Fig. II-10.

Several problems arose from this design, eventually causing the idea to be abandoned. Without the space for a large motor, the backlash introduced by the two-way clutch made it impossible to keep the thumb rigid, and the motor itself was not strong enough to move the thumb if it was under any load at all. The most troublesome issue, however, was the coupling of the DOFs that was caused by the large radius of the CMC joint. As the motor drove the thumb in an opposition/reposition (OR) movement, the paths of the tendons that were used to actuate the thumb in flexion and extension (FE) were shortened and lengthened, resulting in a flexion or extension of the thumb. This movement could theoretically have been compensated for in software by

simultaneously actuating the FE DOF, but instead the design was changed to incorporate bidirectional tendon actuation to drive both the OR and FE DOF, with the FE motor positioned concentric to the CMC joint so as to minimize joint coupling. This resulted in the actuation scheme shown in Fig. II-1.

Another problem encountered arose from the design choice to use bidirectional tendon actuation. Tendon actuation is desirable for prosthetic hands, since it is a far more adaptable and compact method of connecting the output to the motors than any rigid transmissions or linkages that would otherwise be required to achieve the same transmission ratio. Using tendons significantly relaxes any constraints on the precise alignment and location of the motor units, meaning the motors could conceivably be placed in any configuration, so long as tight corners and friction are taken into account. Unidirectional tendons such as those utilized in generations one and two are relatively simple to implement, requiring only a pulley at the motor and a termination point in the digit where the free end of the tendon is attached. To increase the bandwidth and controllability of the precision digits in the third generation hand, bidirectional tendons were introduced into the design, which created several more challenges. The primary challenge was how to maintain tension in the tendon during installation and operation when both ends are attached to the same pulley. The first method was to use two linear springs in the fingertip of each digit to terminate each end of the tendon. First the flexion tendon would be tied to the spring, then the motor would wind up the tendon until the spring was sufficiently compressed. Then the extension tendon would be tied to the other spring, and the motor would relax the tendon until both were slightly compressing the spring. This worked well for installation, but as the tendons stretched during operation, slack would be introduced, and there was no way to remove it without disassembling the hand and repeating the entire installation procedure. It was clear that some sort

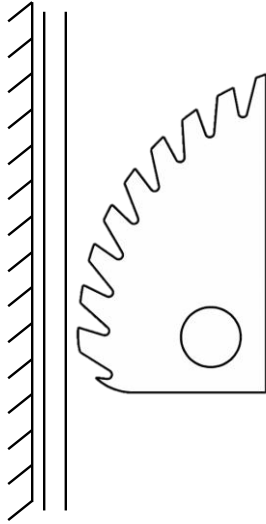


Fig. II-11. Self-locking cam mechanism for bidirectional tendon tightening.

of on-the-fly tensioning mechanism was required to quickly remove tension from the bidirectional digits. There were many complicated solutions to dynamically tension the tendons that were abandoned before implementation, and the first mechanism that was implemented was a self-locking cam like the one pictured in Fig. II-11. In this design, the teeth of the cam would grip the tendon as it was pulled downward, and the eccentricity would cause the tendon to be clamped between the cam and the surface of the digit. While the motor was pulling on the tendon (downward force), the cam would maintain tension, but if there was slack in the tendon when the motor was off, the tendon could be pulled upwards manually to release the cam and remove the slack.

This mechanism worked well in proof of concept prototypes and while under light load, but had less than ideal performance when implemented in the hand prototype. The motors in the hand are capable of providing a large amount of force to the tendon, which when combined with the very low friction coefficient of the tendon itself, caused the cam to slip when under high loads. Additionally, without a spring return mechanism, when the tendon was pulled upward to remove slack, there was no way to immediately return the cam to the lock position. These issues were

solved by simplifying the tensioning mechanism rather than further increasing the complexity of this prototype. The final solution involved clamping the tendon tightly between two small, thin steel plates with two screws. When the tendon is wound between the screws and the plates are clamped, there is sufficient friction to prevent any slipping, and tension can be adjusted by hand and locked with the screws. Once this solution was implemented, the tendons did not slip during all subsequent testing of the hand. The final configuration of this tensioning mechanism is shown in the cross sectional view of the digits in Fig. II-2.

Once the tendon transmission was finalized, the specific configuration of each digit needed to be investigated. While the number of DOFs was dictated by the desired grasping behavior, a lack of active or passive abduction of the fingers meant that the exact position and orientation of each digit's metacarpal phalangeal joint (MCP) was very important in dictating how the hand would grasp larger objects. Many configurations were iterated upon, and the final design was chosen to have digits 3 and 4 (middle and ring fingers) parallel to the longitudinal axis of the palm, and digits 2 and 5 (index and pinky fingers) slightly abducted so as to more easily envelop larger objects. To this end, digit 5 was also rotated slightly out of the plane of the palm about the longitudinal axis of the finger, giving the palm and grasps a more natural rounded shape. The natural anatomy of the CMC joint of digit 1 proved too complicated to be completely replicated in the hand prosthesis, so instead the angle and position of the joint along each axis was chosen to enable the chosen grasps. Specifically, in the reposed or adducted state, the thumb should be able to perform a key grasp, and when abducted, or opposed to the palm, the tip of the thumb should be able to align with either digit 2 or 3. The orientation of the digits in the final design can be seen facilitating the different grasps in Fig. II-9.

Previous generations of the VMG included series elastic elements in the fingertips at the termination point of each tendon. In those designs, these elements enabled velocity control of the tendon position to translate smoothly into force control when the digits contacted an object. Additionally, in digits 3-5 where a single motor drove multiple digits, the elasticity in the fingertips enabled relative motion between them, making conformal grasps possible. In these previous versions, the elastic elements were very stiff, and permitted little relative travel of the tendons. For the third generation, these elastic polymers were replaced by metal springs, which had a great deal more travel and significantly less stiffness. This allowed the new design to conform to a much wider variety of shapes. For digits 1 and 2, the role of the springs was shifted entirely. Rather than rely on the elastic elements to provide the velocity control to force control translation, the new design moved the springs to the extension side of the actuation, and so relied more on the elasticity of the tendon, cosmesis, and object to perform that force translation. The advantage of compliance on the extension side is that the hand can be less resistant to incidental forces acting on the outside of the hand when it is open, thereby reducing the risk of damage while maintaining stiffness in grasping actions, making it less likely to drop held objects.

2.2 Functional Assessment of the Vanderbilt Multigrasp Hand

To test functionality, the VMG hand and MMC were subjected to a series of progressively more taxing assessments designed to simulate the performance of ADLs. Much of the following information was the subject of Dr. Skyler Dalley's dissertation, but is included here since the outcome measures and performance of the hand are relevant to the design. Additionally, designing and carrying out the assessments alongside Dr. Dalley and using the information gained to inform



Fig. II-12. Southampton Hand Assessment Procedure (SHAP).

the design revisions of the hand in order to make it more robust and effective at practical tasks was a large part of the work on the VMG hand.

To assess the functional performance of the hand, the Southampton Hand Assessment Procedure (SHAP) was used. The SHAP is a standardized clinical assessment tool that involves a series of timed tasks designed to assess the ability of the subject to form certain types of grasps, and also to perform a selection of simulated ADLs [58]. In the first half of the assessment the subject must manipulate abstract objects of various shapes, sizes, and weights, and in the second half the subject must execute a series of ADLs (e.g. pouring water, cutting food, using a zipper, turning a key). A picture of the assessment and included objects is shown in Fig. II-12. After completing the assessment, the subject is given a standardized “Index of Function” (IOF) between 0 and 100, with 95-100 being indicative of healthy function. Each grasp is also given an individual score as an indication of where deficiencies might lie.



Fig. II-13. Able bodied adapter used in SHAP assessments.

The assessments were first performed by able-bodied subjects using the VMG attached to an adapter designed to immobilize their intact hand [9]. A picture of this adapter attached to one subject is shown in Fig. II-13. These assessments were primarily used as a troubleshooting tool, and to test the viability of the VMG and MMC as a prosthesis before involving amputee subjects in the testing. The able-bodied tests were conducted with a single subject who was familiar with the MMC. Since it was the first time this subject used the VMG to perform the SHAP test, they were allowed to rehearse the tasks several times until a consistent strategy was developed. Once significant improvement ceased, the fastest times were used in the final calculation of the index of function. These results were compared to the Otto Bock DMC Hand (a single grasp device) and Touch Bionics' i-Limb (a multigrasp device), using results published in [59]. The IOFs for each device were 74, 52, and 87 for the DMC Hand, the i-Limb, and the VMG Hand, respectively. It is difficult to compare directly to the published results since specific experimental protocols may have differed, but the score of 87 for the VMG is very close to healthy function, and gave us great confidence in moving forward with amputee testing.



Fig. II-14. Amputee subject performing a SHAP pouring task.

Subsequent testing was done with a bilateral transradial amputee subject, pictured performing the SHAP in Fig. II-14 [10], [11]. The tests were conducted with a single subject over many trials, in order to present a best case performance scenario, rather than give an indication of average or typical performance over many users. Thus, like the able-bodied case, the subject was allowed to practice the tasks until an effective strategy was developed and significant improvement ceased. Additionally, the subject returned every 1-2 weeks to repeat the assessment until their IOF scores reached a plateau (i.e. a subsequent score improvement of less than 2, which is below the increment considered significant in the SHAP). To provide a comparison to the VMG Hand, four other commercial devices that were owned and used regularly by the subject were tested with the SHAP in a similar fashion:

- Hosmer-Dorrance Corp. 5XA Split-Hook (5XA): single DoF (split hook), body powered, controlled with shoulder abduction
- Motion Control Inc. Electric Terminal Device (ETD): single DoF (split hook), electrically powered, controlled with forearm surface EMG
- Otto Bock MyoHand Variplus Speed (MVS): single DoF (hand), electrically powered, controlled with forearm surface EMG
- Touch Bionics i-Limb Revolution (ILM): six DoF (multigrasp hand), electrically powered, controlled with forearm surface EMG

By the fourth trial, each device had plateaued to its own maximum score. Fig. II-15 shows how the scores for each device evolved over time. Though the VMG Hand performed favorably with respect to the i-Limb and achieved a respectable score in absolute terms (IoF of 87), both multigrasp hands lagged well behind the split hook terminal devices. While these results would seem to indicate that multigrasp hands are inferior to single DoF devices, this conclusion is not supported by the subject's own preferences. In daily use, the subject almost always wears a single-grasp myoelectric ETD on his left arm, and a multigrasp myoelectric i-Limb Revolution on his

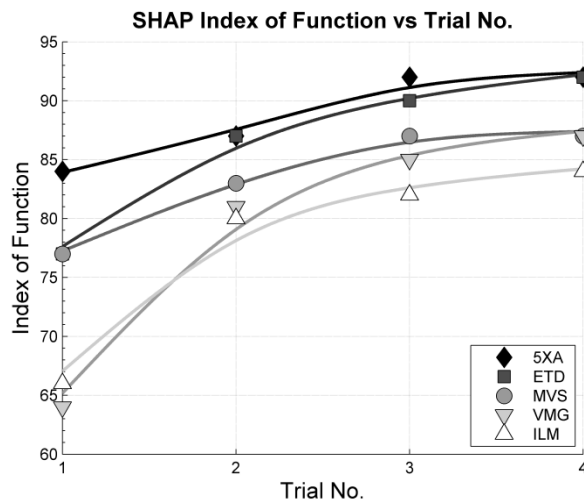


Fig. II-15. Progression of SHAP scores over time.

right (the subject was a bilateral trans-radial amputee). The subject preferred to use the single grasp split hook when high grasp forces were required or when manipulating small objects, while the multigrasp prosthesis was preferred in situations where stability or delicacy is required. From the subject's experiences it is clear that the multigrasp hand is better suited to certain tasks than the split-hook, but the SHAP assessment gives no indication of this. In fact, there were several important functional considerations that were specifically mentioned by the subject that were not covered in the SHAP. These considerations are: the relative stability of grasps, the ability to handle delicate objects, the ability to utilize modern technology such as touch screens, the ability of the prosthesis to use the body as a workspace, the ability to perform compound tasks, and the effect of the prosthesis on compensatory movements required by other muscles in the body. In future hand assessments it might be useful to augment this assessment with additional tasks to address these concerns.

2.3 Winding Temperature Estimation and Regulation for Brushless DC Motors

Throughout early experiments with the VMG prototype, motor burnout was a frequent issue. The motors used in the hand had extremely low winding resistance, and could sink a very large amount of current, meaning that if a bug or glitch resulted in a large reference signal, the motor could be irreparably damaged within seconds. This leaves little room for error, and resulted in many dead motors. This problem was addressed several times by position reference limits at the high-level controller, but since the high-level controller generates position commands, these limits were unintuitive, and prone to being ignored or disabled accidentally when the code was passed on to new researchers. To counteract this, a method was developed to use extra processing power at the servo-amplifier level of code to limit the references sent to the motor in the event of excessive

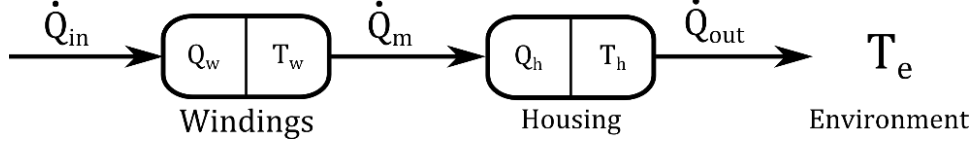


Fig. II-16. Heat transfer diagram for motor thermal model.

heat, thus reducing the risk of burnout. If the winding temperature exceeded the published continuous safe amount, the duty cycle commanded to the motor would attenuate until it reached zero current at the absolute maximum temperature. However, since space and sensor inputs to the boards were limited, there were no temperature sensors, so the winding temperature was estimated via a second order thermal model with the motor current as an input.

Fig. II-16 shows a simplified schematic showing the main elements in the model: the windings, the housing, and the environment. From the first law of thermodynamics, the change in heat of the windings and housing is:

$$\dot{Q}_w = \dot{Q}_{in} - \dot{Q}_m \quad (\text{II-9a})$$

$$\dot{Q}_h = \dot{Q}_m - \dot{Q}_{out} \quad (\text{II-9b})$$

\dot{Q}_w and \dot{Q}_h , or the heat accumulation in the windings and housing, respectively, cause a corresponding change in temperature as follows:

$$\dot{Q}_w = C_w \frac{dT_w}{dt} \quad (\text{II-10a})$$

$$\dot{Q}_h = C_h \frac{dT_h}{dt} \quad (\text{II-10b})$$

Where C_w and C_h are the heat capacities of the windings and housing, respectively. The heat transfer between the bodies in the model, or \dot{Q}_m and \dot{Q}_{out} , is calculated as follows:

$$\dot{Q}_m = h_1(T_w - T_h) \quad (\text{II-11a})$$

$$\dot{Q}_{out} = h_2(T_h - T_e) \quad (\text{II-11b})$$

Where h_1 and h_2 are the thermal conductivities between the windings and the housing, and between the housing and the environment, respectively. The incoming heat to the system, \dot{Q}_{in} , is primarily due to the resistive heating effects of the current passing through the windings, which are equal to:

$$\dot{Q}_{in} = i^2 * R \quad (\text{II-12})$$

Where R is the phase-to-phase winding resistance of the motor, as given on the data sheet. When equations II-9, II-10, II-11, and II-12 are combined, the result is a system of differential equations that can be expressed in state space as follows:

$$\begin{bmatrix} \dot{T}_w \\ \dot{T}_h \end{bmatrix} = \begin{bmatrix} -\frac{h_1}{C_w} & \frac{h_1}{C_w} \\ \frac{h_1}{C_h} & -\frac{h_1 + h_2}{C_h} \end{bmatrix} * \begin{bmatrix} T_w \\ T_h \end{bmatrix} + \begin{bmatrix} \frac{R}{C_w} & 0 \\ 0 & \frac{h_2}{C_h} \end{bmatrix} * \begin{bmatrix} i^2 \\ T_e \end{bmatrix} \quad (\text{II-13})$$

From this representation, these continuous differential equations must be transformed into discrete difference equations to be implemented on the microcontroller. This is done by using a Laplace transform followed by the Tustin approximation to take the equations from the s domain to the z domain. Once in difference equation form, the equation was formulated in fixed point operations, resulting in very little processing time required for the calculation of the temperature in each time step. The temperature estimate is used to attenuate the duty cycle of the motor according to two parameters: T_{safe} and T_{max} , which are the maximum continuous temperature and absolute maximum temperature of the motor, respectively. The temperature limiter occurs after the duty cycle has been calculated by the PID, but before it is sent to the motor PWMs, and alters the calculated duty cycle as follows:

$$DC_{out} = \begin{cases} DC_{in}, & \text{if } T_w \leq T_{safe} \\ DC_{in} * \frac{T_{max} - T_w}{T_{max} - T_{safe}}, & \text{if } T_{safe} < T_w < T_{max} \\ 0, & \text{if } T_w > T_{max} \end{cases} \quad (\text{II-14})$$

Where DC_{out} is the duty cycle commanded to the motor, and DC_{in} is the duty cycle calculated by the PID. Thus, for temperatures below the safe continuous temperature, the duty cycle is unaffected, and for temperatures above the maximum temperature, the duty cycle is set to zero. For temperatures in between the two, the duty cycle is linearly attenuated between the two extremes. The model can be adjusted by varying any of the physical parameters of the motor, as well as the estimated temperature of the environment to make the temperature estimate of the windings more or less conservative. Additionally, the maximum and safe temperatures can be changed to provide more of a buffer zone.

Fig. II-17 shows plots obtained from a test of the algorithm. The winding resistance and thermal conductivity terms were significantly altered to demonstrate the functionality of the

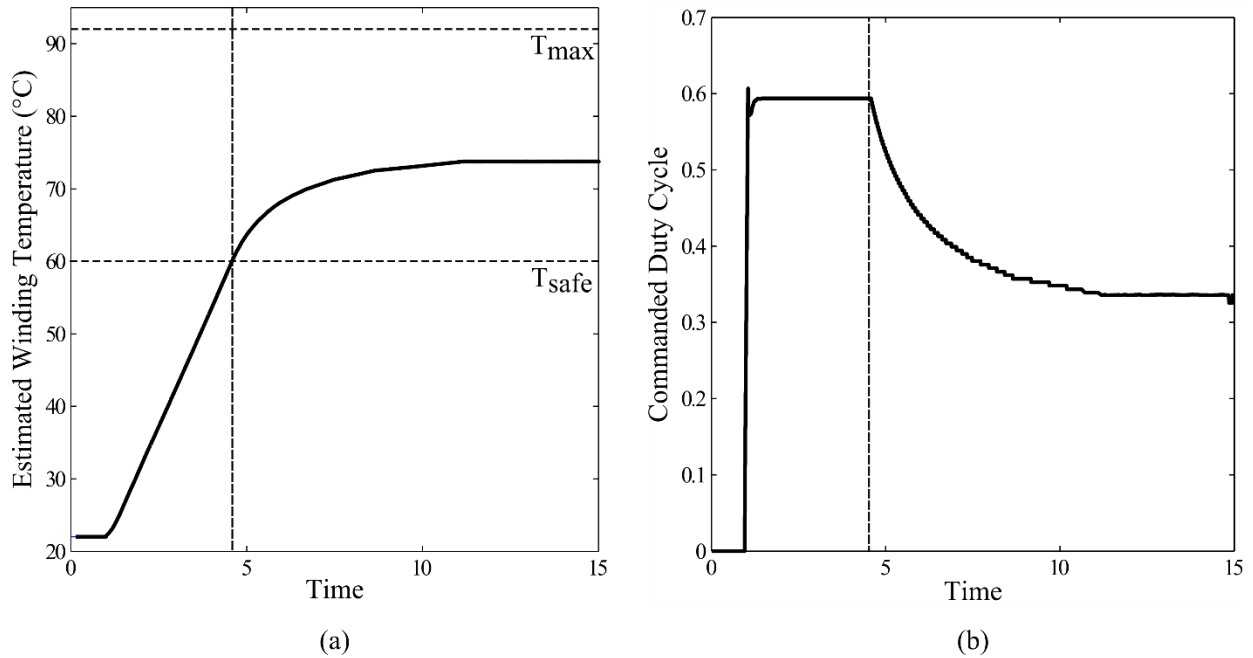


Fig. II-17. Plots illustrating the test of the duty cycle attenuation algorithm. (a) shows the estimate of the winding temperature. (b) shows the commanded duty cycle after attenuation.

algorithm without requiring the motor to operate near its actual maximum temperature. For this test, the maximum allowable temperature was set as 92 °C, and the maximum safe temperature was set to 60 °C. The motor is then given a constantly offset position command, such that the commanded duty cycle to the motor should remain constant. Fig. II-17a shows how the temperature estimation increases steadily until it reaches the maximum safe temperature, at which point the algorithm starts attenuating the duty cycle. In the case of this test, the duty cycle eventually settles into an equilibrium, at which point the current in the windings is creating heat just as fast as the motor is discharging it to the environment. Note that while the two measurements are not directly proportional, the current in the windings is strongly related to the commanded duty cycle, especially when the motor is at stall, as it is here. These tests of extremely conservative circumstances serve to demonstrate that the algorithm is sound, and can be expected to perform similarly in more realistic situations.

CHAPTER III

DESIGN OF A TRANSHUMERAL PROSTHESIS

After the successful design and implementation of a transradial hand prosthesis, the natural progression of this project was to move up the arm and include more joints in the design. The primary goal of the work described in this chapter was to create a transhumeral prosthesis that would serve as a testbed for various control methodologies. It is difficult to iterate on controller design when so many commercial prostheses have closed architecture which does not allow easy or convenient access to control signals or circuitry. To get around this problem, a wrist rotator and elbow prosthesis that are comparable to existing prostheses were designed in order to have a realistic platform on which to test controllers. This chapter begins with a copy of a manuscript that is currently in review for the *IEEE Transactions on Mechatronics* which details the design and assessment of a transhumeral prosthesis. While the paper covers the design of both the wrist and the hand, the specific contribution relevant to this dissertation is the design of the wrist, and the characterization of both the wrist and elbow. The mechanical design of the elbow was done exclusively by Dr. Jason Mitchell, and the embedded system design was done by Don Truex, both of whom are research engineers in the CIM, . Following the manuscript is an addendum discussing the design iterations that went into the wrist prototype, exploring the lessons learned from each prototype and how they led to the final design.

1. Manuscript 2: Design of a Myoelectric Transhumeral Prosthesis

1.1 Abstract

This paper describes a transhumeral prosthesis prototype, intended for the purpose of experimentally investigating design features and control strategies for the control of transhumeral prostheses. The paper specifically focuses on the design and performance characterization of a powered wrist rotator and powered elbow joint, in addition to the embedded system that controls them. In addition to outlining design objectives associated with the wrist and elbow joints, the paper describes the design of both joints, and the embedded system that provides control of them and the arm system. Experimental data is presented that characterizes the performance characteristics of both joints, including data associated with electrical power consumption and audible noise. The arm prosthesis described here is intended to be used with a multigrasp hand prosthesis, previously published by the authors.

1.2 Introduction

There are between 40,000 and 100,000 individuals in the US with major upper extremity limb loss, roughly 40% of whom are transhumeral (above elbow) amputees [13], [14]. Transhumeral prostheses can aid individuals with transhumeral amputation to more capably perform activities of daily living (ADLs). Two major types of functional upper extremity prostheses exist – the body-powered type and the myoelectric type. In the case of a transhumeral prosthesis, both types typically include an elbow joint and a terminal device (often either a split-hook or a hand). The body-powered prosthesis type incorporates Bowden cables, typically a pair, both attached to a shoulder harness worn by the user, such that appropriate movement of the shoulder (e.g., shoulder

flexion and scapular abduction) will generate excursion of the respective cable. Although different variations exist, a common embodiment is the dual-control system, in which one cable (e.g., coupled to shoulder flexion) is used to provide movement of both the elbow and terminal device (i.e., cable excursion will simultaneously actuate both elbow flexion and terminal device opening), while the other cable (e.g., coupled to scapular abduction) is used to lock or unlock the elbow [60]. Because opening the terminal device (against elastic bands) typically requires higher cable forces than flexing the elbow, the actuation cable will typically move only the elbow when the elbow is unlocked, and will move only the terminal device when the elbow is locked. Body-powered prostheses are environmentally robust, relatively low cost, and offer some degree of proprioception and force feedback to the user [61].

Unlike the body-powered type, the myoelectric type of prosthesis utilizes electric motors for actuation of the terminal device and elbow (i.e., rather than a harness and cable). Volitional control of the prosthesis movement is typically provided by a pair of surface electrodes embedded in the prosthesis socket and disposed respectively on the anterior and posterior aspects of the upper arm (i.e., over the biceps and triceps muscle groups, respectively), which measure the surface electromyogram (EMG) of these respective muscle groups. Since the two EMG sites together provide a single bipolar (agonist/antagonist) control signal, the single signal is typically multiplexed between the terminal device and elbow joint by employing a brief co-contraction of the two muscles to switch the control between the two components. Since both the terminal device and elbow are designed to be normally-locked, the component that is not being controlled remains in a locked state. Unlike body-powered prostheses, myoelectric prostheses do not require donning or use of a shoulder harness, and also typically allow operation throughout a larger shoulder range of motion, which enables access to a larger workspace.

Both body-powered and myoelectric transhumeral prostheses, as they are typically employed, are effectively sequential control devices, wherein the single control input (either primary control cable or EMG input) is switched between the terminal device and elbow. Such switching is awkward and inefficient relative to the simultaneous control characteristic of the healthy limb. Note that both types of prostheses also typically include a passive wrist rotation degree-of-freedom (wrist supination and pronation in anatomical terms), which requires external effort (e.g., the contralateral hand) to provide rotation. Actuated wrist rotation is considerably rarer in such prostheses, due largely to the limitations associated with control inputs (i.e., switching between three components rather than two further decreases the efficiency of control).

Patient surveys indicate that greater functionality [62], increased articulation, and simultaneous control of multiple joints [17] are among the top prosthesis functional improvements sought by upper extremity amputees. Since myoelectric prostheses can employ microprocessor control and a variety of sensing modalities, they provide the opportunity to embody considerably more device intelligence, relative to body-powered devices, and therefore offer the potential to provide enhanced functionality, particularly when considering devices with increased degrees-of-freedom (DOFs) or the potential for multi-joint coordinated control.

In order to develop such enhanced functionality, researchers need to develop the associated arm prosthesis hardware. Specifically, an arm prosthesis is a highly interactive device, in terms of its control and physical interaction with the person using it, and in terms of its physical interaction with its environment. Further, such interactions are extremely difficult to model accurately, particularly the interaction and control strategies employed by the human user when conducting ADLs or other manipulation tasks. These include the means by which users resolve kinematic redundancy during manipulation; how increased device DOFs will affect compensatory

movements by intact DOFs; the extent to which cognitive load or control difficulty will affect use of a device feature or DOF; and the ability of a user to control a device feature or component in the absence of an intact neuromuscular control system. As such, although intermediate assessments offer value with respect to initial or partial validation of design features or control strategies, researchers are unable to fully assess the functional value of newly-developed approaches (e.g., on a user's ability to perform ADLs) without experimental implementation in prosthesis hardware on amputee users. Further, such methods are most meaningful when performance is compared to (or contrasted with) the user's performance when using currently-available prostheses. As such, in order to provide meaningful comparative assessments, the functional and performance characteristics (i.e., torque, speed, mass, size) of such hardware should be commensurate with modern commercially-available devices. Ideally, researchers would be able to employ open-architecture versions of commercially-available prosthesis hardware to develop and assess new features and/or control strategies, or investigate functional trade-offs between device complexity and functional efficacy. Despite this, commercial hardware does not generally enable open-architecture access to the sensors, actuators, or embedded system of a device, and therefore precludes investigation or assessment of new control strategies. Further, use of commercial hardware would limit the design features and/or sensory modalities a researcher could implement or investigate, and thus would limit the region of exploration or investigation. Thus, development, investigation, and assessment of design and control features or methods that might enhance the functionality of upper extremity prostheses requires that researchers develop and realize arm prosthesis hardware with functional and performance characteristics commensurate with commercially-available devices. Based on this need, the authors describe herein a transhumeral arm prosthesis design intended for this purpose – that is, intended to provide for the experimental

implementation and assessment of control strategies to improve the functionality of transhumeral prostheses. Such a prosthesis should be characterized by size, mass, torque, and speed characteristics that are commensurate with modern commercial hardware.

Given such motivation, and further facilitated by enabling advances in robotics technology, several designs for various arm components have recently been described. Myoelectric transhumeral prostheses can include various components and be described by varying numbers of active and passive DOFs, since implicit in the need to develop such hardware is the characterization of trade-offs in number and type of DOFs. Despite the variation, the major components include a controllable hand component (i.e., terminal device as per conventional prosthetic semantics), a wrist component, and an elbow component. A substantial proportion of recent related work describes various myoelectric hands, as described by [1], [4], [6], [12], [19]–[26], [43]–[46], [63], [64]. Considerably fewer powered prosthetic wrist designs have been described, as recently surveyed in [65]. Within these powered wrist designs, fewer still have been fully realized and experimentally characterized. Among the electrically-powered devices that have been experimentally characterized are the wrist designs described by [66], [67]. The wrist described in [66] is a single DOF powered device, where the single DOF is intended to be nominally aligned with pronation/supination, but was designed in part to investigate the effect of alternate alignments. The wrist design incorporates a brushless DC motor and a three-stage transmission consisting of a belt drive, planetary gear set, and internal gear set. The wrist measures 65 mm in length, 40 mm in diameter, and has a mass of 87 g. The authors report a measured stall (assumed here to be continuous) torque of 60 mNm, and a speed (assumed here to be no-load) of 250 deg/s. The wrist described in [67] is a two DOF powered device, where the two DOFs are pronation/supination and flexion/extension, respectively. The wrist design incorporates a pair of

DC motors that drive the split portion of a differential (i.e., typically the output portion), which in turn enables control of the two wrist DOFs. The authors report dimensions of 50 mm in length, 30 mm in anterior/posterior width, and 96 or 60 mm medial/lateral width, respectively, for the first and second design versions. The mass was reported as 200 g, measured stall torque of 70 mNm, and (assumed) no-load speed of 175 deg/s. The authors report in the discussion that the speed provided by the wrist was sufficient to be practical, but the (low) measured torque and backdrivable behavior would both be impediments for general use of the wrist prototype. Note that identification of these issues and establishment of practical target specifications is among the value of such experimental hardware.

Similar to powered wrists, relatively few prosthetic elbow designs have been described and experimentally characterized in the recent engineering literature. An elbow prototype was described in [68], which was intended to enable the investigation of impedance-based myoelectric elbow control strategies. The elbow was driven by a DC motor via a two-stage transmission consisting of a belt drive and gear drive, respectively. Another elbow prototype, incorporating a brushless motor and Harmonic drive transmission, was described by [69]. Finally, an arm prototype is described in [70], which employs a custom DC motor that drives the elbow joint through a planetary gear set, two-way clutch, roller screw, and four-bar linkage. The authors could not locate publications describing experimental characterization of these devices, and therefore chose not to report comparative values here.

This paper describes a transhumeral prosthesis prototype, designed for the purpose of experimentally investigating device features and control strategies for upper extremity prostheses. The prosthesis prototype consists of a multigrasp hand, a single-DOF wrist, and an elbow joint. Since the hand was previously reported in [12], this paper focuses on the design of the powered

wrist and elbow components, in addition to the corresponding embedded system, and additionally provides an experimental characterization of the torque and speed characteristics of both joints. Despite a focus on the wrist and elbow components, the hand and some associated characteristics are referenced when describing the functional characteristics (i.e., size, mass, power specifications) of the whole arm system.

1.3 Design Objectives

Each of the three major components of the upper extremity prosthesis described here (i.e., the hand, wrist and elbow) was designed to provide sufficient torque, speed, and range of motion to enable a user to perform typical ADLs. Although conditions of sufficiency have yet to be clearly established in this regard (i.e., hence the motivation in part for design of the prosthesis prototype described here), these values were generally established for purposes of design by a combination of data described in the biomechanical literature characterizing such requirements, and the performance characteristics of existing myoelectric prosthetic components.

1.3.1 Wrist Objectives

The healthy human wrist has three DOFs: pronation/supination (PS), flexion/extension (FE), and radial/ulnar deviation (RUD). Since the weight and complexity of prosthetic devices are generally increased with each additional active DOF, a designer must determine which wrist DOFs, and how many, to include in a wrist design. In addition to size and weight considerations, this determination is further complicated by the lack of direct control signals available to an amputee for use in controlling high DOF prostheses. Ideally a prosthetic wrist should have a minimum amount of active degrees of freedom required to perform ADLs. Range of motion studies indicate that while

all three DOFs are used during typical ADLs, the highest range of motion is associated with the PS DOF [71]. This observation is substantiated by amputee surveys which have reported that users of prosthetic devices rate forearm rotation (PS) as somewhat more desirable than either FE or RUD [17]. Finally, while some commercially available prosthetic wrists provide passive DOFs in FE, no currently available devices offer active DOFs other than PS. In consideration of these factors, the wrist unit described here was designed as a single DOF device with a powered PS DOF. The authors note that the objective of the design presented here is ultimately to conduct experimental assessments that offer insight into the validity of such design assumptions.

With regard to size, a prosthetic wrist should fit within the nominal anthropomorphic envelope, and should be as short as possible in length, to accommodate as many users as possible. As per the anthropometric data presented in [55], the wrist circumference of a 50th percentile male is 17.5 cm. A circular wrist cross-section would therefore correspond to wrist diameter of 5.6 cm, while an elliptical cross-section with a 2:1 aspect ratio would correspond approximately to a major axis (i.e., medial/lateral width) of 7.2 cm and a minor axis (i.e., anterior/posterior width) of 3.6 cm.

With regard to mass, less mass is always preferable in prosthetic devices, particularly since loads are transferred through soft tissue interfaces, rather than through the skeleton. Such rationale, however, does not provide sufficient guidance when establishing mass specifications. As per the premise of this paper, prosthetic arm hardware must be constructed within realistic size and mass constraints, such that researchers can assess the relative functional value of powered components, relative to the additional mass penalty they impose. Thus, the design target for prosthesis mass should always be “as light as possible” [72], subject to the condition that they provide sufficient biomechanical utility to offset added mass, relative to a passive component. Commercial wrist

rotators are in general quite light: the Otto bock wrist rotator has mass between 51 and 96 g depending on the model, and the Utah Arm wrist rotator has a mass between 143 and 168 g [73], [74]. Thus, for a prosthetic wrist to be comparable with commercial models, it should weigh no more than 200 g, and preferably less.

The primary kinetic and kinematic performance requirements of a wrist are related to the range of motion (ROM), rotational speed, and torque of the joint. Studies of wrist motion during activities of daily living have found that approximately 100 deg of rotation is sufficient for performing most tasks [71], [75]. This figure is considered to be a minimum desired range, as the maximum range of motion of a healthy wrist is closer to 180 deg, and some commercial prostheses are capable of more than 360 deg of rotation [73]. Thus the design objective was established as a minimum PS ROM of 180 deg.

Relatively little data exists regarding sufficient wrist torques and speeds required to perform ADLs. In the absence of clear guidance with respect to sufficient wrist rotational speeds, the authors note that a previously published paper on wrist design [67] indicated 175 deg/s was sufficiently fast to be practical. Further, using existing commercial devices as a reference, the Otto Bock wrist is capable of between 130 and 160 deg/s, while the Utah Arm ProWrist Rotator is capable of 300 deg/s. In consideration of these points of reference, and since as previously mentioned a research prosthesis should have comparable capabilities to the commercial state-of-the-art, the nominal target for rotational speed for the wrist unit described here was established at 150 deg/s.

With regard to torque, a study of the maximum twisting moment produced by able-bodied individuals indicates torques ranging from approximately 1 to 30 Nm, depending on the orientation and shape of the object being manipulated [76]. Such measurements, however, represent maximal

values, and do not characterize the values sufficient to perform ADLs. Further, in the case of an active wrist prosthesis, it is assumed that the principal function of the prosthesis is to position or reposition the orientation of the hand to facilitate grasp or release of objects oriented along various axes in the workspace, rather than perform active twisting movements. That is, the objective is to position the hand, and to resist twisting moments, but not necessarily to perform (twisting) work on the environment. As such, the wrist torque should be sufficient to re-orient an offset load in the hand. For example, rotating a 500 mL bottle of water, if held by the end of the bottle, would require 280 mNm of torque. Rotating a typical carpenter's hammer (i.e., approximately 500 g), when held at the base of the handle, would require approximately 1.4 Nm. The Utah Arm ProWrist Rotator, as a point of reference, provides an active torque of 1.7 Nm. In consideration of these requirements and points of reference, the target torque for the wrist unit described here was established at 1.5 Nm.

Finally, given that the primary task of the wrist is to orient the hand and maintain that orientation, another important design requirement is non-backdrivability. Such behavior was also suggested by [67] as an important characteristic for practical use. This characteristic eliminates power consumption required to passively hold objects, and decouples the maximum continuous holding torque from the active driving torque (i.e., decouples holding torque from the motor characteristics). Finally, since repositioning of the wrist presumably occurs at a relatively low duty cycle, and since the holding torque is decoupled from the active torque by the non-backdrivability of the design, the torque specification of 1.5 Nm is a continuous rating for the wrist, but can correspond to the peak torque rating of the wrist motor.

To summarize, the prosthetic wrist was designed to nominally achieve the following performance objectives:

- A single active PS DOF, i.e., a wrist rotator
- Range of motion at least 180 deg
- Active torque in PS of 1.5 Nm
- Maximum angular velocity in PS of 150 deg/s
- Non-backdrivable behavior
- Mass less than 200 g
- Circumference less than 17.5 cm (nominally, 7.2 cm by 3.6 cm)
- Length as short as possible

1.3.2 Elbow Objectives

The length of the proximal section of the elbow should be as short as possible, in order to accommodate as many users as possible (i.e., users with long residual limb length). Although the length of the proximal segment should be as short as possible, it is reasonable to assume a minimum forearm length of 23.3 cm, which corresponds to the forearm length of a 25th percentile female arm. If the wrist rotator unit is assumed to have a length of 3.5 cm, the target minimum length for the elbow unit would be 19.8 cm. Further, as per the anthropometry data provided in [55], the elbow circumference of a 50th percentile male is approximately 28 cm, while the corresponding flexed forearm circumference is approximately 30 cm. Assuming circular cross-sections, these correspond to elbow diameters of 8.9 and 9.6 cm, respectively. As such, the major dimensions of the elbow unit should be nominally 9 to 9.5 cm near the proximal end of the forearm.

A target mass can be approximated from anthropometry data by estimating elbow mass as the sum of half the forearm mass and half the upper arm mass. According to [54], this results in a target mass of approximately 1.9 kg for a 50th percentile male. Specifying such a target mass for

the elbow, however, is problematic for the same reasons as previously mentioned for wrist mass – namely, the soft-tissue interface has less tolerance for mass than the healthy limb. In [72], it is suggested that a reasonable target for a prosthetic device (taking into consideration the soft-tissue socket interface) is 500 g for the hand, and 1.5 kg for the rest of the arm, resulting in a whole arm mass target of 2 kg. If the mass of a hand is assumed to be 500 g, and the mass of the wrist 200 g (see above), then the target mass of the elbow would be approximately 1.3 kg. Ideally a prosthetic device would be lighter, as indicated by the mass of common commercial prosthetic arm systems, which commonly have mass in the range of 1.4 to 1.6 kg [77], [78].

The ROM of a healthy elbow is typically between 0 deg (fully extended) to approximately 146 deg (fully flexed), although a ROM between 30 and 130 deg has been shown to be sufficient for most ADLs [79], [80]. Given that sufficiency is the objective for specifying design targets, a minimum target ROM of 100 deg was chosen for the powered elbow (i.e., providing a ROM between 30 and 130 deg), with a greater ROM being preferable if possible.

A few studies have been conducted characterizing the elbow torque and speed required to perform ADLs. A survey of upper limb movement requirements conducted by [75] reports that the elbow undergoes a maximum angular velocity of approximately 250 deg/s while executing typical ADLs, which corresponds to a time of approximately 0.4 s to move through the minimum targeted ROM. Torque specifications can be found from a study by [81] which contained an inverse dynamic analysis on ten subjects performing ten different ADLs. This study found that the maximum elbow torque (averaged among all subjects) was 5.8 Nm in flexion (measured while raising a block to head height). As a point of reference, the Otto Bock DynamicArm exceeds this amount of torque by offering a maximum lift of 6 kg [77], which would correspond to a torque of approximately 14 Nm for a 50th percentile female arm, or 16 Nm for a 50th percentile male arm. In

consideration of these requirements and points of reference, the target torque for the elbow unit described here was established at 16 Nm, which was assumed sufficient to conduct most ADLs, and also to be competitive with existing commercial products.

Finally, unlike the wrist, which is assumed to provide a positioning and holding functionality, the elbow is assumed to provide dual functionalities, which include positioning and holding in certain situations (e.g., reaching), and kinematically-constrained following in other situations (e.g., opening a door or a drawer). As such, the elbow must switch between high output impedance and low output impedance states. In commercially-available devices, the latter behavior is typically referred to as “free-swing” mode. Although various approaches are available for the provision of such functionality, the authors choose to do so here by employing a low-output-impedance design, and to selectively increase the output impedance using feedback gains in the elbow position feedback controller (i.e., emulating a stiff system via feedback control of the elbow joint). With this approach, the elbow can provide position-and-hold functionality, or can alternatively be passively back-driven (via the shoulder) when coupled to a kinematic constraint.

To summarize, the design objectives for the powered elbow prosthesis are as follows:

- Minimum range of motion from 30 deg to 130 deg flexion (where 0 deg flexion corresponds to full extension of the elbow)
- Active torque of approximately 16 Nm
- Maximum angular velocity of 250 deg/s
- Open-loop back-drivable actuation
- Mass less than 1.3 kg (or total arm mass less than 2 kg), less if possible
- Major diameter approximately 9.5 cm near proximal end
- Maximum forearm length of 19.8 cm

- Back-drivable behavior to facilitate shoulder-driven closed-chain manipulation tasks

1.4 Design of Arm Components

1.4.1 Wrist Design

Recall that the wrist is intended for low-power position-and-hold functionality, with maximum torque of 1.5 Nm and maximum (no-load) speed of 150 deg/s. These torque and speed characteristics are not expected simultaneously; rather it is assumed here that maximum torque should be available at half maximum speed, in which case the wrist should be capable of a maximum output power of approximately 2 W (i.e., 1.5 Nm @ 1.3 rad/s, intermittent). Although efficiency of a transmission is difficult to accurately predict, it is reasonable to assume a nominal range of efficiencies between 15% and 35% for a high transmission gear ratio with friction-based non-backdrivability. Assuming this nominal inefficiency, a 5 W (continuous) Maxon EC-max 16 brushless DC motor (6-volt winding) was selected to power the wrist, based on its small form factor and relatively high output torque (3.2 mNm continuous). Assuming between a 15% and 35% transmission efficiency, and that the brushless motor can produce between 5 and 9 mNm for low duty-cycle operation, the required transmission ratio would be bracketed between estimates of 475 (assuming 9 mNm @ 35% efficiency) and 2000 (assuming 5 mNm @ 15% efficiency). In order to provide these ranges of transmission, and to provide non-backdrivable behavior, a three-stage transmission was selected, consisting of an initial planetary gearhead stage, followed by an interchangeable spur gear stage, followed by a worm gear stage, as shown in the cut-away CAD model in Fig. III-1. Specifically, a Maxon planetary gearhead provides a speed reduction ratio of 29:1, while the worm gear output stage provides a ratio of 30:1. The interchangeable second stage consists of a set of spur gears with three ratio options – 75:34, 62:47, or 47:62. Note that the last

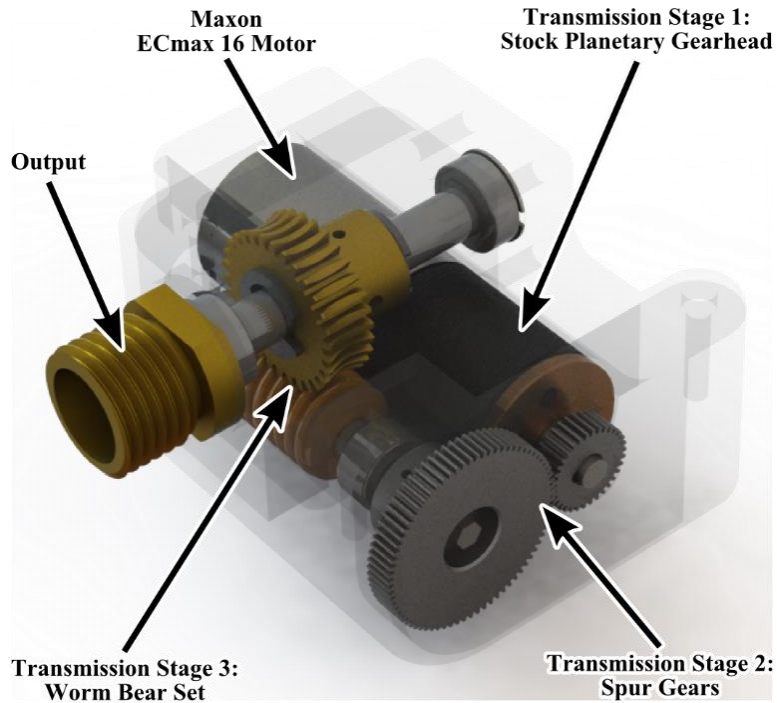


Fig. III-1. CAD model of wrist unit.

is a speed increase rather than reduction. Thus, with the three second-stage configurations, the overall transmission ratio can be adjusted to be 1919:1, 1147:1, or 660:1, respectively, which essentially spans the previously stated assumptions of transmission efficiency and intermittent motor torque capability. Further, since as previously discussed, the precise requirements of wrist torque and speed to best enable ADLs is not yet clear, adjustability of overall transmission ratio will facilitate the experimental assessment of functional trade-offs in this regard. Regarding the third stage, note the worm gear was chosen primarily because it provides a high gear ratio in a small space; provides the design objective of non-backdrivability; and enables the motor to be oriented along the medial/lateral aspect of the wrist, and thus facilitates geometric requirements.

The wrist interfaces with a multigrasp hand, previously described by the authors [12], via a small bolt circle of cap screws, and with the elbow unit via a (standard body-powered) threaded connector. Note that (although this paper is focused on a transhumeral prosthesis), the use of a

standard body-powered threaded connector at the proximal end of the wrist was selected to enable use of a subjects' existing body-powered socket when conducting experimental assessment of the hand and wrist combination with transradial subjects. With regard to materials, the cover and support structure were machined from aluminum, and each of the transmission shafts from stainless steel. The second-stage and worm gears are stock components, the former machined from steel and the latter from brass. All shafts are supported by ball bearings, and all are preloaded axially with bearing preload springs. Both the spur gear and worm gear sets are located within housing compartments that are packed with grease (to increase efficiency and decrease audible noise). Finally, position sensing for closed-loop control is provided by Hall Effect sensors embedded in the brushless DC Motor.

1.4.2 Elbow Design

The elbow was designed for maximum torque output of 16 Nm and maximum (no-load) speed of 250 deg/s (4.4 rad/s). Assuming, as with the wrist, maximum torque capability is expected at half no-load speed, the elbow should be capable of 35 W of power, in this case assumed intermittent. Since the elbow will be a backdrivable transmission, with considerably lower transmission ratio relative to the wrist, a transmission efficiency of 75% was assumed for the motor selection. Given the nominal power and torque output, a 100 W Maxon EC60 14-pole brushless DC motor (12-v winding) was selected, based on its nominal power output and relatively high torque/mass ratio. The EC60 is rated at a continuous torque capability of almost 300 mNm, with intermittent torque capability strongly related to the heat-sinking configuration (i.e., the manner in which the motor is mounted). Based on prior experience with this motor, the authors assumed an intermittent torque capability of approximately 600 mNm (i.e., approximately twice the continuous torque rating).

Given this assumption, and assuming 75% transmission efficiency, a transmission ratio of 35:1 is required. In the elbow unit, this transmission ratio is provided by a three-stage transmission consisting of two chain stages (ratio of 5.1:1 and 2.9:1, respectively), followed by a cable-drive output stage (with a ratio of 2.4:1). Chain drives were chosen for the first two stages for their high efficiency, low weight, and compactness. The output stage incorporates a cable drive for high efficiency; zero backlash; lack of chordal action, and ability to minimize the elbow dimension on the proximal side of the elbow joint. Note that although the two chain drives introduce some backlash and chordal action into the transmission, the reduction stage provided by the cable drive attenuates the presence of these effects at the elbow joint, such that they are essentially negligible as observed at the output (i.e., at the elbow).

The fabricated elbow unit, along with a forearm spacer, is shown in Fig. III-2. The proximal end of the elbow includes a standard transhumeral socket interface, such that experimental assessments can be performed using a subject's daily-use socket. The distal end is designed to

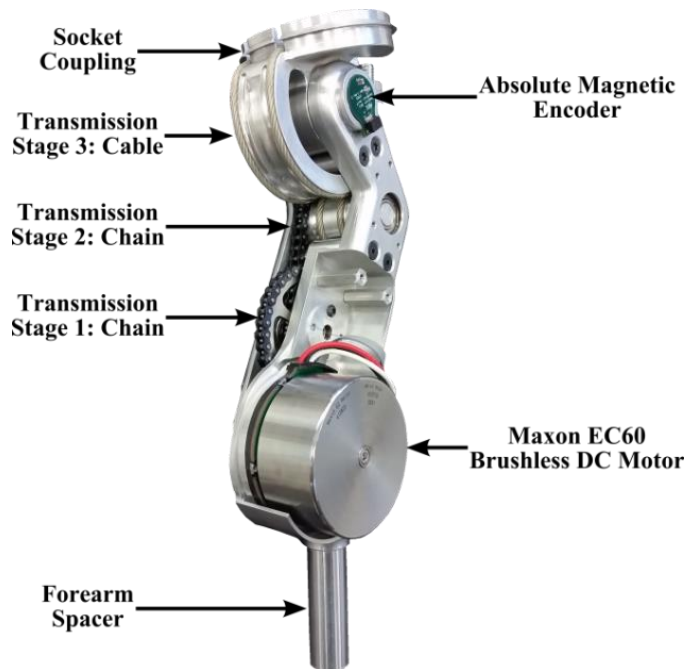


Fig. III-2. Elbow prosthesis prototype.

either interface with the previously described powered wrist rotator, or directly with the previously reported multigrasp hand (i.e., if used without the prosthetic wrist). A forearm spacer, which can be fabricated in varying lengths, is inserted between the elbow and either wrist or hand to adjust the length of the forearm to match a user's contralateral forearm. Structural components of the elbow and cable pulleys were machined from 7075 aluminum, and the chain sprockets machined from 4140 steel. All structural components were designed to have a minimum static safety factor of three relative to expected maximum loading conditions. Position sensing in the elbow is provided by the motor's Hall Effect sensors, fused with an Austria Microsystems AS5145 absolute magnetic encoder that measures the angle of the elbow joint.

1.4.3 Embedded System Design

An embedded system was designed for the prosthesis to provide the functionality diagramed in Fig. III-3. The major components of the embedded system include: 1) battery and power conditioning circuitry; 2) four-quadrant brushless motor drivers for wrist and elbow brushless motors; 3) angle measurement of the wrist and elbow joints; 4) 9-axis inertial measurement unit (IMU) to measure inertial arm motion (for investigation of arm control strategies); 5) 8-channel EMG measurement and signal conditioning; 6) microcontroller for on-board signal conditioning and control functionality; 7) a CAN bus for communication with host computer, for controller prototyping, data measurement, and diagnostics; and 8) a CAN bus and control circuitry for interaction with and control of embedded system within hand prosthesis. Note that the hand prosthesis embedded system, referenced in Fig. III-3 but not shown here, is described separately in [12]. The embodiment of this embedded system, along with identification of major componentry, is shown in Fig. III-4. The asymmetric shape of the embedded system is to facilitate

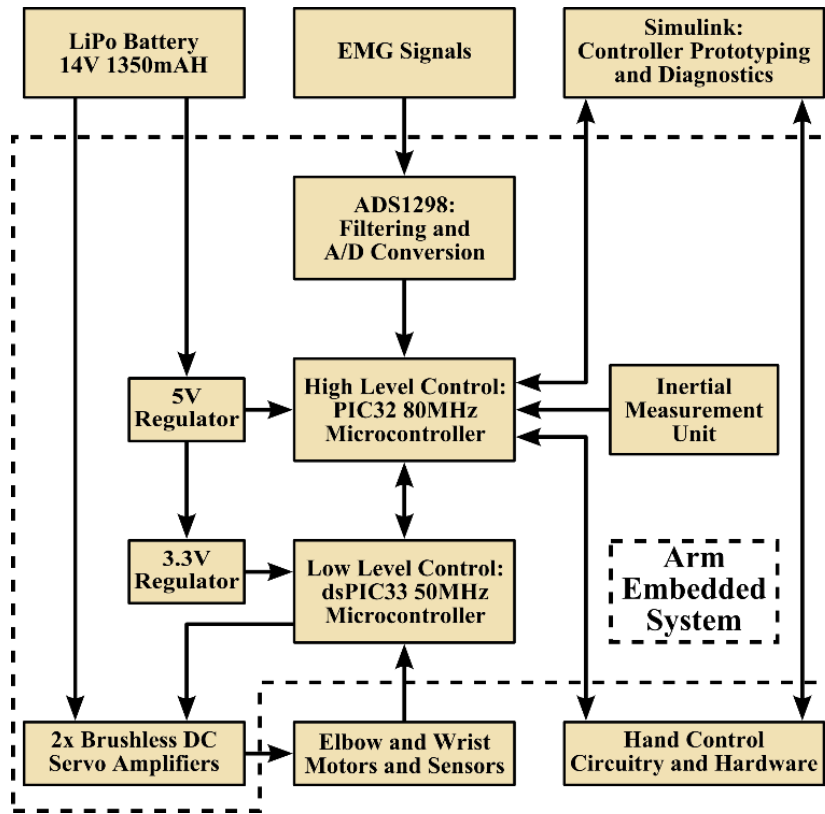


Fig. III-3. Block diagram of arm embedded system.

mounting on the elbow unit, such that the prosthesis remains within the anthropomorphic envelope, as shown in Fig. III-5.

The embedded system consists of a single four-layer circuit board that is designed to be mounted directly to the powered elbow prosthesis as shown in Fig. III-5. The system is capable of executing the high level control of each joint such that the prosthesis can be completely self-contained, although it also supports tethered control where motor position commands are generated by a PC running Simulink with MATLAB Real-Time Windows Target. The board utilizes two microcontrollers: a 50 MHz Microchip dsPIC33, and an 80 MHz Microchip PIC32. The PIC32 generally performs higher-level control, while the dsPIC generally lower-level control. Specifically, the dsPIC33 provides Hall-sensor-based brushless motor block commutation and closed-loop PID current control for the wrist and elbow motors at a PWM rate 45 kHz, with a

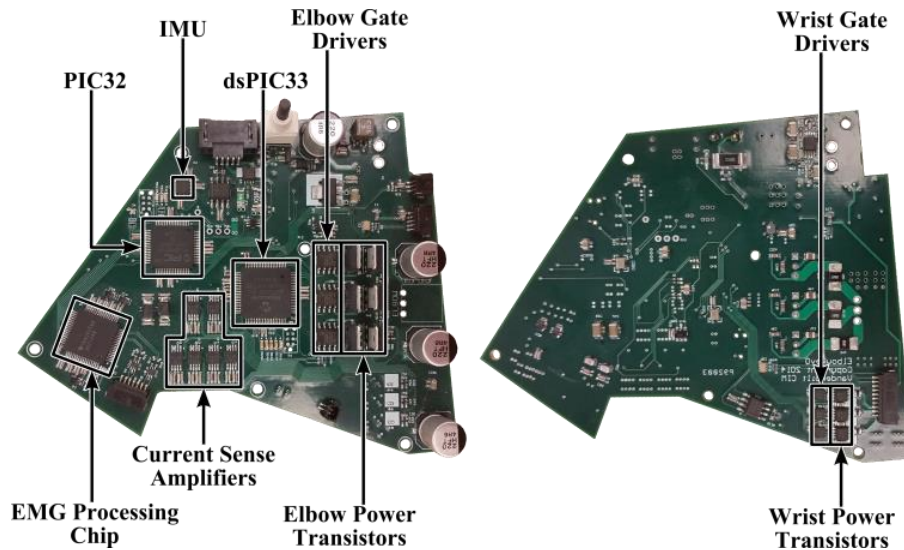


Fig. III-4. Top and bottom view of arm embedded system.

current control loop that runs at 5 kHz. Based on the transistor ratings and trace widths on the board, the wrist amplifier is capable of supplying 5 A continuous current to the wrist motor, while the elbow servoamplifier is capable of 50 A continuous. Inertial measurement is provided by an Invensense MPU-9250 9-axis IMU, and EMG measurement by a Texas Instruments ADS1298 8-channel analog front end with 24-bit analog to digital converter to process EMG signals. The PIC32 reads all data (i.e., joint angle data from the dsPIC33, 9-axis IMU data from the IMU, EMG measurement from the EMG circuitry, and motor angle and current data from the hand), and either sends it to the host computer (if running in tethered mode), or performs control computations directly if running in untethered mode. Based on the control computations, the PIC32 sends commands to the hand servoamplifiers (located within the hand) via the CAN bus, and to the wrist and elbow servoamplifiers (in the dsPIC33), respectively. The high-level control loop in the PIC32 runs at a sampling rate of 500 Hz. On-board communication is based on a serial peripheral interface

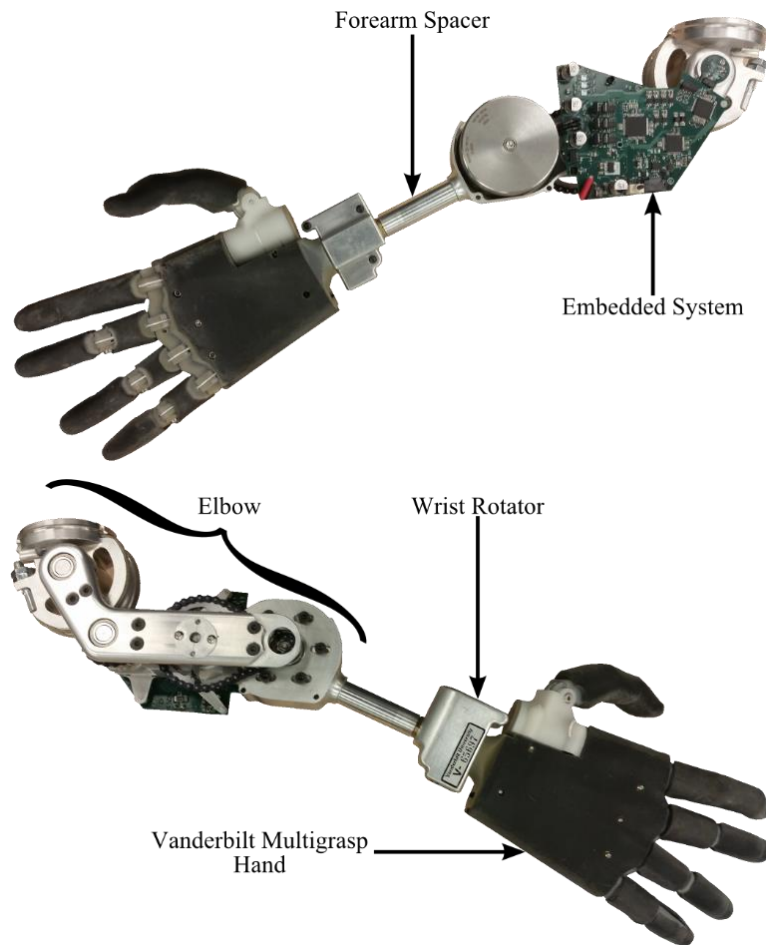


Fig. III-5. Labeled photograph of fully assembled arm prosthesis.

(SPI) bus, while a controller area network (CAN) serial interface is used to communicate between the arm board and hand board, and between arm board and PC.

1.5 Performance Characteristics

1.5.1 Range of Motion, Size and Mass

A photograph of the assembled arm, including elbow, wrist, and (previously published) multigrasp hand is shown in Fig. III-5. A video is included in the supplemental material that depicts basic arm movements, and also demonstrates the free-swing (i.e., backdrive) capability of the elbow. With

regard to measured wrist characteristics, the wrist is mechanically capable of continuous 360 deg of rotation in either direction, but since the prototype currently lacks slip rings through which to transmit the motor control signals, the wrist is constrained in software to rotate within a 180 deg ROM. Slip rings may be incorporated at a later date, should a continuous 360 deg ROM be desirable. The assembled wrist measures 5.5 cm in the medial/lateral dimension, 3.5 cm in the anterior/posterior dimension, and 3.7 cm in the proximal/distal dimension, and has a mass of 175 g. The circumference at the largest section of the wrist is 16.4 cm, which corresponds

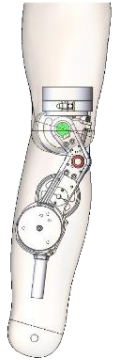



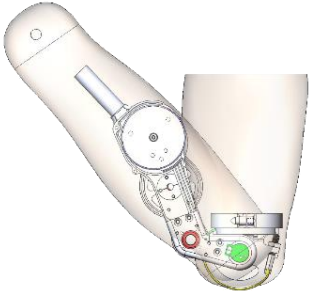

Full Extension - Sagittal Plane		Full Extension - Frontal Plane	
Model	Photograph	Model	Photograph
			
Full Flexion - Sagittal Plane			
Model		Photograph	
			

Fig. III-6. Solid models and corresponding photographs of elbow prosthesis illustrating its ROM.

approximately to a 10th percentile male wrist. As such, ROM, size, and mass objectives were met for the wrist design.

The elbow, which is pictured in the context of a 50th percentile male arm, is shown in Fig. III-6. The elbow is capable of a ROM from 15 deg flexion to 145 deg flexion (i.e., total ROM of 130 deg). The length of the proximal segment of the prosthesis is 3.0 cm, the minimum length of the distal (i.e. forearm) segment is 17.4 cm (i.e., when the forearm spacer is not used), and the maximum width at the proximal end of the forearm is 5.0 cm. The mass of the elbow unit is approximately 1.0 kg. As such, ROM, size, and mass objectives were met for the elbow design.

Note that although the arm prototype shown in Fig. III-6 does not include a battery, the system was designed to incorporate a 12 v, 2.9 Ah lithium ion battery pack consisting of three 18650 lithium ion cells, with a total mass of 145 g. Combining the mass of this battery pack with the 175 g wrist unit, 1000 g elbow unit, 50 g embedded system, and 550 g hand (see [12]), results in a total arm mass of 1.9 kg. As such, the arm system falls within the 2 kg mass design goal previously described.

1.5.2 Joint Speed Measurement

The torque and speed performance characteristics of both the wrist and elbow units were experimentally quantified. In these characterizations, the previously described embedded system was used for closed-loop control of the wrist and elbow axes, with either desired (exogenous) position or current commands (as appropriate) generated by a PC running Simulink Real-Time Windows Target and sent to the embedded system over the CAN bus (see Fig. 3). In all experimental characterizations, the system was powered by a 12 v benchtop DC power supply, rather than by the 12 v lithium-ion battery pack expected to power the arm. Regardless, the use of

Wrist and Elbow Performance Characteristics				
Component	Wrist			Elbow
Transmission Ratio	1919:1	1147:1	660:1	35:1
Maximum Torque (Nm)	2.63	1.53	0.982	18.4
Maximum Angular Velocity in rpm (deg/s)	14.5 (87)	24.2 (145)	40 (240)	82 (490)
Estimated Time to Travel Full ROM (s)	2.1	1.2	0.75	0.39
Motion Tracking Bandwidth (Hz)	0.67	1.1	1.7	1.5

Table III-1. Wrist and Elbow Performance Characteristics.

a DC power supply instead of lithium-ion battery is not expected to change the performance characteristics, since the current supplied by the DC power supply was electronically limited to a value less than the continuous discharge current rating of the lithium-ion battery pack.

Due to the high transmission ratio of the wrist unit, the maximum joint angular velocity is limited by the back-EMF of the motor operating at the 12 v potential of the power supply. As such, the maximum wrist joint speed is a direct function of the second-stage transmission ratio. As given in Table 1, the maximum angular velocity of the wrist, as measured by motor Hall sensing, is approximately 90 deg/s, 145 deg/s, and 240 deg/s, respectively, for the three different transmission ratio configurations. In order to further characterize the speed of movement, the closed-loop servo-controlled joint motion bandwidth was measured by commanding a sinusoidal position signal with a peak-to-peak amplitude of half the expected ROM (i.e., 90 deg for the wrist unit), and measuring the relative magnitude between the commanded and actual motion across a given frequency band. These data for the wrist unit are reported in Table III-1 for each of the three transmission ratios. The corresponding frequency response for each is shown in Fig. III-7. Note that the corresponding

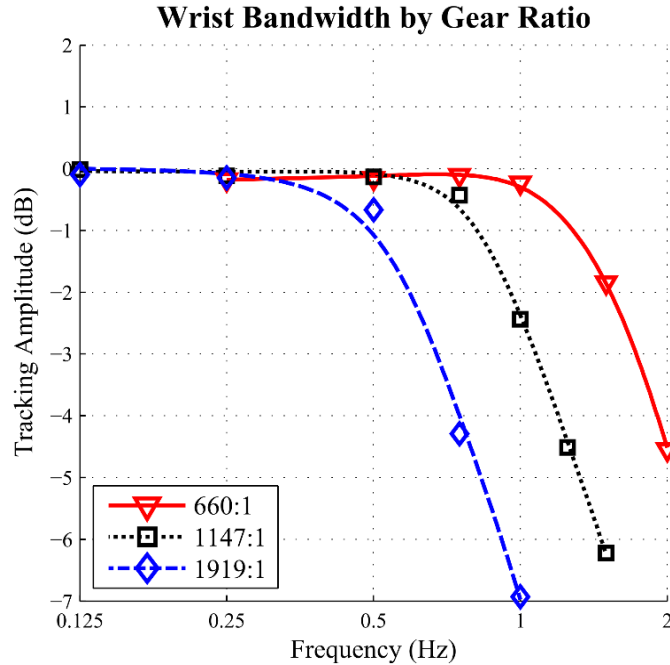


Fig. III-7. Closed loop position tracking bandwidth for each wrist transmission configuration.

-3 dB tracking bandwidth of the wrist joint is in the 1-2 Hz range for the respective transmission configurations.

Due to its relatively small transmission ratio, the maximum angular velocity of the elbow is more a function of its maximum acceleration (within its 130 deg ROM) than its back EMF (i.e., more a function of maximum current than driving voltage). In particular, the maximum realistic angular velocity of the elbow is constrained by the total acceleration that can be achieved within half of the elbow ROM, since the elbow must decelerate in the second half of the ROM so as to not strike the hard-stop. As such, the maximum attainable angular velocity for the elbow was measured via commanding a position step response under closed-loop control with a magnitude of 130 degrees (full elbow ROM) to the elbow. In these experiments, the peak current was electronically limited to 20 A, which corresponds to the maximum continuous output of the intended battery pack. Also, since the maximum speed is limited by acceleration (and therefore

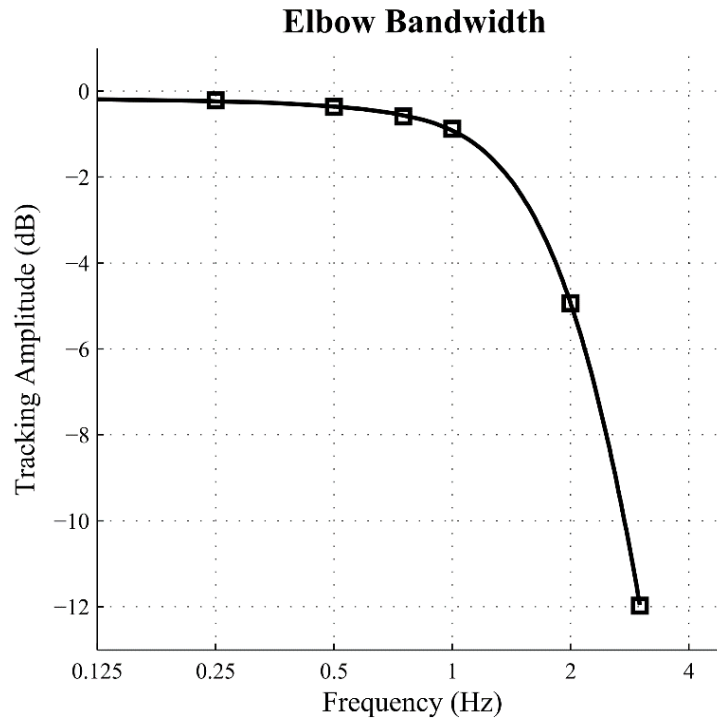


Fig. III-8. Closed loop position tracking bandwidth for elbow.

affected by rotational inertia about the elbow, as well as gravitational loads), all elbow speed characterizations were conducted with the wrist, multigrasp hand, and forearm spacer (for 50th percentile male) in place. Under these conditions, the maximum elbow angular velocity was measured to be 490 deg/s, as reported in Table III-1. Additionally, as with the wrist joint, the bandwidth of elbow trajectory tracking was characterized, under the same nominal conditions, using a half-ROM of 65 deg for the peak-to-peak position amplitude. The resulting frequency response is shown in Fig. III-8, indicating a -3 dB motion tracking bandwidth of approximately 1.5 Hz. As indicated by Table III-1, the measured speed characteristics at the low and medium wrist transmission ratios meet the design objectives for wrist speed, while the measured characteristics for the elbow are well beyond the associated design objective.

1.5.3 Joint Torque Measurement

For both the wrist and the elbow, the maximum active output torque was measured by commanding a specified motor current, and measuring the joint torque output using a force gage (Exttech Instruments model 475044) attached orthogonally via a lever arm to the output of each respective component. Based on the specification of each motor and their respective heat sinking configurations (both a thermally heat sinked into an aluminum structure), a maximum intermittent current factor of approximately two above the continuous (non-heat-sinked) rating was selected as appropriate and reasonable. As such, the torque was measured for a current command of 2 A for the wrist unit, and 20 A for the elbow unit. The maximum joint torque was measured by recording the maximum torque over a one-second period, and averaging the resultant measurements over 10 trials. The resulting maximum wrist unit torques were measured as 1.0, 1.5, and 2.6 Nm, respectively, for the small, medium, and large wrist transmission ratios. Note that, given the known current input to the motors and measured torque output, the drive-train efficiency corresponding to each of the wrist transmissions can be calculated as 19%, 17%, and 17%, respectively, for the small, medium, and large wrist transmission ratios (all of which are within the originally assumed range of efficiencies for the motor selection process, although on the low end of the range).

The corresponding maximum torque measured at the elbow was 18.4 Nm. This torque corresponds to lifting 7.7 kg for a 50th percentile female forearm length, or lifting 7.0 kg for a 50th percentile male forearm length. Given the known current input and measured torque output of the elbow, the elbow transmission provides an efficiency of 85%, which is somewhat greater than the efficiency assumed during the motor selection process.

The results for measured torque capability for each joint and each configuration are summarized in Table III-1. As indicated by Table III-1, the measured torque characteristics at the

medium and high wrist transmission ratios meet the design objectives for wrist torque, while the measured torque characteristics for the elbow exceed the elbow torque design objective.

The passive torque of the wrist and elbow were measured differently, as there were opposite design goals for each component. The wrist is intended to provide a large holding torque, so that heavy objects will not passively rotate the wrist. Since the non-backdrive feature results from the worm gear output stage of the transmission, the maximum holding torque is a function of the yield strength of various components (i.e., worm and worm gear, bearings, shafts, etc). As such, the holding torque of the wrist is assumed to be much greater than the active torque; since the authors were unwilling to destructively test the wrist, however, the holding torque was not experimentally characterized. The design objective in the case of the elbow, however, is to minimize the backdrive torque. This was measured using the same experimental setup previously described for elbow torque measurement, but without commanding any current to the elbow motor. In this case, the maximum torque required to move the elbow in the plane perpendicular to gravity was approximately 1.5 Nm (i.e., about 8% of the maximum active torque). Since the elbow unit produces more than this torque under gravitational loads, the elbow unit will fully extend under its own mass when in the vertical plane (i.e., when subjected to gravity). A video included in the supplemental material demonstrates the backdrive capability of the elbow unit.

1.5.4 Power Measurements and Battery Life

In addition to the nominal performance criteria, it is also useful to understand the electrical power requirements of an arm prosthesis, since practical implementation of such a device requires it be powered using a battery pack. The electrical power required to operate the wrist and elbow was determined by measuring the energy consumed while performing motions which simulate the

component tasks of ADLs. For each test, the current consumed by the embedded system (which provided power to all components of the arm) at constant voltage was measured using a current probe (Agilent model 1146A). Total power required by the embedded system was computed by integrating the current supplied at constant voltage to the embedded system over the trial duration to obtain the total electrical energy required from the power supply. Since the wrist will primarily be used to preposition the hand, and is not intended to provide active rotating torques, the ADLs for the wrist were approximated by attaching the multigrasp hand [12] to the wrist and commanding a sinusoidal position command (full ROM) at a moderate frequency (0.15 Hz), which corresponds to the same maximum velocity as a half-bandwidth sinusoid, but performed over a full ROM. For these experiments, the wrist was configured with the intermediate transmission ratio of 1147:1, since that ratio met both the torque and speed objectives, and was therefore determined to have the best balance between torque and speed. Operating under these conditions, the electrical power used by the embedded system integrated over 10 cycles was measured, and is listed in Table III-2.

Representative elbow tasks can be broadly classified into three categories: positioning the hand (e.g., reaching), actively lifting objects, and statically holding objects. Hand positioning tasks

Wrist and Elbow Power Usage				
Test	Positioning			Static Hold
	Unloaded		Loaded	
Component	Wrist	Elbow	Elbow	Elbow
Measured Energy	8.1 J	8.64 J	25.6 J	17.4 J/s
Cycles per Battery Charge	15,000	14,400	4,880	120 min
Cycles per Gram of Battery Weight	103	99	34	50 s

Table III-2. Wrist and Elbow Power Usage.

were modelled in the same manner as with the wrist: a 100 deg peak-to-peak sinusoid signal at 0.5 Hz (half bandwidth) was commanded to the elbow of the whole arm system (i.e., with hand, wrist, and spacer), but otherwise without a load attached to the hand. For the active lifting task, the same experiment was conducted, but with the hand grasping a 1 kg mass. In each case, the measured power was integrated over 20 cycles of movement. Finally, since the elbow is back-drivable, power is required to hold the elbow in a static position. This task, and the power required by it, was simulated by measuring the average current required by the elbow to hold a 1 kg weight in the hand when the forearm was oriented perpendicular to gravity (i.e., elbow angle of 90 deg, where the upper arm was aligned with the gravity vector) for a duration of 50 s. The results of these experiments are listed in Table III-2.

The battery pack designed for use in the arm prosthesis is a 12 v, 2.9 Ah pack, consisting of three (high-drain) 18650 lithium ion cells, which collectively have a mass of 145 g. As such, the total energy in the battery pack is approximately 125 kJ (i.e., the gravimetric energy density is 860 J/g). Based on the power measurements previously described, and using the battery pack described, a single charge of the battery pack would provide for 15,000 (unloaded) ROM cycles of the wrist; 14,400 (unloaded) ROM cycles of the elbow; 4,880 loaded (with 1 kg mass) ROM cycles of the elbow; or 120 min (i.e., 2 hours) of static holding (of a 1 kg mass); or some linear combination of these movements. Note that these estimates do not include the power required by the hand (which is estimated in [12]). These estimates are listed in Table III-2, along with an estimated normalized per unit mass of the battery pack.

1.5.5 Audible Noise Measurement

Although audible noise objectives were not specified, an arm prosthesis should preferably be characterized by a minimal amount of audible noise during operation. The amount of audible noise was characterized for the wrist and elbow units by mounting each device in a compliant mount to minimize vibrations transmitted to the test bench; commanding sinusoidal movement through the full ROM at the half-bandwidth frequency of each respective joint; and using a sound-level meter (Center model 325) to measure the audible noise level at a distance of 1 meter at several locations around each device. The resulting average noise levels were measured as 53.6 dBA and 51.7 dBA, respectively, for the wrist and elbow joints. As a point of reference, ambient noise in an office environment is estimated to be 45 dBA [82], and a change of less than approximately 3 dB is imperceptible to the human ear.

1.6 Conclusion

The authors describe the design of a transhumeral arm prosthesis consisting of a multigrasp hand, wrist rotator, and elbow. The paper focuses on the design and performance characterization of the wrist and elbow units, since the hand design and performance characterization has been previously reported. The prosthesis is intended as a research platform to better inform the design and functional trade-offs associated with upper extremity prostheses, and to enable the experimental investigation and assessment of control strategies for improving the functionality of them. In future work, the authors intend to use the prosthesis to conduct studies with transhumeral amputee subjects to assess the relative value of additional DOFs (i.e., at the hand and wrist); to assess the validity of design assumptions and objectives (e.g., mass, torque, and speed characteristics); and to investigate methods of control that enable effective use of arm function.

2. Addendums to Manuscript 2

2.1 Powered Wrist Rotator Design Iterations

Before the wrist design as presented in manuscript 2 was finalized, it went through two other major design iterations centered around the specific actuator and transmission configuration. Recall that the design goals for the prosthetic wrist were specified as follows:

- A single active PS DOF, i.e., a wrist rotator
- Range of motion at least 180 deg
- Active torque in PS of 1.5 Nm
- Maximum angular velocity in PS of 150 deg/s
- Non-backdrivable behavior
- Light and compact enough to fit within the anatomical envelope

The first version of the wrist concentrated primarily on the mechanism that would enable the non-backdrivable behavior. The strategy to accomplish this initially was to design a larger version of the two-way clutch mechanism already present in the hand actuation units, and the first generation of the wrist served as a proof-of-concept for this idea. Because of the size and complexity of the scaled-up two-way clutch mechanism, it wasn't possible to fit a gear reduction into the anatomical envelope, so the active torque was provided by a larger, high-torque motor (Maxon EC45 Flat motor) without a gearhead mounted concentrically to the axis of rotation.

Fig. III-9 shows the first prototype of the wrist attached to the VMG Hand, as well as CAD models showing the completed design and a cross-section of the two-way clutch. In the cross-section view (Fig. III-9b), the green component is rigidly attached to the input shaft, the red component is rigidly attached to the output shaft, and the blue parts are rolling bearings that act as

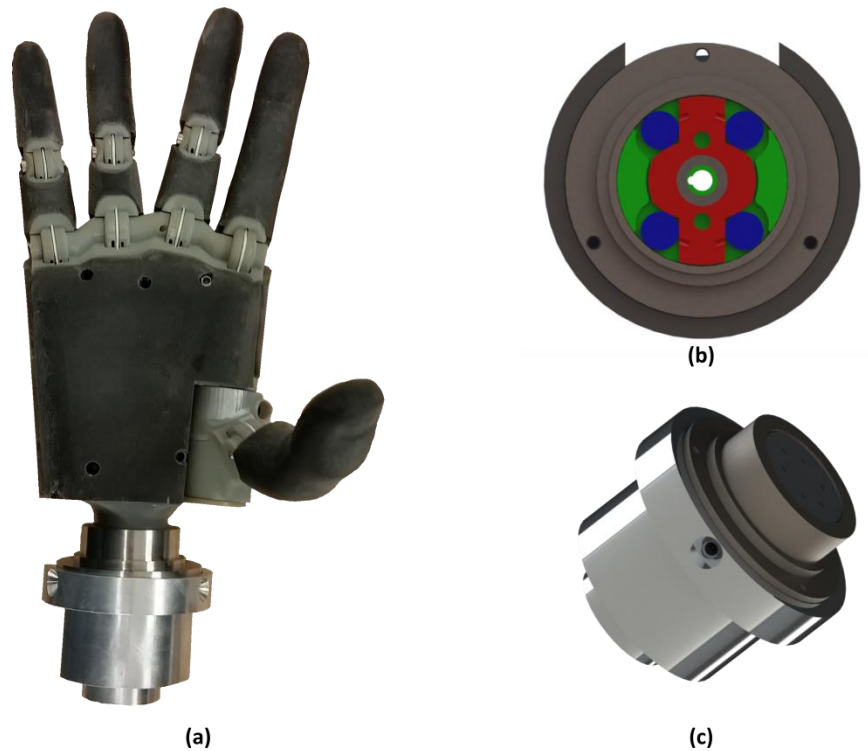


Fig. III-9. First generation of wrist prototype. (a): Photograph of wrist attached to the VMG hand. (b): CAD model of cross-section of two-way clutch mechanism. (c): CAD model of first generation wrist.

the locking mechanism. The function of this mechanism is identical to the one already described in [4], allowing the motor to drive the output shaft while preventing the output from driving the motor. When the input (green) is driven, the concave surfaces roll the bearings away from the housing and up against the output (red), causing the output to rotate with the input. When a force is applied to the output, however, the bearings are forced against the housing, preventing the input shaft from receiving any torque.

While the two-way clutch worked as expected when scaled up in size, the first prototype had several shortcomings. First of all, the wrist rotator was bulky and heavy, and would add an unacceptable amount of length and mass to the system. Secondly, operating the electric motor at the low speeds and high torques required for a prosthetic wrist does not provide an optimal power to weight ratio, since DC motors generate maximum power at higher speeds and lower torques.

Thus, the best case scenario for the active torque provided by the wrist would be approximately 100 mNm, which was insufficient for smooth control of the wrist position. This problem could have been solved by attaching a stock gearhead to the motor, but even the smallest gearheads would have increased the overall size of the wrist by at least 50%. Since the wrist was already exceeding the desired size and mass envelope, a stock gearhead was deemed infeasible and the determination was made to redesign the wrist using a non-backdrivable high-ratio transmission.

The second generation of the wrist was used to test more combinations of motors and gears to find the right combination of motor power and transmission ratio. The configuration of the motor and transmission in the second version ended up very closely resembling the final design. Unlike the final version, though, the second generation wrist used only a 2-stage transmission, with a Maxon EC-16 30 watt motor. The two stages of the transmission were identical to the final two stages of the final design: a set of interchangeable spur gears, and a worm gear set connected to the output. The key part of this design was the 30:1 worm gear set in the third and final stage. The inclusion of the worm gear allows a large gear ratio in a small volume, but the most important benefit is that it ensures the wrist will not be backdrivable. Since the worm gear cannot drive the worm, the passive torque capability of the wrist will be limited only by the thrust loads of the bearings that hold the shaft in place and the yield strength of the gears themselves. The performance of the two-stage transmission was promising enough that only small iterations were required for the final version of the wrist. The gear reduction brought the torque and speed of the wrist closer to the desired performance, but for the final version the motor was replaced by a smaller one with a stock transmission to meet the stated torque and speed requirements.

The performance and properties of the final version of the wrist far exceeded the first prototype. As can be seen in Fig. III-10, the second generation is far smaller in each dimension

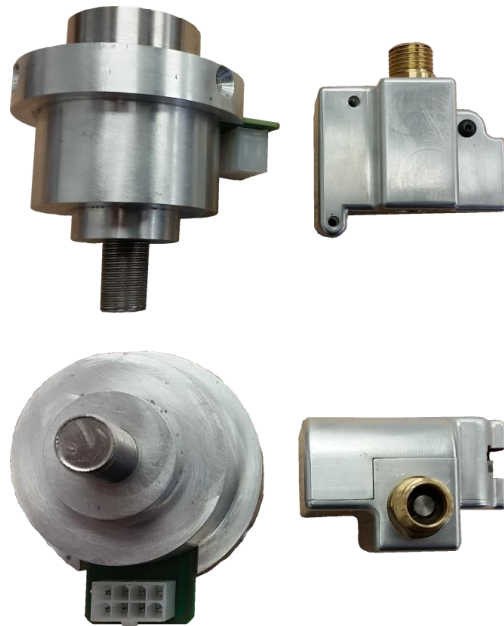


Fig. III-10. Side-by-side comparison of the first and final versions of the wrist.

than the first generation. It is also less than half the mass (175g vs. 370g), and has many times the maximum output torque, as presented in manuscript 2.

CHAPTER IV

COORDINATED CONTROL OF A PROSTHETIC WRIST

As stated previously, the overall goal of the transhumeral prosthesis design was to create a reliable and open testbed to develop and test control methodologies, much as the VMG Hand was used to great effect to iterate and assess the MMC. The transhumeral prosthesis described in chapter 3 was likewise used to develop coordinated control strategies of the wrist and elbow. There have been no examples in the literature to date of prosthesis controllers that offer true coordinated control of multiple prosthetic and natural joints, and so the challenge to create such a controller serves as the backdrop for the following chapter. The majority of the chapter is devoted to reprinting a manuscript that was submitted to the *IEEE Transactions on Neural Systems and Rehabilitation Engineering*, and is currently in review. The paper explores the use of alternative sensor information (specifically inertial data) to coordinate the movement of prosthetic joints with the user's sound joints. This manuscript is followed by an addendum that outlines some of the difficulties and strategies in interpreting IMU data into useable information. Not all of the principles explored in the addendum were eventually used in the presented controller, but they nevertheless provide important context for the interpretation of IMU data.

1. Manuscript 2: Inertial-Measurement-Based Synergistic Wrist Rotation Control for a Myoelectric Arm Prosthesis

1.1 Abstract

This paper describes a control method to enhance control of a myoelectric prosthesis containing a wrist rotator. Rather than exclusively utilize electromyogram (EMG) for the control of all myoelectric components, a method is described that utilizes inertial measurement (from 6-axis inertial measurement unit, or IMU) to control wrist rotation in coordination with (intact) upper arm movement. The method was implemented on a transradial prosthesis prototype with a powered wrist rotator and hand, and the efficacy of the method was assessed on five healthy subjects, who wore the prototype using an able-bodied adaptor, while performing activities of daily living (ADLs). The assessments compared the ability to perform ADLs using the combined EMG/IMU-based control method, with their ability to perform the same ADLs using a conventional, sequential EMG control approach. Results of the assessment indicate that subjects were able to perform the tasks 33% faster on average with the EMG/IMU-based method, relative to a conventional sequential EMG method.

1.2 Introduction

Upper extremity prostheses often entail multiple degrees-of-freedom (DOFs). A transradial prosthesis, for example, may include the combination of powered hand and wrist components, while a transhumeral prosthesis may include hand, wrist, and elbow components. Additionally, recent advances in compact and power dense motors, batteries, and microprocessors has increased the technological viability of further increasing the number of DOFs in such prostheses, including

the potential for multi-articulating hands [12], [19], and compact powered single and multi-DOF wrists [65]. The existing conventional method for control of multiple powered components is to use a two-site EMG interface, which provides a single (bidirectional) control input to the prosthesis, and to multiplex this input between powered components (or DOFs) via a brief muscular co-contraction (i.e., to switch between components). This sequential approach is generally inefficient (relative to simultaneous healthy movement) even with two DOFs to control, and becomes less efficient with more device DOFs. As such, a control approach that facilitates the simultaneous control of arm components would increase the viability and potential efficacy of arm prostheses with multiple powered components.

The need for improvement in arm prostheses is further indicated by surveys of upper extremity amputees. Such surveys indicate that fewer than 50% of amputees regularly use their prosthetic devices, with higher rejection rates present in transhumeral populations [15], [83]. Surveys of amputees additionally report a desire for devices with higher functionality, but also a desire for more intuitive and coordinated control [17]. Higher DOF prosthetic systems have the potential to provide greater functionality than lower DOF devices, but utilization of this potential will likely require more robust and intuitive control schemes than the current convention of two-site EMG multiplexing.

One means of simultaneous multi-joint prosthesis control is to use pattern recognition methods, such as those employed by [27], [29], [31], [32], [41], [84]. Pattern recognition approaches generally incorporate multiple (i.e., more than two) EMG sites and additionally consider these multiple EMG inputs over a finite window of time, both of which effectively increase the observability of a given intended movement. Based on this input, these methods train a model that classifies a pattern of EMG input into a given movement, and subsequently performs

the simultaneous control of multiple DOFs. Although such methods offer an effective approach to simultaneous movement, they generally require more than two EMG sites/electrodes, and since the methods use windows of data in time, they generally entail an increased input/output movement delay relative to the two-site EMG approach, which has no fundamental dependency on the time-history of (EMG) input. Another limitation of such methods is the sensitivity to the model of EMG input. EMG measurements can lack repeatability, due to factors such as movement or relocation of EMG electrodes, changes in skin conductivity, muscle fatigue, and variations in loading of the limb (which can change the relative amount of muscular co-contraction). The conventional two-site EMG approach, in contrast, is not a model-based approach, and therefore is less sensitive to EMG variability.

Given the challenges associated with limited availability and consistency of EMG information, an attractive possibility for improving the control of multi-DOF myoelectric arm prostheses is to supplement the EMG information with additional measurements. Given the recent availability, compactness, and low cost of microelectromechanical systems (MEMS) based 6-axis inertial measurement units (IMUs), supplementing EMG with inertial measurement information is one potentially promising means of enhancing multi-DOF myoelectric arm control. The use of IMU information to improve arm control was also suggested in a relatively recent perspectives article [85]. Among the possibilities, IMUs can be used to provide information regarding the motion of the user's residual limb, which can enable a controller to leverage existing movement synergies between the residual limb and prosthesis. This approach was also the motivation for a recent paper investigating such synergies [86]. It is the aim of this paper to use such synergies to inform use of IMU information to enhance prosthesis control, and specifically synergies between upper arm abduction and adduction and wrist rotation. It is hypothesized that such an approach

will enable faster performance in ADLs that are facilitated by wrist use, relative to existing sequential EMG controllers. Based on this hypothesis, the authors present herein the design, implementation, and assessment of a controller that integrates IMU and EMG information for the control of a multi-DOF arm. A control approach is described for the control of a transradial prosthesis consisting of a myoelectric hand and wrist rotator, where IMU measurement is used to control the wrist component based on movement synergies with the upper arm, and EMG is used to control the hand component. Since the control of the wrist is coordinated with the movement of the residual limb, the authors refer to the method as a coordinated control. Although the method is described, implemented, and assessed in the context of a transradial prosthesis, the method is also directly applicable to wrist rotation control in a transhumeral prosthesis.

1.3 Coordinated Control Approach

Individuals with upper extremity amputation generally compensate for the lack of wrist motion control during manipulation tasks with compensatory motions of their torso and upper arm [87], [88]. Observations of these motions indicate that individuals use a high degree of shoulder ab/adduction to accommodate wrist mobility deficiencies in rotation (i.e., pronation/supination), and when the shoulder range of motion is exceeded, shoulder ab/adduction is supplemented by movement of the torso in the frontal plane (i.e., sideways leaning). These empirical observations are supported by studies reported in [86], which give quantitative evidence for the coupling of shoulder ab/adduction and wrist pronation/supination in manipulation tasks. These motion synergies are an essential motivation for the controller described here, specifically with regard to coordinating the motion between the intact shoulder and prosthetic wrist, thereby facilitating control of the wrist joint, and reducing the need for compensatory movements of the torso.

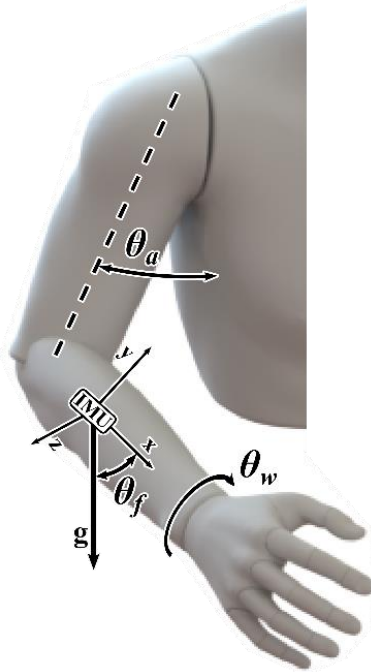


Fig. IV-1: Diagram showing location of IMU on arm and motions used in the coordinated controller.

Given the synergy between frontal plane upper arm motion and wrist rotation, the general control approach of the coordinated controller is to use the upper arm angle with respect to the vertical in the frontal plane (labeled as θ_a in Fig. IV-1) to control wrist rotation. In cases when the torso remains vertical, this angle will be the same as the shoulder ab/adduction angle. When the coordinated controller is active, the wrist (rotational) angular velocity is directly proportional to θ_a , as measured from a neutral position where the arm is slightly abducted away from the torso, but where the plane defined by the forearm and upper arm remains essentially in the sagittal. A positive value of θ_a (upper arm angle), which indicates shoulder abduction, results in a wrist angular velocity in the pronation direction, whereas a negative value (shoulder adduction) will generate a wrist angular velocity in the supination direction. Returning the upper arm to a small band around the neutral position (i.e., $\theta_0^{lb} \leq \theta_a \leq \theta_0^{ub}$) will result in zero angular velocity (i.e., will maintain a stationary wrist angle). The dead-band is defined by the lower and upper bounds

of upper arm angle (θ_0^{lb} and θ_0^{ub}). The coupling between upper arm angle and wrist rotation velocity ($\dot{\theta}_w$) is adjusted by specifying the velocity gains k_{ad} and k_{ab} for the adduction and abduction regions, respectively. Referring to the angles defined in Fig. IV-1, the wrist angular velocity when in the coordinated control mode is as follows:

$$\dot{\theta}_w = \begin{cases} k_{ad} * (\theta_a - \theta_0^{lb}), & \text{if } \theta_a < \theta_0^{lb} \\ 0, & \text{if } \theta_0^{lb} \leq \theta_a \leq \theta_0^{ub} \\ k_{ab} * (\theta_a - \theta_0^{ub}), & \text{if } \theta_a > \theta_0^{ub} \end{cases} \quad (IV-1)$$

The user activates or deactivates the synergistic wrist controller described by (IV-1) via a compound switching condition. Specifically, toggling into and out of (IV-1) requires the upper arm be held within the neutral position band ($\theta_0^{lb} \leq \theta_a \leq \theta_0^{ub}$), and also that the elbow be flexed so that the forearm elevation angle, as measured by the IMU and defined as θ_f , falls within a band specified by θ_t^{lb} and θ_t^{ub} (which corresponds to holding the forearm in an approximately vertical orientation). When these conditions are met for a period of 0.5 s, the IMU-based coordinated control of the wrist mode will be toggled on or off. Fig. IV-2 shows a state chart illustrating the switching conditions of the coordinated wrist controller, as compared to a traditional sequential EMG co-contraction controller.

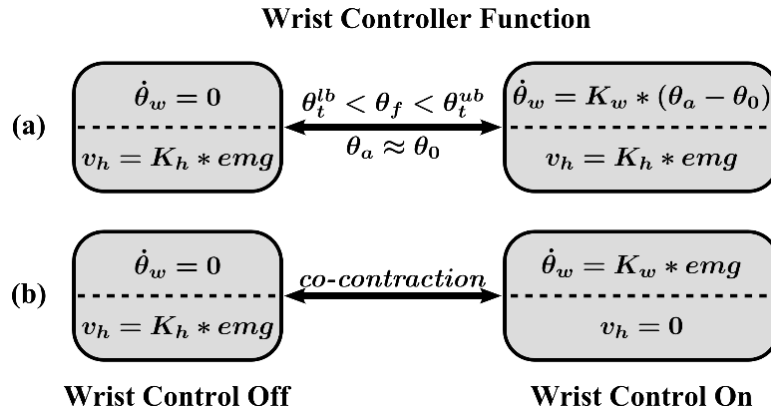


Fig. IV-2: Wrist controller configurations used in assessment. (a): IMU coordinated controller, IMU controlled wrist, EMG controlled hand. (b): EMG sequential controller, EMG controlled wrist and hand.

It is important to note that the synergistic wrist controller does not require the use of EMG, and as such, EMG is preserved for other use in the arm controller. In the case of a transradial prosthesis (such as the one used herein), EMG can therefore be used exclusively for control of the myoelectric hand, such that user can simultaneously control the hand and wrist by using simultaneous EMG and upper arm movement, respectively.

1.4 Assessment Procedure

The ability of the coordinated wrist controller to facilitate ADLs was assessed and compared with a conventional sequential EMG control approach in a set of experiments in which five healthy subjects wore a transradial prosthesis prototype using an able-bodied adaptor that allowed them to affix the prosthesis prototype to their intact arm. Details regarding the implementation of the controller in the prosthesis prototype are described in the following sections.

1.4.1 Prosthesis Prototype

The controller was implemented on a transradial arm prosthesis prototype consisting of a multigrasp hand and single DOF wrist rotator. The multigrasp hand used in the assessments is the Vanderbilt Multigrasp Hand (VMG), previously described in [12], and previously demonstrated in functional assessments in [10]. The VMG is capable of performing 8 different grasps and postures, which are accessed via a Multigrasp Myoelectric Controller (MMC), described in [6]. The MMC enables access to the set of grasps and postures provided by the VMG via a finite state machine that uses a (standard) two-site EMG input (i.e., EMG electrodes on the anterior and posterior aspects of the forearm, respectively), in addition to measurement of the hand

configuration and joint torques (technically, measurement of actuation tendon displacements and forces).

The wrist rotator used in the assessments was developed by the authors in order to enable the implementation and assessment of the coordinated wrist control approach described here. The wrist rotator unit consists of a single DOF in pronation/supination, and provides an experimentally measured active torque of 1.5 Nm and maximum rotational speed of 145 deg/s, as configured for the experiments described here. The wrist is non-backdrivable, and therefore provides a holding torque considerably greater than the 1.5 Nm of active torque. The prosthesis prototype was designed to be operated via an onboard microcontroller and battery, but for the purposes of the experiments reported here, the hand and wrist were tethered to a benchtop DC power supply and a PC running Simulink, which provided high-level arm control (i.e., equation (IV-1)) and facilitated data acquisition. The high-level PC control was supplemented by an embedded system on the arm, which performed IMU and EMG signal conditioning and low-level position and current control and motor commutation via a 50 MHz Microchip dsPIC33 and an 80MHz Microchip PIC32 microcontroller.

Coordinated Controller Parameters		
Parameter		Value
θ_a	θ_0^{ub}	25°
	θ_0^{lb}	-10°
θ_f	θ_t^{ub}	170°
	θ_t^{lb}	145°
k	k_{ab}	1.5
	k_{ad}	1.5

Table IV-1: Coordinated controller parameters.

The control law described in equation (IV-1) was implemented on the above hardware with the nominal controller parameters shown in Table IV-1. One of the subjects preferred thresholds that were 10-15 degrees offset from the nominal values, but most subjects performed the tasks with the settings in Table IV-1. In all cases, the thresholds were adjusted (as desired by the subject) during initial practice sessions, and were kept constant throughout all recorded assessments. Note that the dead band for θ_a is slightly offset in the abduction direction, which made it easier for subjects to perform the adduction movements required for wrist supination. Similarly, the trigger band for θ_f is slightly less than 90° , which compensates for the slight angle in the elbow when it is fully flexed.

1.4.2 Able-bodied Adapter and Motion Capture

Healthy subjects wore the prosthesis prototype using an able-bodied adapter, which allowed free elbow motion while immobilizing the intact wrist. The combined mass of the able-bodied adapter and transradial prosthesis prototype was approximately 1.5 kg. In addition to the adaptor and prosthesis, the subjects also donned a motion capture shirt on their upper body, which used 4 markers to track the location of their lower back, neck, upper arm, and wrist. A subject wearing

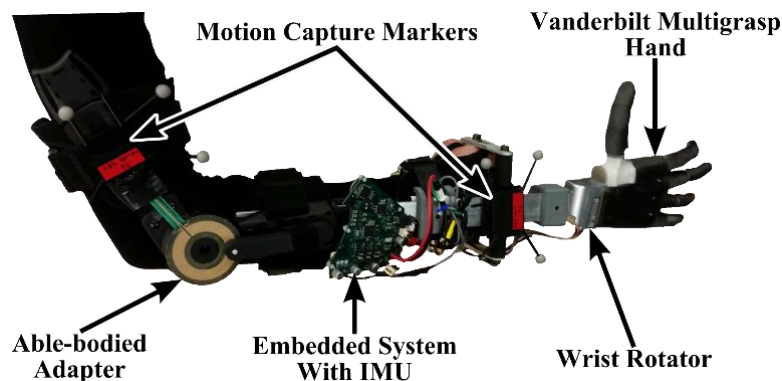


Fig. IV-3: Able-bodied adapter. Note that the brace immobilizes wrist rotation while allowing free elbow rotation.

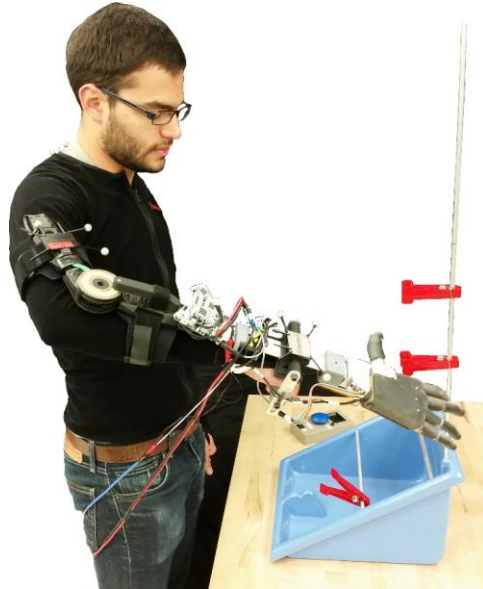


Fig. IV-4: Subject performing Clothespin Relocation Test (CRT).

the able-bodied adapter and motion capture markers is shown in Fig. IV-3. The same subject shown performing one of the assessment tasks with the experimental apparatus is shown in Fig. IV-4.

1.4.3 Obtaining Arm Angles from IMU Measurements

The arm orientation information used by the controller as described in the controller approach and defined in Fig. IV-1 was computed in real-time with data measured by a six-axis IMU mounted to the forearm of the prosthesis prototype. Fig. IV-1 illustrates the placement of the IMU on the forearm, showing the orientation of the local frame and the directions of upper arm frontal plane angle (θ_a), wrist pronation (θ_w), and forearm elevation (θ_f). In the case of a transradial prosthesis, the upper arm frontal plane angle (θ_a), which is used to control wrist rotation, cannot be measured directly by the IMU, since the IMU is located in the forearm. To calculate this angle, first the gravity vector is projected onto each of the principle planes of the IMU's coordinate frame as follows:

$$\theta_x^a = \text{atan2}\left(\frac{-a_z}{a_y}\right), \quad \theta_y^a = \text{atan2}\left(\frac{a_z}{a_x}\right), \quad \theta_z^a = \text{atan2}\left(\frac{a_x}{a_y}\right) \quad (\text{IV-2})$$

where θ_x^a denotes a rotation about the x-axis (in the yz plane), as measured by the accelerometer (similarly for θ_y^a and θ_z^a), and

$$\hat{g}^a = [a_x \quad a_y \quad a_z] \quad (\text{IV-3})$$

is the normalized gravity vector as measured by the accelerometer.

For the orientation of the IMU coordinate system shown in Fig. IV-1, θ_a is exactly equal to θ_x^a , since the gravity vector has significant components in only the yz plane if the elbow remains flexed at a right angle. In a similar fashion, $\theta_a = \theta_y^a$ if the elbow is in a fully flexed or fully extended configuration. Since the magnitude of the gravity vector in the corresponding plane gives an approximation of the contribution of that angle to the total motion, the calculation of the upper arm angle for any elbow configuration becomes:

$$\theta_a^a = \sqrt{a_y^2 + a_z^2} * \theta_x^a + \sqrt{a_x^2 + a_z^2} * \theta_y^a \quad (\text{IV-4})$$

This approximation of θ_a^a is then low-pass filtered at 3 Hz to determine a value for θ_a that is less sensitive to high frequency motions of the arm prosthesis. In this case, the angle measurement was not supplemented with gyroscope measurements, since the only relatively low-frequency angle information of was of interest (i.e., angle information was intentionally limited to lower frequencies to decrease sensitivity to high-frequency movements).

To calculate θ_f for the switching condition, the accelerometer-based angle estimates were fused with angular velocity measurements from the gyroscope to improve the improve the high-frequency content of the measurement and to mitigate effects of linear accelerations of the arm, both of which improved ability to toggle the coordinated controller on and off.

1.4.4 EMG Measurement

EMG signals were obtained via two bipolar Ag/AgCl disposable electrodes manufactured by Myotronics, Inc. The electrodes were attached to the anterior and posterior surfaces of the forearm in the approximate vicinity of the flexor carpi radialis and extensor carpi radialis muscles. A third electrode was attached to the elbow to serve as a ground reference for the EMG signals. The signals were differentially pre-amplified at a gain of 100 and then converted to a digital signal by a Texas Instruments ADS1298 8-channel analog front end with a 24-bit analog to digital converter. The digital signals were then sent to the PIC32, where they were low-pass filtered at 500 Hz to remove noise, high-pass filtered at 20 Hz to remove DC offset, and rectified. Finally, the signals were low-pass filtered at 2 Hz to provide an envelope representing the integration of local EMG.

The processed EMG were further normalized based on data obtained from each subject prior to their use of the controller. The user was directed to perform flexion, extension and co-contraction actions, and these average values were used to normalize the processed signals and set the co-contraction thresholds. To detect co-contractions, a 100-point moving average of each of the EMG signals was compared to these pre-recorded co-contraction thresholds. When both signals were above their respective thresholds, the system registers a co-contraction. The velocity reference for the hand controller (in the case of the coordinated control approach), or for both the hand and wrist controller (for the sequential approach) was calculated by taking the difference in the two EMG signals.

1.4.5 Assessment Tasks

The Clothespin Relocation Test (CRT) and a custom task designated as the Compound Manipulation Task (CMT) were collectively used to assess the performance of the hand/wrist

prosthesis controllers. These tasks were chosen over other assessments such as the Southampton Hand Assessment Procedure (SHAP) to focus the assessment on tasks that fundamentally involve both the wrist and hand. These tasks generally involve grasping, use of the wrist, and subsequent releasing of an object, and therefore entail collective use of both the hand and wrists joints.

The CRT is adapted from the Royland Graded Pinch Exerciser [89], and is shown in Fig. IV-4. Before the start of the task, three of the 2 lb clothespins (the red clothespins included in the test) were affixed to the middle horizontal rod. The test began when the subject started a timer with the contralateral hand (the hand not being assessed). The subject then relocated each of the three clothespins to the vertical rod one at a time, then returned each to the horizontal rod, and finally stopped the timer.

The CMT was designed by the authors specifically for this assessment, and uses several of the abstract objects included in the SHAP. The CMT task required each subject to manipulate several abstract objects in a specific sequence. Before the start of the task, each of the objects was placed in a respective location on the far side of the SHAP tray (relative to the subject), while each subject placed his or her manipulating hand at his or her side in a neutral pose (i.e., hand hanging by the side of the body). The subject then started the timer with his or her contralateral hand, and moved each object to its corresponding location on the near side of the SHAP tray. After the last object was placed, the timer was stopped. The subject was instructed to manipulate each object with the type of grasp specified by the SHAP for that specific object (i.e., a lateral pinch, cylindrical, or spherical grasp). Due to the specified sequence of object manipulation, restriction of the grasp type ensured that the subject was required to rotate his or her wrist approximately 90 degrees between each object so that the hand was properly oriented for each grasp. An illustration of this task is shown in Fig. IV-5. As such, this assessment task should characterize the efficacy

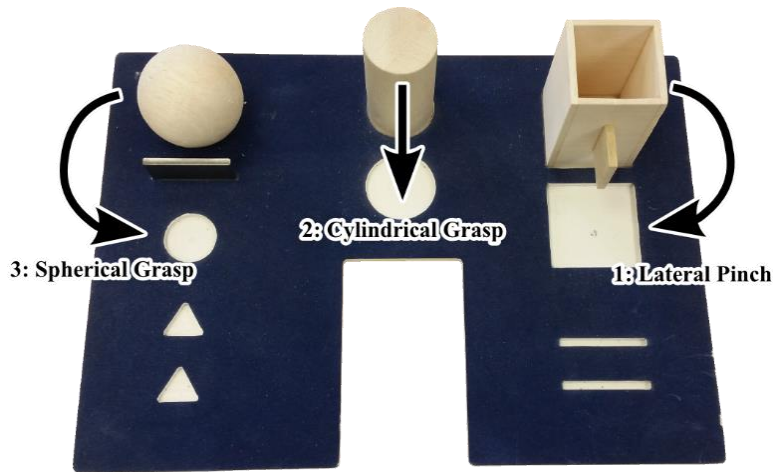


Fig. IV-5: Diagram illustrating the procedure of the Compound Manipulation Task (CMT).

of a wrist controller in re-orienting the wrist while performing a succession of manipulation tasks, each of which require a different wrist orientation.

As previously mentioned, the assessments were conducted using 5 able-bodied subjects (4 male, 1 female, mean age 27 yrs). The experiments were approved by the Vanderbilt University Institutional Review Board, and each subject provided informed consent. Over the course of several days, the 5 subjects performed both tasks multiple times with the coordinated controller, a sequential EMG controller, and additionally, for purposes of reference, for the cases of wearing the transradial prosthesis with a fixed wrist, and for the case without a prosthesis (i.e., manipulation with the healthy limb). For each subject, a complete set of assessments was performed for four cases: first without a prosthesis (i.e., with the healthy limb); second with the prosthesis without a wrist joint; third with the prosthesis with the coordinated controller; and fourth, with the prosthesis with the sequential EMG controller. Note that each case was completed on a different day, so it was assumed that any fatigue effects would not crossover from one case to another. Further, it was assumed that, by assessing the sequential EMG controller last, that case would most likely have the benefit of any long-term learning effects (i.e., the order was chosen to minimize bias towards

the coordinated control approach). Note that the order could have alternatively been randomized, although given the small number of subjects, the authors felt a consistent order of presentation that minimized bias toward the coordinated control approach was preferable.

For each case, subjects were given 5-10 minutes to practice each task. Other than the constraints on the specific grasps to be used in the CMT (as specified by the SHAP), no instructions or constraints were given regarding performance of each task. Subjects repeated each task until task completion times fell within 10% of the mean of the three most recent trials, after which it was assumed that task learning effects had effectively plateaued. Excluding the case without the prosthesis, subjects generally performed each task 6-10 times before task completion times plateaued. Once the learning plateau was achieved, only the last three trials were considered for the performance assessment (i.e., the data reported below is taken only from the three trials of each task performed after learning effects had substantially subsided).

1.5 Results

The performance of the subjects for each task was quantified through self-timing and recording torso motion via a motion capture system. Specifically, the motion of the torso in the coronal plane of the body (abduction of the torso) was used as the metric for assessing compensatory motion, since it is this motion that most directly causes pronation in the wrist. The total motion of the marker in question was represented by taking the average absolute abduction of the torso motion with respect to time. The mean of the absolute value of the signal is a convenient measure in that it is a single number that represents the amount of movement that exists in the signal relative to the neutral position of the torso. Distilling the coronal plane motion of the torso into a single number in this manner facilitates comparisons of torso movement between tasks.

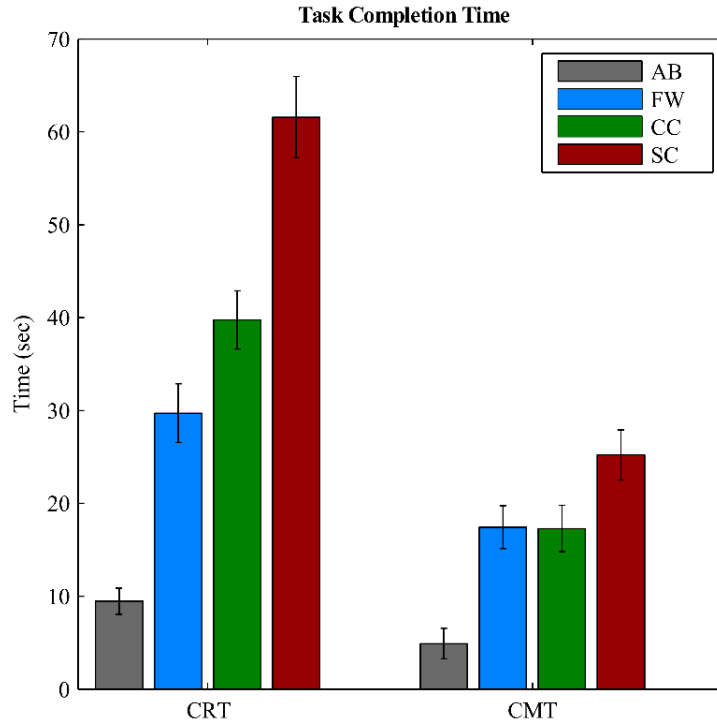


Fig. IV-6: Mean task completion time and standard deviations for able-bodied case (AB), fixed wrist case (FW), coordinated controller (CC), and sequential controller (SC).

Fig. IV-6 and Fig. IV-7 show the means and standard deviations of the completion times across all subjects for the 3 last trials of each case and task, along with the average frontal plane motion (also averaged across all subjects). The data corresponding to these figures for the prosthesis cases with coordinated and sequential controllers is displayed in Table IV-3. As shown in the table, the coordinated controller was on average characterized by a mean CRT completion time of 39.8 s and a mean CMT completion time of 17.3 s, while the sequential controller was characterized by corresponding times of 61.6 s and 25.2 s, respectively. As such, the coordinated controller enabled completion of the CRT and CMT on average 35.2% and 31.5% faster, respectively, than the sequential controller. A paired t-test of the respective data indicates that the differences in means in the completion times in all cases was statistically significant (with

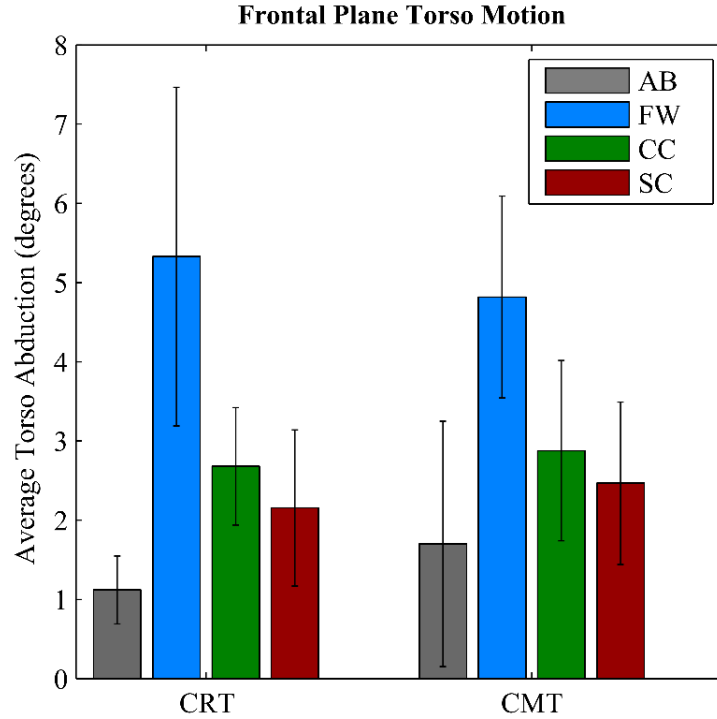


Fig. IV-7: Torso displacement means and standard deviations for able-bodied case (AB), fixed wrist case (FW), coordinated controller (CC), and sequential controller (SC).

confidence levels above 99%). Averaging the two tasks the coordinated controller enabled subjects to complete the tasks 33.3% faster than the sequential controller.

As also reported in Table IV-3, the coordinated controller was on average characterized by an average rectified mean torso motion of 2.7 and 2.9 deg, respectively, for the CRT and CMT, while the sequential controller was on average characterized by a mean torso motion of 2.2 and 2.5 deg, respectively, for the two tasks. As indicated by the relatively large standard deviations (relative to the mean values) in Table IV-3, however, and as verified by a paired t-test of the motion data, the differences in means in the torso motion is not statistically significant (confidence levels of 24% and 15% for the CRT and CMT, respectively). As such, the results indicate that the coordinated controller enables on average a 33.3% faster task completion relative to a sequential control approach, with the same level of torso motion.

Coordinated Control Performance Data			
Measurement	Task	Mean	Std. Deviation
Time (s)	CRT	39.8	3.13
	CMT	17.3	2.5
Motion (deg)	CRT	2.68	0.741
	CMT	2.88	1.14
Sequential Control Performance Data			
Measurement	Task	Mean	Std. Deviation
Time (s)	CRT	61.6	4.38
	CMT	25.2	2.70
Motion (deg)	CRT	2.15	0.986
	CMT	2.47	1.02

Table IV-3: Performance data for the coordinated and sequential controllers.

Coordinated Controller vs. Sequential Controller			
Measurement	Task	Percent Difference	P-Value
Time	CRT	35.2*	0.00095*
	CMT	31.5*	0.00048*
Motion	CRT	-34.9	0.24
	CMT	-18.0	0.15

Table IV-2: Statistical analysis of coordinated controller compared with sequential controller.

1.6 Discussion

Observations of the trials and feedback from the subjects indicate that the significant reduction in time is partially due to the uninterrupted hand control present in the coordinated controller. With the sequential controller, a switching signal was required whenever control was transferred from the wrist to the hand. In tasks requiring frequent switching between hand and wrist control, the time lost to switching and to mentally readjusting control strategies became significant. This was not a factor with coordinated controller, since the always-active hand and wrist control enabled the

subject to make movements that were faster and generally less discrete. Additionally, qualitative feedback from the subjects indicated that using the coordinated controller was less tiresome than the fixed wrist case, and required less concentration and mental effort than the sequential controller.

The motion data obtained from the fixed wrist configurations confirmed the trends stated in the literature, in which compensatory motions are required in the absence of wrist rotation. Specifically, the fixed wrist configuration resulted in much more torso motion, and these differences were statistically significant. However, the completion times for the fixed wrist case were also lower on average than when using a wrist rotator, with either the coordinated or sequential wrist controllers, as indicated in Fig. IV-6.

1.7 Conclusion

In this paper, the design and assessment of an IMU based coordinated wrist controller for a prosthetic wrist rotator was presented. The controller uses the motion of a user's upper arm as measured by an IMU to control wrist rotation. The efficacy of the controller was assessed on 5 able-bodied subjects, and compared to a sequential EMG wrist controller, while performing two tasks designed to represent activities of daily living that would be facilitated by wrist rotation. Based on the assessment, the coordinated control approach enabled subjects to complete tasks on average 33.3% faster than the sequential controller. As such, this work indicates that IMU information may have value with respect to improving the control of upper extremity myoelectric prostheses, particularly prostheses with multiple powered components. The controller should be evaluated in studies involving upper extremity amputee subjects to fully assess its value in facilitating ADLs.

2. Addendums to Manuscript 3

2.1 IMU Data Interpretation and Sensor Fusion

In early versions of the coordinated wrist controller, it was assumed that the complete orientation of the forearm and/or upper arm would be required to make control decisions based on the motion of the arm. Though the final form of the controller only required measurements from three accelerometer axes and one gyroscope axis, several methods of producing an accurate measurement of the arm's orientation in three-dimensional space were investigated before settling on the simplified version. This section gives a brief background to some of the nomenclature and existing strategies of sensor fusion, and then details the efforts taken to create a sensor fusion algorithm for the wrist controller.

2.1.1 Mathematical Representations of Rotation

In this section, vectors and axes will be expressed either in the fixed (or world), or the body (or moving) frame. The fixed frame is fixed to the earth and does not move, whereas the body frame is attached to the IMU and moves with the arm. To define an orientation (i.e. a relative rotation) in three-dimensional space, three independent measurements are required. The most general representation of rotations uses a 3x3 orthogonal matrix, which is actually 6 independent variables, meaning that several are redundant. This representation has the advantage of making vector transformations a simple act of matrix and vector multiplication. However, the downside is the larger number of variables, and the increase in operations required for each transformation.

Euler angles are the simplest representation of a spatial rotation, and are constructed using only three rotations. With Euler angles, any rotation can be expressed as three rotations about three

different axes, i.e. a rotation θ about the Z-axis, followed by a rotation ϕ about the new Y-axis, and then a rotation ψ about the Z-axis again. This example would be referred to as ZYZ Euler angles. There are many different valid combinations of Euler angles that can be used to express rotation (for example XYZ, or YXZ), and different representations can be optimal depending on the specific application. Euler angles have the advantage of being easily translatable into physical quantities, and requiring the least number of variables to track (the minimum of 3 independent measurements). Unfortunately, Euler angle representations also fall victim to singularities, also referred to as gimbal lock when referring to a physical system. This occurs when two of the rotation axes align, leading to a situation where not every orientation change can be expressed by a change in the Euler angles. In other words, the singularity causes the corresponding rotation matrix to drop rank, and the system to lose a degree of freedom.

Quaternions are a 4-dimensional complex vector quantity consisting of a scalar real component and a vector imaginary component that are in some ways a compromise between Euler angles and rotation matrices. The added degree of redundancy compared to Euler angles eliminates singularities, while still having fewer variables than rotation matrices, and requiring fewer operations to perform transformations. Quaternions can represent both vectors and rotations, and have a special set of mathematical operations for multiplication and applying rotation transformations. Though quaternions do not directly translate into any physical quantity, they can be readily constructed from an axis-angle rotation formulation, in which a rotation is expressed as a finite rotation about a single axis.

2.1.2 Sensor Fusion

When calculating orientation, in general the accelerometer and magnetometer signals are more suitable for low frequency information, while the gyroscope signals are more suitable for high frequency information. The accelerometer and magnetometer measurements are essentially the body-frame representation of the gravity and magnetic north vectors, respectively, and thus provide an absolute reference for orientation. The transformation between the fixed and body coordinate frames at any point can be determined by comparing the measurements to the representations of those vectors in the fixed frame. However, this transformation is only really valid when the IMU is stationary, as any movement will cause an acceleration, resulting in accelerometer measurements that are not entirely caused by gravity.

On the other hand, the gyroscope signals provide angular velocities, but there are no steady-state values they can be compared to at each time step. The velocities can be integrated to give a measurement of the principal angles of rotation (in essence, XYZ Euler angles), but random noise in the signals will inevitably cause those integrated values to drift randomly. This causes significant inaccuracies in the steady state orientation measurement over time, resulting in a measurement that is used best as a relative reference for orientation.

The challenge of sensor fusion is to combine the gyroscope measurements, which are accurate over short time scales or when the IMU is in motion, with the accelerometer and magnetometer measurements, which are accurate over long time scales or when the IMU is stationary. A popular method of fusing the sensor information is to use a Kalman filter, which uses statistical analysis and the estimated variance of the signals to combine multiple unreliable measurements to produce a single, more precise measurement. The Kalman filter has been used to great effect in research and commercial applications of IMU sensor fusion, but was not fully

investigated for the coordinated wrist controller described here due to the complexity in formulation and implementation.

A somewhat more straightforward method for sensor fusion is to use a complementary filter. A complementary filter simply applies a high-pass filter to the gyroscope measurements (removing the steady state content in the signal), applies a low-pass filter to the accelerometer and magnetometer measurements (removing the transient content in the signals), and adds them together. The cutoff frequencies for each filter in this case are equal, so that the overall filter has a unity gain throughout all frequency ranges. A complementary filter has the advantage of being straightforward in implementation and conceptualization, and still very effective at fusing different signals. As such, it was eventually used in the final controller design to fuse the partial orientation information that ended up being relevant to the controller.

2.1.3 Calculating Orientation from Reference Vectors

A complementary filter is a straightforward way to combine quantities obtained from multiple signals, but the process of converting raw sensor data from very different types of sensors into forms that can be readily combined is not trivial. The method outlined here involves producing a quaternion from each of the signals, and then combining the different quaternions using the complementary filter. For the gyroscope, it is most convenient to express the small rotation at each time step as a differential quaternion. This is because finite rotations are not commutative, so if each gyroscope signal is integrated and then combined with the other measurements, the results will not be accurate. Infinitesimal rotations, however, can be applied in any order, and can be obtained from the gyroscope measurements by multiplying the velocity measurement by the

sample time. This gives three differential rotations about each principal axis. In general, a quaternion can be calculated from an axis-angle representation as follows:

$$q = \hat{n}_x \sin\left(\frac{\theta}{2}\right) \hat{i} + \hat{n}_y \sin\left(\frac{\theta}{2}\right) \hat{j} + \hat{n}_z \sin\left(\frac{\theta}{2}\right) \hat{k} + \cos\left(\frac{\theta}{2}\right) \quad (\text{IV-5})$$

Using small angle approximations and combining three such quaternions, the differential quaternion representing the gyroscope measurements at each time step is:

$$q_g = \frac{\omega_x dt}{2} \hat{i} + \frac{\omega_y dt}{2} \hat{j} + \frac{\omega_z dt}{2} \hat{k} + 1 \quad (\text{IV-6})$$

The first algorithm used to find a quaternion from the absolute sensors was derived from one used in the transfemoral prostheses project in the Center for Intelligent Mechatronics, and used only the accelerometer measurements, since only a 6-axis IMU was available. This method involved finding an axis and angle that represents the rotation between the fixed and body frames, and then converting that into a quaternion. If the accelerometer measurement gives a normalized gravity vector as measured in the body frame of

$$\hat{g}_b = [a_x \quad a_y \quad a_z] \quad (\text{IV-7})$$

and the gravity vector in the fixed frame is expressed as

$$\hat{g}_f = [0 \quad -1 \quad 0] \quad (\text{IV-8})$$

then the axis of rotation that transforms the fixed frame into the body frame is equal to the cross product of equation IV-7 and IV-8.

$$\hat{n} = \hat{g}_b \times \hat{g}_f = [a_z \quad 0 \quad -a_x] \quad (\text{IV-9})$$

The angle of rotation can be found from the dot product as follows:

$$\theta = \cos^{-1}(\hat{g}_b \cdot \hat{g}_f) \quad (\text{IV-10})$$

Once the axis and angle have been calculated, the rotation can be expressed as a quaternion using equation IV-5:

$$q_a = \hat{n}_x \sin\left(\frac{\theta}{2}\right) \hat{i} + 0\hat{j} + \hat{n}_z \sin\left(\frac{\theta}{2}\right) \hat{k} + \cos\left(\frac{\theta}{2}\right) \quad (\text{IV-11})$$

The problem with this formulation is that while it works very well at calculating the orientation of the IMU in the planes that contain the gravity vector (i.e. the vertical planes), it provides absolutely no heading information (i.e. orientation in the horizontal plane). This can be seen from equation IV-11: since the \hat{j} component of the quaternion is always zero, there will always be some orientation information that can never be expressed by this quaternion. Conceptually, this makes sense: if a rigid body is rotated about the gravity vector, the perceived force of gravity on the body at its center of mass will not change at all. While this deficiency was not significant in a lower limb prosthesis where the vast majority of motion takes place in the vertical plane, the lack of heading information seriously degrades the ability of the IMU to determine certain shoulder motions, such as flexion/extension when the shoulder is abducted.

Thus, in order to fully characterize motion of the upper arm, it was necessary to utilize a 9-axis IMU which contains a magnetometer in addition to an accelerometer. Since the magnetometer provides another reference vector, this one pointing to magnetic north, it can provide the heading information that the accelerometer-based algorithms lacked. Since finite rotations are not commutative and cannot be easily added together, the accelerometer and magnetometer quaternions cannot be calculated independently and later added. Instead, a single quaternion must be calculated using both measurements. One method of achieving this is to create an orthonormal basis for the body frame using the two measured vectors. If \hat{g}_b is the normalized measured gravity vector, and \hat{m}_b is the normalized measured magnetic north vector, one such basis would be:

$$\hat{b}_1 = \|\hat{g}_b \times \hat{m}_b\|, \quad \hat{b}_2 = -\hat{g}_b, \quad \hat{b}_3 = \|\hat{b}_1 \times \hat{b}_2\| \quad (\text{IV-12})$$

Due to the properties of rotations, these can be used to create a rotation matrix directly:

$$R_{f-b} = [\hat{b}_1 \quad \hat{b}_2 \quad \hat{b}_3] \quad (\text{IV-13})$$

Since the basis vectors were chosen such that the corresponding rotation matrix expressed in the fixed frame is identity, this matrix represents the rotation matrix of the body frame relative to the fixed frame.

This method for calculating the rotation is straightforward and simple, but it gives the added complexity of transforming the rotation matrix into a quaternion in order to be combined with the gyroscope measurement. This conversion is non-unique, and sorting out all of the signs of the quaternions and managing the wrap-around effects dynamically were very difficult. It is far more desirable to calculate the quaternion from the two vectors directly: several methods for this are explored in [90]. These methods were developed for the attitude determination of spacecraft using vectors to the sun and earth's magnetic field, but are readily applied to this case. Using the direct quaternion method outlined in this paper which treats both measurements equally, the quaternion calculated from the two absolute reference vectors is:

$$q_a = c * [(\hat{g}_b - \hat{g}_f) \times (\hat{m}_b - \hat{m}_f), \quad \hat{m}_b \cdot \hat{m}_f - \hat{g}_b \cdot \hat{g}_f] \quad (\text{IV-14})$$

where c is the normalization factor required to make q_a a unit quaternion.

Once the two quaternion estimations are calculated from the gyroscope (q_g) and the absolute reference sensors (q_a), they are passed through the complementary filter and combined. The gyroscope quaternion is high-pass filtered, the absolute reference quaternion is low-pass filtered, and then they are multiplied to combine the rotations and produce an aggregate vector. Unfortunately, the fused orientation was never brought to the point where it was completely reliable, since the noise inherent in the accelerometer and magnetometer signals proved very problematic. Several different methods were tried to form the quaternions and combine them, including preliminary investigation into the implementation of a Kalman filter, but those efforts

were abandoned when it became clear that the desired functionality of the wrist controller could be achieved without a complete estimation of the arm orientation. Since the controller only needed a few specific measurements (e.g. forearm elevation and shoulder abduction), those values could be calculated directly from the sensor data as described in manuscript 3, rather than derived from the orientation quaternion. This greatly simplified the algorithm and made it far more reliable.

CHAPTER V

CONCLUSION

This dissertation has presented the design and characterization of an upper extremity prosthetic system. Work on this project has focused on a balance between mechanical design, device assessment, and controller design. The mechanical design work presented here has culminated in the construction of a complete, self-contained transradial prosthesis, including a multi-grasp hand and powered wrist rotator. Through the process of many design iterations, these devices have proven capable of performing the vast majority of activities of daily living that a typical amputee would find necessary. These capabilities were characterized in the abstract by testing the raw speed, force, and functionality of each device, and also in more practical assessments. These assessments included many occasions where amputee and able-bodied test subjects used the devices to perform simulated activities of daily living, proving the utility of the designs in real-world situations. Finally, a novel wrist controller was presented which enables the coordinated control of multiple prosthetic and sound joints. This controller uses the orientation of the intact upper arm to control the rotation of the wrist, leaving EMG signals free to control the hand. This technique can be readily applied to transradial or transhumeral prostheses, providing more convenient and natural access by amputees to the DOFs granted by advanced multi-joint prostheses. In aggregate, the completed prosthesis described here represents a convenient testbed for the development of additional novel upper limb controllers, which will hopefully eventually be made available to enhance the capabilities of amputees.

1. Recommended Future Work

As previously mentioned, the hardware presented in this dissertation was designed to be a versatile and effective testbed for the development of upper extremity control strategies. To this end, future work on this project should include further refinement of existing controllers, and the application of the IMU-based coordinated controller to additional limbs. Specifically, there is a need to produce intuitive controllers for transhumeral and shoulder disarticulation prostheses. As the level of amputation increases and more natural joints are missing, the problem of finding control signals and the challenges amputees face in using a prosthesis become more and more severe. In future work, the use of IMU signals to control both the elbow and the wrist should be investigated as a way to provide much needed control inputs to supplement EMG signals.

Additionally, to fully investigate the efficacy of these controllers, they should be tested on amputee subjects in addition to able-bodied subjects. Amputees who have adapted to use of a prosthesis have very different movement strategies than able bodied subjects, and it would be useful to see if the performance trends are consistent across both groups. This would also provide more compelling evidence for the effectiveness of these IMU-based coordinated controllers in real situations.

REFERENCES

- [1] T. E. Wiste, S. A. Dalley, T. J. Withrow, M. Goldfarb, T. E. Wiste, T. J. Withrow, and M. Goldfarb, "Design of a Multifunctional Anthropomorphic Prosthetic Hand with Extrinsic Actuation," *IEEE/ASME Trans. Mechatronics*, vol. 14, no. 6, pp. 699–706, 2009.
- [2] S. A. Dalley, T. E. Wiste, H. A. Varol, and M. Goldfarb, "A Multigrasp Hand Prosthesis for Transradial Amputees," in *IEEE International Conference of the Engineering in Medicine and Biology Society*, 2010, pp. 5062–5065.
- [3] S. A. Dalley, H. A. Varol, and M. Goldfarb, "Continuous Position and Force Control of a Multigrasp Myoelectric Transradial Prosthesis," in *Myoelectric Controls/Powered Prosthetics Symposium (MEC)*, 2011, pp. 79–81.
- [4] T. E. Wiste, S. A. Dalley, H. A. Varol, and M. Goldfarb, "Design of a Multigrasp Transradial Prosthesis," *ASME J. Med. Devices*, vol. 5, no. 3, pp. 1–7, 2011.
- [5] S. A. Dalley, H. A. Varol, and M. Goldfarb, "Multigrasp Myoelectric Control for a Transradial Prosthesis," in *IEEE International Conference on Rehabilitation Robotics*, 2011, pp. 1–6.
- [6] S. A. Dalley, H. A. Varol, and M. Goldfarb, "A method for the control of multigrasp myoelectric prosthetic hands," *IEEE Trans. Neural Syst. Rehabil. Eng.*, vol. 20, no. 1, pp. 58–67, 2012.
- [7] N. A. Alshammary, S. A. Dalley, and M. Goldfarb, "Assessment of a multigrasp myoelectric control approach for use by transhumeral amputees," in *IEEE International Conference of the Engineering in Medicine and Biology Society*, 2012, pp. 968–971.
- [8] D. A. Bennett, S. A. Dalley, and M. Goldfarb, "Design of a hand prosthesis with precision and conformal grasp capability," in *IEEE International Conference of the Engineering in Medicine and Biology Society*, 2012, pp. 3044–3047.
- [9] S. A. Dalley, D. A. Bennett, and M. Goldfarb, "Preliminary functional assessment of a multigrasp myoelectric prosthesis," in *IEEE International Conference of the Engineering in Medicine and Biology Society*, 2012, pp. 4172–4175.
- [10] S. A. Dalley, D. A. Bennett, and M. Goldfarb, "Functional assessment of a Multigrasp Myoelectric prosthesis: An amputee case study," in *Proceedings - IEEE International Conference on Robotics and Automation*, 2013, pp. 2640–2644.

- [11] S. A. Dalley, D. A. Bennett, and M. Goldfarb, "Functional assessment of the vanderbilt multigrasp myoelectric hand: A continuing case study," *Engineering in Medicine and Biology Society (EMBC), 2014 36th Annual International Conference of the IEEE*. pp. 6195–6198, 2014.
- [12] D. A. Bennett, S. A. Dalley, D. Truex, and M. Goldfarb, "A Multigrasp Hand Prosthesis for Providing Precision and Conformal Grasps," *IEEE/ASME Trans. Mechatronics*, vol. 20, no. 4, pp. 1697–1704, 2015.
- [13] K. Ziegler-Graham, E. Mackenzie, P. Ephraim, T. Trivison, and R. Brookmeyer, "Estimating the Prevalence of Limb Loss in the United States: 2005 to 2050," *Arch. Phys. Med. Rehabil.*, vol. 89, no. 3, pp. 422–429, 2008.
- [14] NLLIC-Staff, "Amputation Statistics by Cause: Limb Loss in the United States," National Limb Loss Information Center, 2008.
- [15] J. Davidson, "A survey of the satisfaction of upper limb amputees with their prostheses, their lifestyles, and their abilities," *J Hand Ther*, vol. 15, no. 1, pp. 62–70, 2002.
- [16] P. J. Kyberd, D. J. Beard, J. J. Davey, and J. D. Morrison, "A Survey of Upper-Limb Prosthesis Users in Oxfordshire," *J. Prosthetics Orthot.*, vol. 10, no. 4, pp. 85–91, 1998.
- [17] D. J. Atkins, D. C. Y. Heard, and W. H. Donovan, "Epidemiological overview of individuals with upper-limb loss and their reported research priorities," *J. Prosthetics Orthot.*, vol. 8, no. 1, pp. 2–10, 1996.
- [18] M. Zecca, S. Micera, M. C. Carrozza, and P. Dario, "Control of multifunctional prosthetic hands by processing the electromyographic signal," *Crit. Rev. Biomed. Eng.*, vol. 30, no. 4–6, pp. 459–485, 2002.
- [19] J. T. Belter, J. L. Segil, A. M. Dollar, and R. F. Weir, "Mechanical design and performance specifications of anthropomorphic prosthetic hands: A review," *J. Rehabil. Res. Dev.*, vol. 50, no. 5, p. 20, 2013.
- [20] Y. Kamikawa and T. Maeno, "Underactuated five-finger prosthetic hand inspired by grasping force distribution of humans," in *IEEE/RSJ Int. Conf. Intelligent Robots and Systems*, 2008, pp. 717–722.
- [21] P. J. Kyberd and J. L. Pons, "A comparison of the Oxford and Manus intelligent hand prostheses," in *Proc. IEEE Int. Conf. Robotics and Automation*, 2003, vol. 3, pp. 3231–3236.

- [22] L. Zollo, S. Roccella, E. Guglielmelli, M. C. Carrozza, and P. Dario, "Biomechatronic design and control of an anthropomorphic artificial hand for prosthetic and robotic applications," *IEEE/ASME Trans. Mechatronics*, vol. 12, no. 4, pp. 418–429, 2007.
- [23] C. Cipriani, M. Controzzi, and M. C. Carrozza, "The SmartHand transradial prosthesis," *J. Neuroeng. Rehabil.*, vol. 8, no. 1, 2011.
- [24] S. Jung and I. Moon, "Grip force modeling of a tendon-driven prosthetic hand," in *Int. Conf. Control, Automation and Systems*, 2008, pp. 2006–2009.
- [25] C. M. Light and P. H. Chappell, "Development of a lightweight and adaptable multiple-axis hand prosthesis," *Med. Eng. Phys.*, vol. 22, no. 10, pp. 679–684, 2000.
- [26] Y. Losier, A. Clawson, A. Wilson, E. Scheme, K. Englehart, P. Kyberd, and B. Hudgins, "An Overview of the UNB Hand System," in *Myoelectric Controls/Powered Prosthetics Symp.*, 2011, vol. 1, pp. 251–254.
- [27] F. C. P. Sebelius, B. N. Rosén, and G. N. Lundborg, "Refined myoelectric control in below-elbow amputees using artificial neural networks and a data glove," *J. Hand Surg. Am.*, vol. 30, no. 4, pp. 780–789, 2005.
- [28] M. Vuskovic and D. Sijiang, "Classification of prehensile EMG patterns with simplified fuzzy ARTMAP networks," in *International Joint Conference on Neural Networks*, 2002, vol. 3, pp. 2539–2544.
- [29] J. Zhao, Z. Xie, L. Jiang, H. Cai, H. Liu, and G. Hirzinger, "EMG control for a five-fingered underactuated prosthetic hand based on wavelet transform and sample entropy," in *IEEE/RSJ International Conference on Intelligent Robots and Systems*, 2006, pp. 3215–3220.
- [30] L. H. Smith, L. J. Hargrove, B. A. Lock, and T. A. Kuiken, "Determining the optimal window length for pattern recognition-based myoelectric control: Balancing the competing effects of classification error and controller delay," *Ieee Trans. Neural Syst. Rehabil. Eng.*, vol. 19, no. 2, pp. 186–192, 2011.
- [31] L. Hargrove, Y. Losier, B. Lock, K. Englehart, and B. Hudgins, "A real-time pattern recognition based myoelectric control usability study implemented in a virtual environment," in *IEEE International Conference of the Engineering in Medicine and Biology Society*, 2007, pp. 4842–4845.

- [32] G. Li, A. E. Schultz, and T. A. Kuiken, "Quantifying Pattern Recognition-Based Myoelectric Control of Multifunctional Transradial Prostheses," *Neural Syst. Rehabil. Eng. IEEE Trans.*, vol. 18, no. 2, pp. 185–192, 2010.
- [33] J. C. Baits, R. W. Todd, and J. M. Nightingale, "The feasibility of an adaptive control scheme for artificial prehension," *Proc. Inst. Mech. Eng.*, vol. 183, no. 3J, pp. 54–59, 1968.
- [34] M. Rakic, "The 'Belgrade Hand Prosthesis,'" *Proc. Inst. Mech. Eng.*, vol. 183, no. 3J, pp. 60–67, 1968.
- [35] J. M. Nightingale, "Microprocessor control of an artificial arm," *J. Microcomput. Appl.*, vol. 8, no. 2, pp. 167–173, 1985.
- [36] P. H. Chappell and P. J. Kyberd, "Prehensile control of a hand prosthesis by a microcontroller," *J. Biomed. Eng.*, vol. 13, no. 5, pp. 363–369, 1991.
- [37] P. J. Kyberd, O. E. Holland, P. H. Chappell, S. Smith, R. Tregidgo, P. J. Bagwell, and M. Snaith, "MARCUS: a two degree of freedom hand prosthesis with hierarchical grip control," *IEEE Trans. Rehabil. Eng.*, vol. 3, no. 1, pp. 70–76, 1995.
- [38] C. M. Light, P. H. Chappell, B. Hudgins, and K. Englehart, "Intelligent multifunction myoelectric control of hand prostheses," *J. Med. Eng. Technol.*, vol. 26, no. 4, pp. 139–146, 2002.
- [39] D. P. J. Cotton, A. Cranny, P. H. Chappell, N. M. White, and S. P. Beeby, "Control Strategies for a Multiple Degree of Freedom Prosthetic Hand," in *Measurement & Control*, 2006, vol. 40, no. 1, pp. 24–27.
- [40] C. Cipriani, F. Zaccone, S. Micera, and M. C. Carrozza, "On the shared control of an EMG-controlled prosthetic hand: analysis of user-prosthesis interaction," *IEEE Trans. Robot.*, vol. 24, no. 1, pp. 170–184, 2008.
- [41] L. Miller, R. Lipschutz, K. Stubblefield, B. Lock, H. Huang, T. Williamsiii, R. Weir, and T. Kuiken, "Control of a Six Degree of Freedom Prosthetic Arm After Targeted Muscle Reinnervation Surgery," *Arch. Phys. Med. Rehabil.*, vol. 89, no. 11, pp. 2057–2065, 2008.
- [42] C. Sollerman and A. Ejeskär, "Sollerman Hand Function Test: A Standardised Method and its Use in Tetraplegic Patients," *Scand. J. Plast. Reconstr. Surg. Hand Surg.*, vol. 29, no. 2, pp. 167–176, 1995.

- [43] H. Huang, L. Jiang, Y. Liu, L. Hou, H. Cai, and H. Liu, "The Mechanical Design and Experiments of HIT/DLR Prosthetic Hand," in *IEEE Int. Conf. Robotics and Biomimetics*, 2006, pp. 896–901.
- [44] I. N. Gaiser, C. Pylatiuk, S. Schulz, A. Kargov, R. Oberle, and T. Werner, "The FLUIDHAND III: A Multifunctional Prosthetic Hand," *Am. Acad. Orthotists Prosthetists*, vol. 21, no. 2, p. 6, 2009.
- [45] A. D. Deshpande, Z. Xu, M. J. V Weghe, B. H. Brown, J. Ko, L. Y. Chang, D. D. Wilkinson, S. M. Bidic, and Y. Matsuoka, "Mechanisms of the Anatomically Correct Testbed Hand," *IEEE/ASME Trans. Mechatronics*, vol. 18, no. 1, p. 12, 2013.
- [46] M. C. Carrozza, B. Massa, S. Micera, R. Lazzarini, M. Zecca, and P. Dario, "The Development of a Novel Prosthetic Hand-Ongoing Research and Preliminary Results," *IEEE/ASME Trans. Mechatronics*, vol. 7, no. 2, pp. 108–114, 2002.
- [47] C. L. Taylor and R. J. Schwarz, "The Anatomy and Mechanics of the Human Hand," *Artif. Limbs*, vol. 2, no. 2, pp. 22–35, 1955.
- [48] M. R. Cutkosky, "On grasp choice, grasp models, and the design of hands for manufacturing tasks," *Robot. Autom. IEEE Trans.*, vol. 5, no. 3, pp. 269–279, 1989.
- [49] N. Smaby, M. E. Johansen, B. Baker, D. E. Kenney, W. M. Murray, and V. R. Hentz, "Identification of Key Pinch Forces Required to Complete Functional Tasks," *J. Rehabil. Res. Dev.*, vol. 41, no. 2, pp. 215–224, 2004.
- [50] R. G. Radwin and S. Oh, "External Forces in Submaximal Five-Finger Static Pinch Prehension," *Ergonomics*, vol. 35, no. 3, pp. 275–288, 1992.
- [51] R. F. Weir, "Design of Artificial Arms and Hands for Prosthetic Applications," in *Standard Handbook of Biomedical Engineering and Design*, M. Kutz, Ed. New York: McGraw-Hill, 2003, pp. 32.1–32.61.
- [52] D. H. Silcox, M. D. Rooks, R. R. Vogel, and L. L. Fleming, "Myoelectric Prostheses. A Long Term Follow up and a Study of the use of Alternate Prostheses," *J. Bone Jt. Surgery-American Vol.*, vol. 75A, no. 12, pp. 1781–1789, 1993.
- [53] A. Kargov, C. Pylatiuk, R. Oberle, H. Klosek, T. Werner, W. Roessler, and S. Schulz, "Development of a multifunctional cosmetic prosthetic hand," in *IEEE International Conference on Rehabilitation Robotics*, 2007, pp. 550–553.

- [54] C. E. Clauser, J. T. McConville, and J. W. Young, "Weight, Volume, and Center of Mass of Segments of the Human Body," Wright Patterson Air Force Base, Dayton, 1969.
- [55] C. C. Gordon, T. Churchill, C. E. Clauser, B. Bradtmiller, J. T. McConville, I. Tebbetts, and R. A. Walker, "1988 Anthropometric survey of U.S. army personnel: summary statistics interim report," United States Army Natick Research, Development and Engineering Center, Natick, Massachusetts, 1989.
- [56] P. J. Kyberd, C. Wartenberg, L. Sandsjö, S. Jönsson, D. Gow, J. Frid, C. Almström, and L. Sperling, "Survey of Upper-Extremity Prosthesis Users in Sweden and the United Kingdom," *JPO J. Prosthetics Orthot.*, vol. 19, no. 2, pp. 55–62, 10.1097/JPO.0b013e3180459df6, 2007.
- [57] C. Pylatiuk and S. Schulz, "Using the Internet for an Anonymous Survey of Myoelectrical Prosthesis Wearers," *Myoelectric Controls Symposium*. Fredericton, New Brunswick, Canada, 2005.
- [58] C. M. Light, C. Chappell, and P. J. Kyberd, "Establishing a standardized clinical assessment tool of pathologic and prosthetic hand function: Normative data, reliability, and validity," *Arch. Phys. Med. Rehabil.*, vol. 83, no. 6, pp. 776–783, 2002.
- [59] O. Van Der Niet Otr, H. A. Reinders-Messelink, R. M. Bongers, H. Bouwsema, and C. K. Van Der Sluis, "The i-Limb hand and the DMC Plus hand compared: A case report," *Prosthet. Orthot. Int.*, vol. 34, no. 2, pp. 216–220, 2010.
- [60] C. L. Taylor, "The Biomechanics of Control in Upper-Extremity Prostheses," *Artif. Limbs*, vol. 2, no. 3, pp. 4–25, 1955.
- [61] J. A. Doubler and D. S. Childress, "An analysis of extended physiological proprioception as a prosthesis-control technique," *J. Rehabil. Res. Dev.*, vol. 21, no. 1, pp. 5–18, 1984.
- [62] E. Biddiss, D. Beaton, and T. Chau, "Consumer design priorities for upper limb prosthetics," *Disabil. Rehabil. Assist. Technol.*, vol. 2, no. 6, pp. 346–357, 2007.
- [63] P. Geethanjali and K. K. Ray, "A Low-Cost Real-Time Research Platform for EMG Pattern Recognition-Based Prosthetic Hand," *IEEE/ASME Transactions on Mechatronics*, vol. 20, no. 4, pp. 1948–1955, 2015.
- [64] W. Chen, C. Xiong, and S. Yue, "Mechanical Implementation of Kinematic Synergy for Continual Grasping Generation of Anthropomorphic Hand," *Mechatronics, IEEE/ASME Transactions on*, vol. 20, no. 3, pp. 1249–1263, 2015.

- [65] N. M. Bajaj, A. J. Spiers, and A. M. Dollar, “State of the Art in Prosthetic Wrists: Commercial and Research Devices,” in *Proc. IEEE Int. Conf. Rehabilitation Robotics*, 2015, pp. 331–338.
- [66] A. Zinck, O. Stavadahl, E. Biden, and P. J. Kyberd, “Design of a Compact, Reconfigurable, Prosthetic Wrist,” *Appl. Bionics Biomech.*, vol. 9, no. 1, pp. 117–124, 2012.
- [67] P. J. Kyberd, E. D. Lemaire, E. Scheme, C. MacPhail, L. Goudreau, G. Bush, and M. Brookesshaw, “Two-degree-of-freedom powered prosthetic wrist,” *The Journal of Rehabilitation Research and Development*, vol. 48, no. 6, p. 609, 2011.
- [68] C. Abul-Haj and N. Hogan, “An emulator system for developing improved elbow-prosthesis designs,” *IEEE Trans. Biomed. Eng.*, vol. 34, no. 9, pp. 724–737, 1987.
- [69] J. W. Sensinger and R. F. F. Weir, “User-modulated impedance control of a prosthetic elbow in unconstrained, perturbed motion,” *IEEE Trans. Biomed. Eng.*, vol. 55, no. 3, pp. 1043–1055, 2008.
- [70] J. Sensinger, J. Lipsey, T. Sharkey, A. Thomas, L. Miller, K. Turner, J. Ochoa, and T. Idstein, “Initial Experiences with the RIC Arm,” in *Proc. Myoelectric Controls/Powered Prosthetics Symp.*, 2014, pp. 227–229.
- [71] J. Aizawa, T. Masuda, T. Koyama, K. Nakamaru, K. Isozaki, A. Okawa, and S. Morita, “Three-dimensional motion of the upper extremity joints during various activities of daily living,” *J. Biomech.*, vol. 43, no. 15, pp. 2915–2922, 2010.
- [72] P. Kyberd, D. Gow, and P. Chappell, “Research and the Future of Myoelectric Prosthetics,” in *Powered Upper Limb Prostheses—Control, Implementation and Clinical Application*, A. Muzumdar, Ed. Berlin: Springer-Verlag, 2004.
- [73] Ottobock, “10S17 Electric Wrist Rotator Instructions for Use.” [Online]. Available: http://professionals.ottobockus.com/cps/rde/xbcr/ob_us_en/ifu_647h204_electric_wrist_rotator.pdf. [Accessed: 01-Jan-2015].
- [74] MotionControl, “FACT SHEET - Wrist Rotator.” [Online]. Available: <http://www.utaharm.com/files/>. [Accessed: 01-Jan-2015].
- [75] M. A. Buckley, A. Yardley, G. R. Johnson, and D. A. Cams, “Dynamics of the Upper Limb during Performance of the Tasks of Everyday Living—A Review of the Current Knowledge Base,” *Proc. Inst. Mech. Eng. Part H J. Eng. Med.*, vol. 210, no. 4, pp. 241–247, 1996.

- [76] L. Peebles and B. Norris, "Filling 'gaps' in strength data for design," *Appl. Ergon.*, vol. 34, no. 1, pp. 73–88, Jan. 2003.
- [77] Ottobock, "DynamicArm Patient Information." [Online]. Available: http://www.ottobock.com/cps/rde/xbcr/ob_com_en/646D229-INT-07-1206w.pdf. [Accessed: 01-Jan-2015].
- [78] MotionControl, "Utah Hybrid Arm." [Online]. Available: <http://www.utaharm.com/files/>.
- [79] B. F. Morrey, L. J. Askew, and E. Y. Chao, "A biomechanical study of normal functional elbow motion.," *J. Bone Joint Surg. Am.*, vol. 63, no. 6, pp. 872–877, 1981.
- [80] D. J. Magermans, E. K. J. Chadwick, H. E. J. Veeger, and F. C. T. Van Der Helm, "Requirements for upper extremity motions during activities of daily living," *Clin. Biomech.*, vol. 20, no. 6, pp. 591–599, 2005.
- [81] I. A. Murray and G. R. Johnson, "A study of the external forces and moments at the shoulder and elbow while performing every day tasks.," *Clin. Biomech. (Bristol, Avon)*, vol. 19, no. 6, pp. 586–94, Jul. 2004.
- [82] J. Bradley and B. Gover, "Criteria for acoustic comfort in open-plan offices," in *Proc. 33rd Int. Congr. and Expo. on Noise Control Engineering*, 2004, pp. 22–25.
- [83] K. A. Raichle, "Prosthesis use in persons with lower- and upper-limb amputation," *J. Rehabil. Res. Dev.*, vol. 45, no. 7, pp. 961–972, 2008.
- [84] L. H. Smith, T. A. Kuiken, and L. J. Hargrove, "Real-time simultaneous myoelectric control by transradial amputees using linear and probability-weighted regression," in *Proceedings of the 2015 International Conference of the IEEE Engineering in Medicine and Biology Society*, 2015, pp. 1119–1123.
- [85] N. Jiang and K.-R. Muller, "Myoelectric control of artificial limbs-is there a need to change focus," *IEEE Signal Process. Mag.*, vol. 29, no. 5, pp. 152–150, 2012.
- [86] F. Montagnani, M. Controzzi, and C. Cipriani, "Exploiting Arm Posture Synergies in Activities of Daily Living to Control the Wrist Rotation in Upper Limb Prostheses: a Feasibility Study," in *Proceedings of the 2015 International Conference of the IEEE Engineering in Medicine and Biology Society*, 2015, pp. 2462–2465.

- [87] S. L. Carey, M. Jason Highsmith, M. E. Maitland, and R. V. Dubey, "Compensatory movements of transradial prosthesis users during common tasks," *Clin. Biomech.*, vol. 23, no. 9, pp. 1128–1135, 2008.
- [88] J. S. Landry and E. N. Biden, "Optimal Fixed Wrist Alignment for Below-Elbow, Powered, Prosthetic Hands," in *Proceedings of the 2002 MyoElectric Controls/Powered Prosthetics Symposium*, 2002.
- [89] L. A. Miller, K. A. Stubblefield, R. D. Lipschutz, B. A. Lock, and T. A. Kuiken, "Improved myoelectric prosthesis control using targeted reinnervation surgery: a case series," *IEEE Trans Neural Syst Rehabil Eng*, vol. 16, no. 1, pp. 46–50, 2008.
- [90] L. Markley, "Attitude determination using two vector measurements," in *NASA CONFERENCE PUBLICATION*, 1999, pp. 39–52.